

## TABLE OF CONTENTS

	Page
INTRODUCTION .....	1
CHAPTER 1 LITERATURE REVIEW .....	19
1.1 Introduction.....	19
1.2 Liposomes .....	19
1.2.1 Classification of liposomes .....	21
1.2.2 Liposomes applications.....	22
1.3 Liposomes production methods .....	27
1.4 Liposome production using micromixers .....	28
1.4.1 Molecular diffusion-based micromixers for liposome production .....	29
1.4.2 Chaotic advection-based micromixers for liposome production .....	35
1.4.3 Fluid lamination and folding.....	40
1.4.4 Micromixers for liposome production evolution .....	42
1.5 Patents and companies working on the field.....	43
1.6 Chapter 1 conclusions .....	45
CHAPTER 2 LIPOSOME FORMATION IN DEAN DYNAMICS FLOW BASED MICROMIXERS DEVICES: THEORY, MATERIALS, AND METHODS .....	47
2.1 Liposome formation theory.....	47
2.2 Nanoprecipitation method and mixing.....	49
2.3 Mixing theory.....	51
2.4 Mixing and liposome production relationship .....	54
2.5 Numerical modeling.....	55
2.6 Micromixer design and fabrication.....	59
2.7 Mixing imaging.....	61
2.8 Lipid preparation.....	63
2.9 Liposomes production using micromixers.....	64
2.10 Liposome characterization .....	66
2.10.1 Dynamic light scattering .....	67
2.10.2 Nanoparticle tracking analysis.....	70
2.10.3 Zeta potential (electrokinetic potential) .....	72
2.10.4 Transmission electron microscopy .....	73
2.11 Chapter 2 conclusions .....	74
CHAPTER 3 LIPOSOME PHYSICOCHEMICAL CHARACTERISTICS MODELING .....	77
3.1 Identifying the most significant factors. ....	78
3.1.1 Screening experiments .....	78
3.1.2 Liposome size significant factors.....	81
3.1.3 Liposome PDI significant factors .....	83
3.1.4 Liposome zeta potential significant factors .....	84

3.1.5	Conclusions on the most significant factors .....	85
3.2	Surface response-based modeling of liposome characteristics in a periodic disturbance mixer.....	86
3.2.1	Introduction.....	86
3.2.2	Materials and methods .....	87
3.2.3	Results and discussion .....	91
3.2.4	Conclusions.....	101
3.3	Chapter 3 conclusions .....	102
CHAPTER 4      PARAMETRIC STUDY OF THE FACTORS INFLUENCING LIPOSOME PHYSICOCHEMICAL CHARACTERISTICS IN A PERIODIC DISTURBANCE MIXER .....		
4.1	Introduction.....	103
4.2	Materials and methods .....	104
4.2.1	Lipid preparation.....	104
4.2.2	Liposome characterization .....	104
4.2.3	Statistical analysis .....	106
4.3	Results and discussion .....	106
4.3.1	Alternating centripetal force direction induces mixing .....	107
4.3.2	Intensity- based size vs number-based size validation .....	109
4.3.3	TFR controls liposome size .....	111
4.3.4	FRR controls liposome size in a defined range .....	113
4.3.5	Lipid concentration influences liposome size.....	115
4.3.6	Lipid fatty acid chain length influence over liposome size .....	118
4.3.7	Temperature and liposome size are negatively correlated.....	119
4.3.8	Liposomes are stable in the long term .....	120
4.3.9	Liposome production rate .....	122
4.4	Chapter 4 conclusions .....	122
CHAPTER 5      THE EFFECT OF DIFFERENT ORGANIC SOLVENTS IN LIPOSOME PROPERTIES PRODUCED IN A PERIODIC DISTURBANCE MIXER: TRANSCUTOL®, A POTENTIAL ORGANIC SOLVENT REPLACEMENT .....		
5.1	Introduction.....	125
5.2	Materials and methods .....	127
5.2.1	Lipids preparation and nanoparticle production .....	127
5.2.2	Nanoparticle characterization .....	128
5.2.3	Experimental design and statistical analysis.....	128
5.3	Results and discussion .....	129
5.3.1	Liposome production using different organic solvents.....	129
5.3.2	Concentration effects on liposomes produced with ethanol and Transcutol® .....	134
5.3.3	Temperature effects on liposomes produced with ethanol and Transcutol® .....	136
5.3.4	Liposome size stability .....	139

CHAPTER 6	FUTURE WORK: TOWARDS BIOMEDICAL APPLICATIONS .....	143
6.1	Alternative microfabrication process: 3D printing .....	143
6.2	Geometry optimization for an improved liposome production yield.....	145
6.3	Approaches to facilitate liposome production implementation .....	145
6.4	EVs characterization for cancer research.....	146
6.5	Gene delivery applications.....	147
CONCLUSIONS .....		149
RECOMMENDATIONS.....		151
APPENDIX I PUBLICATIONS DURING PH.D. STUDIES.....		155
BIBLIOGRAPHY .....		157





## LIST OF TABLES

	Page
Table 1.1	Head-groups classification with examples..... 21
Table 1.2	Liposome classification ..... 22
Table 1.3	Approved liposome formulations ..... 23
Table 3.1	Factors and levels tested in the experimental screening design..... 79
Table 3.2	Initial low and high experimental levels per variable ..... 89
Table 3.3	CCCR design results for the 29 runs..... 91
Table 3.4	Grouping information using the Tukey method at a 95% confidence level..... 96
Table 3.5	Statistically significant coefficients for each model ( $p < 0.05$ ) and model statistics summary ..... 98
Table 4.1	DLS vs NTA characterization..... 109
Table 4.2	Theoretical vs. Measured particle concentration produce at FRR = 1 TFR = 18 mL/h ..... 122
Table 5.1	Experimental design. All the experiments were performed at FRR = 8.56 and TFR = 18 mL/h..... 128



## LIST OF FIGURES

	Page
Figure 0.1      Type of nanodrugs particles.....	3
Figure 0.2      Nanomedicines market value .....	3
Figure 0.3      Liposome applications summary .....	4
Figure 0.4      Structural liposome model, encapsulated, and surface elements.....	6
Figure 0.5      Nanoparticle accumulation .....	7
Figure 1.1      a Structure of POPC lipid molecule b Lipid bilayer thickness c Lipid vesicle .....	20
Figure 1.2      Liposomes loaded with Dil red dye in the retina space .....	26
Figure 1.3      Flow focusing production method (a) Numerical model (b) DiIC <sub>18</sub> fluorescence intensity during liposome formation.....	30
Figure 1.4      Schematic of 3D-MHF liposome formation device.....	32
Figure 1.5      a) Numerical models comparing the ethanol concentration profiles for VFF and MHF devices   b) Photograph of multilayer VFF with an aspect ratio of 100:1 .....	34
Figure 1.6      Mixing inside a SHM.The micrographs are a cross-section view at different distances from the beginning of the channel.....	36
Figure 1.7      Herringbone structures induce chaotic advection of the laminar streams. Dimensions of the mixing channel are 200µm x 79 µm, and herringbone structure is 31 µm high and 50 µm thick.....	37
Figure 1.8      Chaotic advection-based microfluidic Device (CA-MD).....	39
Figure 1.9      Liposome production using micromixers evolution .....	43
Figure 2.1      Schematic showing the liposome formation process explained by energetic considerations.....	48
Figure 2.2      Energy diagram of lipid aggregates as they move from phospholipid aggregates to SUVs.....	49

Figure 2.3	Mutual diffusion coefficient for the binary mixture ethanol-water dependent on concentration. In black, the experimental data, in red, the 5th order polynomial.....	58
Figure 2.4	Mixing of ethanol and water in a microfluidic device. Experimental vs. numerical modeling .....	59
Figure 2.5	PDM. The micromixer consists of two inlets a micromixing channel and an outlet.....	60
Figure 2.6	Micromixer fabrication process .....	61
Figure 2.7	Micromixing imaging A) Food dyes imaging in two dimensions. In blue-stained water and in orange ethanol B) Fluorescence dyes imaging in three dimensions .....	62
Figure 2.8	Mixing imaging experimental setup .....	63
Figure 2.9	Lipid preparation process. From left to right, lipid mixture, chloroform removal, and organic solvent dilution.....	64
Figure 2.10	Liposome production experimental setup A) Schematic B) Photography of the functional experimental setup .....	65
Figure 2.11	Particle size distribution A) By number B) By volume C) By intensity .....	68
Figure 2.12	Zetasizer S90 workflow. From left to right, inserting the sample, equipment, and results .....	69
Figure 2.13	NTA Measurements A) Nanosight NS500 B) Sample results are taken from NS500 C) Image of the scattered light of nanoparticles .....	71
Figure 2.14	Diagram showing the potential as a function of the distance from the particle's surface in a colloidal dispersion.....	72
Figure 2.15	Philips Tecnai T12 electron microscope.....	73
Figure 2.16	General methodology for investigating the liposome formation process in Dean Flow Dynamics based micromixers .....	75
Figure 3.1	Dean Forces-based micromixers A) CEA based on flow lamination B) PDM, based on alternatively shifting centripetal forces.....	78
Figure 3.2	A) Screening experiments steps B) Lipids used in the screening experiments .....	80

Figure 3.3	Experimental setup V) DMPC:CHOL:D 5:4:1 10 mM X) DMPC:CHOL 1:1 40 mM Y) DMPC: CHOL 1:1 10 mM Z) DMPC: CHOL: DHP 5 :4 :1 40 mM.....	81
Figure 3.4	Fit screening model for size A) Main effects plots for size B) Pareto chart of effects.....	82
Figure 3.5	Normalized size distribution by intensity of two samples, produced by a CEA micromixer, in blue a Z-Average of 236.6 nm and in orange 160.7 nm for a FRR of 1 and 5 .....	83
Figure 3.6	Fit screening model for PDI A) Main effects plots for PDI B) Pareto chart of effects.....	84
Figure 3.7	Fit screening model for zeta potential A) Main effects plots for PDI. B) Pareto chart of effects .....	85
Figure 3.8	Periodic disturbance micromixer A) Microchannel dimensions B) Microscope image of the PDM C) Schematic representation of the liposome formation process .....	87
Figure 3.9	CCCR design graphical representation.....	90
Figure 3.10	Surface Response Model derived from the Central Composite Circumscribed Rotatable Design Data. The model level of significance is $p < 0.05$ A) 3-dimensional B) Contours representation .....	94
Figure 3.11	PDI Surface Response Model as well as the $R^2$ , $R^2$ -adjusted, and $R^2$ -predicted. The model has a $p < 0.05$ A) 3-dimensional B) Contours representation.....	95
Figure 3.12	Zeta potential measurements result for the nine different conditions. The error bars show $1.96\sigma$ , indicating the limits of 95% confidence ( $n = 3$ ).....	97
Figure 3.13	Z-average (nm) vs. FRR ( $n = 3$ ). Error bars indicate $\pm 1$ standard deviation (SD) for samples and SE fit for the model prediction.....	98
Figure 3.14	Mixing efficiency at different FRRs. Each data point corresponds to a cross-section for a total of 11 data points from 1–11.....	100
Figure 3.15	Numerical simulations comparing the concentration profiles at FRR = 1 and FRR = 3 at a constant TFR = 18 mL/h A) Top view of the mixing channels and position of the cross-sections B) Cross-sections at different FRRs.....	101

Figure 4.1	Micromixing in PDM at a FRR = 1 and TFR = 18 mL/h (A) Confocal image showing a top view of the PDM (B) Micromixer numerical model with the ethanol flow in red and the water flow in blue. Milli-Q. The bar represents the ethanol concentration (C) Cross-sections of the confocal images and their numerical model counterparts.....	107
Figure 4.2	Mixing index versus time for a constant FRR = 8.56 at various TFR (5-20 mL/h). Each data point corresponds to the 11 different cross sections in the diagram below.....	108
Figure 4.3	Size distribution by number normalized for the same sample produced at FRR = 1 and TFR = 18 mL/h. Characterized in the DLS (blue) and NTA (orange).....	110
Figure 4.4	Size distribution by number normalized for the same sample produced at FRR = 1 and TFR = 18 mL/h. Characterized in the DLS (blue) and NTA (orange).....	111
Figure 4.5	Effect of the TFR on various liposome properties.....	112
Figure 4.6	The effect of FRR over liposomes properties .....	114
Figure 4.7	Initial lipid concentration effects over liposome size .....	116
Figure 4.8	Liposome properties produced using DSPC, cholesterol, and DHP in a molar ratio 5:4:1 .....	118
Figure 4.9	Temperature effects on liposome properties.....	120
Figure 4.10	Liposomes stability after 50 days diameter mean +/- 1 SD A) Liposome sample synthesized at FRR = 12 and TFR = 18 mL/h, nm B) FRR = 8.56 TFR = 20 mL/h T = 70 °C .....	121
Figure 4.11	Liposomes produced at FRR = 8.56 TFR=18 mL/h, initial lipid concentration of 10 mM, T = 40 °C made of DMPC:CHOL:DHP at a molar ratio 5:4:1 three months after production .....	121
Figure 5.1	Liposomes synthesized using an FRR = 8.56 and TFR = 18 mL/h at 40 °C using different organic solvents with a 10 mM lipid concentration A) Z-Average and PDI. The bars indicate +/- 1 SD n = 3 B) Size Distribution by Intensity Normalized .....	130
Figure 5.2	Liposomes synthesized using an FRR = 8.56 and TFR = 18 mL/h at 40 °C using different organic solvents with a 10 mM lipid concentration A) Diameter by number. The bars indicate +/- 1 SD n = 3 B) Size Distribution by Number Normalized .....	131

Figure 5.3	Nanoparticle formation process. The increase of the aqueous solvent concentration, and hence the polarity of the mixture, causes the lipids to self-assemble in disk-shaped structures, which finally bend and close into liposomes ..... 132
Figure 5.4	Zeta Potential of liposomes synthesized using an FRR = 8.56 and TFR = 18 mL/h at 40 °C ..... 133
Figure 5.5	Liposomes synthesized using two different organic solvents and different lipid concentrations at 40 °C, with an FRR = 8.56 and TFR = 18mL/h A) Average size and PDI. The bars indicate +/- 1 SD n = 3 B) Size Distribution by Intensity Normalized for ethanol C) Size Distribution by Intensity Normalized for Transcutol® ..... 135
Figure 5.6	Zeta Potential of liposomes synthesized using two different organic solvents and different lipid concentrations at 40 °C, with an FRR = 8.56 and TFR = 18mL/h. The bars indicate +/- 1 SD n = 3 ..... 136
Figure 5.7	Liposomes synthesized using two different organic solvents and different production temperatures at 10 mM lipid concentration, with an FRR = 8.56 and TFR = 18mL/h A) Average size and PDI. The bars indicate +/- 1 SD n = 3 B) Size Distribution by Intensity Normalized for ethanol C) Size Distribution by Intensity Normalized for Transcutol® ..... 137
Figure 5.8	Zeta Potential of liposomes synthesized using two different organic solvents and different production temperatures at 10 mM lipid concentration, with an FRR = 8.56 and TFR = 18mL/h. The bars indicate +/- 1 SD n = 3 ..... 138
Figure 5.9	Liposome size evolution synthesized with ethanol at 40 °C using an FRR = 8.56 and TFR = 18mL/h. 1-day vs. 50 days after synthesis characterization A) Size Distribution by Intensity of the least changing sample synthesized with a 5 mM lipid concentration B) Size Distribution by Intensity of the most changing sample synthesized with a 40 mM lipid concentration ..... 139
Figure 5.10	Liposome size evolution synthesized with Transcutol® using an FRR = 8.56 and TFR = 18mL/h. 1-day vs. 50 days after synthesis characterization A) Size Distribution by Intensity of the least changing sample produced at 40 °C and with a 40 mM lipid concentration B) Size Distribution by Intensity of the most changing sample produced at 70 °C and with a 10 mM lipid concentration ..... 140
Figure 5.11	Liposome size evolution synthesized with Transcutol® using an FRR = 8.56 and TFR = 18mL/h. 1-day vs. 50 days after synthesis

characterization A) Size Distribution by Intensity of the least changing sample produced at 40 °C and with a 40 mM lipid concentration B) Size Distribution by Intensity of the most changing sample produced at 70 °C and with a 10 mM lipid concentration ..... 141

Figure 6.1 Microfabrication process of 3D printed-PLA-COC device A) PLA device and COC “ceiling” B) 3D printing the microfluidic device C) A completed device with connectors ..... 144

Figure 6.2 Factors influencing gene delivery systems production..... 148



## LIST OF ABBREVIATIONS

ACS	American Chemical Society
AFA	Adaptative focused acoustics
ANOVA	Analysis of variance
AO	Antioxidants
CAGR	Compound annual growth rate
CA-MD	Chaotic advection-based microfluidic device
CCCR	Central composite circumscribed rotatable
CEA	Contraction-expansion array
CHOL	Cholesterol
CL	Cationic liposomes
CM	Crisscross micromixer
COC	Cyclic olefin copolymer
CONACyT	<i>Consejo Nacional de Ciencia y Tecnología</i>
DEPC	1,2-Dierucoyl-sn-glycero-3-phosphocholine
DHP	Dicetyl phosphate
DiIC18	1,1'-dioctadecyl-3,3,3',3'-tetramethylindocarbocyanine perchlorate
DLIN-	(6Z,9Z,28Z,31Z)-heptatriacont-6,9,28,31-tetraene-19-yl 4-
MC3-DMA	(dimethyl amino) butanoate
DLS	Dynamic light scattering
DMPC	1,2-dimyristoyl-sn-glycero-3-phosphocholine
DMPG	Dimyristoylphosphatidylglycerol

DODAC	N-N-dioleoyl-N, N-dimethyl ammonium chloride
DoE	Design of experiments
DOPC	1,2-dioleoyl-sn-glycero-3-phosphocholine
DOPE	1,2-dioleoyl-sn-glycero-3-phosphoethanolamine
DOPS	1,2-dioleoyl-sn-glycero-3-phospho-L-serine
DOTAP	Dioleoyl-3-trimethylammonium propane
DOTMA	1,2-di-O-octadecenyl-3-trimethylammonium propane
DPPG	1,2-Dihexadecanoyl-sn-Glycero-3-Phospho-1'-rac-glycerol
DS	Delivery systems
DSPC	1,2-distearoyl-sn-glycero-3-phosphocholine
DSPG	1,2-distearoyl-sn-glycero-3-phospho-(1'-rac-glycerol)
EMA	European medicines agency
EPC	Egg 1,2-dioleoyl-sn-glycero-3-ethylphosphocholine
EPG	Egg L- $\alpha$ -phosphatidylglycerol
EPR	Enhanced retention and permeability effect
EVs	Extracellular vesicles
FDA	Food and Drug Administration
FDM	Fused deposition modeling
FRR	Flow rate ratio
GMP	Good manufacturing practices
HSPC	L- $\alpha$ -phosphatidylcholine
IC	Initial concentration

IEEE	Institute of Electrical and Electronics Engineers
iLiNP	Invasive lipid nanoparticle production device
IPA	Isopropyl alcohol
Lipid T	Lipid mixture type
LNPs	Liposome nanoparticles
LUV	Large unilamellar vesicles
ME	Mixing efficiency
MHF	Microfluidic hydrodynamic focusing
MI	Mixing index
MLV	Multilamellar vesicles
MR	Magnetic resonance
Mtype	Mixer type
NDS	Nanoparticle delivery system
NTA	Nanoparticle tracking analysis
OLV	Oligolamellar vesicles
PA	Phosphatidic acid
PBS	Phosphate buffer saline solution
PC	Phosphatidylcholine
PCS	Photo correlation spectroscopy
PDI	Polydispersity index
PDM	Periodic disturbance mixer
PDMS	Polydimethylsiloxane

## XXVIII

PE	Phosphatidylethanolamine
PEG-DSPE	1,2-distearoyl-sn-glycero-3-phosphoethanolamine-N-[amino(polyethylene glycol)-2000]
PG	Phosphatidylglycerol
PI	Phosphatidylinositol
PLA	Poly-lactic acid
PLGA	Poly lactic-co-glycolic acid
POPC	1-palmitoyl-2-oleoyl-sn-glycero-3-phosphocholine
PS	Phosphatidylserine
RSC	Royal Society of Chemistry
RSM	Response surface methodology
SAW	Surface acoustic waves
SHM	Staggered herringbone micromixer
siRNA	Small interfering ribonucleic acid
SL	Stealth liposomes
SLA	Stereolithography
SM	Sphingomyelin
SU-8	Substrate with 8 epoxy
SUV	Small unilamellar vesicles
TEM	Transmission electron microscopy
TFF	Tangential flow filtration
TFR	Total flow rate

UM	Uveal melanoma
VFF	Vertical flow focusing
ZP	Zeta potential



## LIST OF SYMBOLS

$\mu$	Dynamic viscosity
A	Lipid area
$A_{do}$	Surface area of disk 0
c	Concentration
D	Diffusion coefficient
$De$	Dean number
$D_H$	Hydraulic diameter
$d_h$	Hydrodynamic diameter
$D_{s0}$	Diameter of sphere 0
$D_{s1}$	Diameter of sphere 1
e	Lipid bilayer thickness
F	External force
h	Half diameter in a pipe.
j	Diffusion flux
k	Boltzmann constant
N	Molar flux
n	Number
$N_A$	Avogadro's number
p	Pressure
P	Production rate
Q	Total flow rate

$Q_{as}$	Aqueous solvent flow rate
$Q_{os}$	Organic solvent flow rate
$r_h$	Particles Ratio or Liposome Ratio
$R$	Volumetric source for the species
$R_c$	Ratio of curvature
$Re$	Reynolds number
$T$	Temperature
$u$	Flow velocity
$x$	Distance
$X$	Increasing proportion
$\eta$	Viscosity
$\nu$	Kinematic viscosity
$\rho$	Fluid density
$\sigma$	Standard deviation



## INTRODUCTION

Liposomes are vesicles made of lipids. Lipids are organized in lipid bilayers forming sphere shape structures that can encapsulate multiple substances. This property makes liposomes suitable for drug delivery applications. Along 50+ years in liposome research, various preparation methods have been proposed; however, the vast majority of them are batch-based, and mostly production rates are only suitable for laboratory scale production. Moreover, reproducibility is a significant concern required to meet the standards of regulatory agencies. Batch methods do not have the required consistency. These problems delay or block the research, development, and production of liposomes and prevent them from reaching patients worldwide (Hua, de Matos, Metselaar, & Storm, 2018).

Between 1995 and 2005, significant advances were made in microfabrication, especially in soft lithography allowing researchers to produce microfluidic devices with channels in the order of micrometers in relatively easy few steps. These advancements opened an entirely new world of opportunities to investigate the micromixing phenomenon and its applications.

Micromixers offer a suitable alternative for liposome production. Tunable size monodispersed liposome nanoparticles (LNPs) can be produced in a continuous flow, improving reproducibility. Unfortunately, micromixers yield, in general, is too low for industrial-scale production, while the ones that are suitable for mass production clog and are challenging to fabricate. Other mixing strategies and micromixers designs might help to solve this conundrum. However, only a few micromixers have been studied and explicitly characterized for liposome production; furthermore, important variable interactions have not been addressed. This work objective is to investigate liposome formation in micromixers that are based on Dean's flow dynamics. This type of micromixers uses chaotic advection and Taylor dispersion to accelerate the mixing process. The conditions under which LNPs are produced, as well as crucial factors that direct and control liposome physicochemical characteristics such as size, size distribution, and zeta potential were investigated.

## 0.1 Rationale

Pharmacy word originates from the Greek word *pharmakon*, which has different meanings, including remedy and poison. For years, this dichotomy has been accepted. This acceptance meant for patients that sometimes the cure was worse than the disease. Several therapeutic agents must be administered at high doses, increasing toxic effects. For patients, removing or reducing the poisonous part of the remedy would mean a better quality of life. Having a way of releasing the correct dose at the right location without producing side effects, the magic bullet of Paul Ehrlich was an elusive feat until recently (Ehrlich, 1913).

Delivery systems (DS) consists of a shell or structure that functions as a carrier and a cargo that can include genes, drugs, imaging labels, among others. This cargo could be enclosed inside the transport vehicle as well as ligated to its exterior. Most of the DS used in the biomedical field are in the range of 3-200 nm. DS protect their cargo from degradation, offering an extended circulation time inside the human body. Due to their properties such as size and modified surfaces added with specific moieties, DS can target specific organs, tissues, and cells. DS that are in the range of nanometers are called nanoparticle delivery systems (NDS). There are several types of nanoparticles, such as polymeric conjugates, micelles, dendrimers, viral nanoparticles, carbon nanotubes, and liposomes (Cho, Wang, Nie, Chen, & Shin, 2008). Figure 0.1 shows the different types of nanoparticles.

In terms of market potential, nanopharmaceuticals are expected to grow to 168.91 billion by 2026, with a compound annual growth rate (CAGR) of 22.1%, as shown in Figure 0.2. This market growth is supported by liposomes and polymer delivery systems (Business-Wire, 2019).

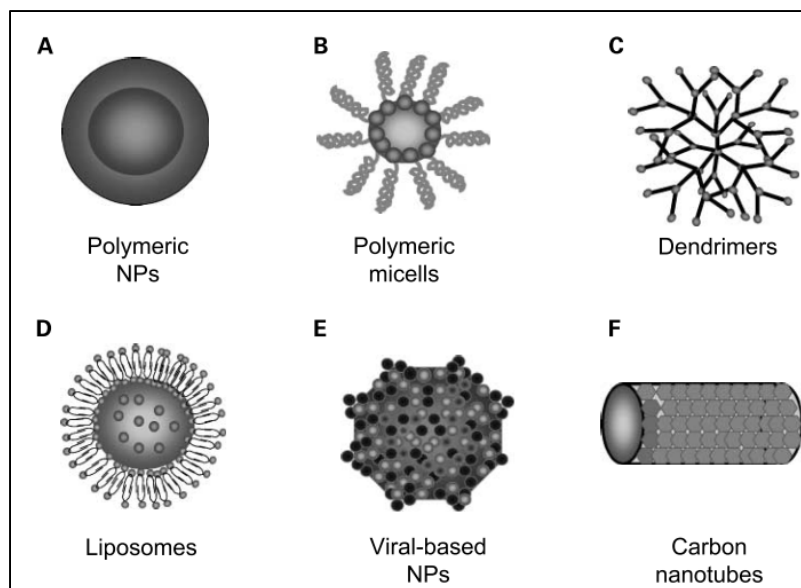


Figure 0.1 Type of nanodrugs particles  
Taken from Cho et al. (2008, p.1312)

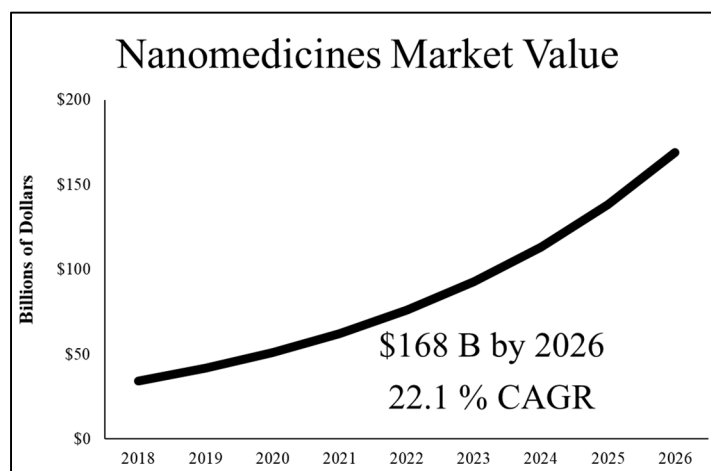


Figure 0.2 Nanomedicines market value  
Adapted from Business-Wire (2019)

Liposomes have proven to be one of the most versatile nanoparticles, considering the number of approved products in the market. The first approved nanodrug was a liposomal carrier (Doxil®). Nanoparticles applied in the medical field is growing (Havel, 2016). This type of nanoparticles has established a precedent and paved the way for regulations in the area of

nanopharmaceuticals (Food & Administration, 2018). So far, 17 liposome-based drug formulations have been approved (Leung, Amador, Wang, Mody, & Bally, 2019).

Liposomes applications range from drug delivery systems, gene delivery systems, vaccines imaging, and analytical applications. These vesicles can encapsulate both imaging labels and therapeutic substances, also known as theragnostics (Pattni, Chupin, & Torchilin, 2015). Additionally, applications in the field of cosmeceuticals have been explored (Rahimpour & Hamishehkar, 2012; Van Tran, Moon, & Lee, 2019). Figure 0.3 summarizes Liposomes applications.

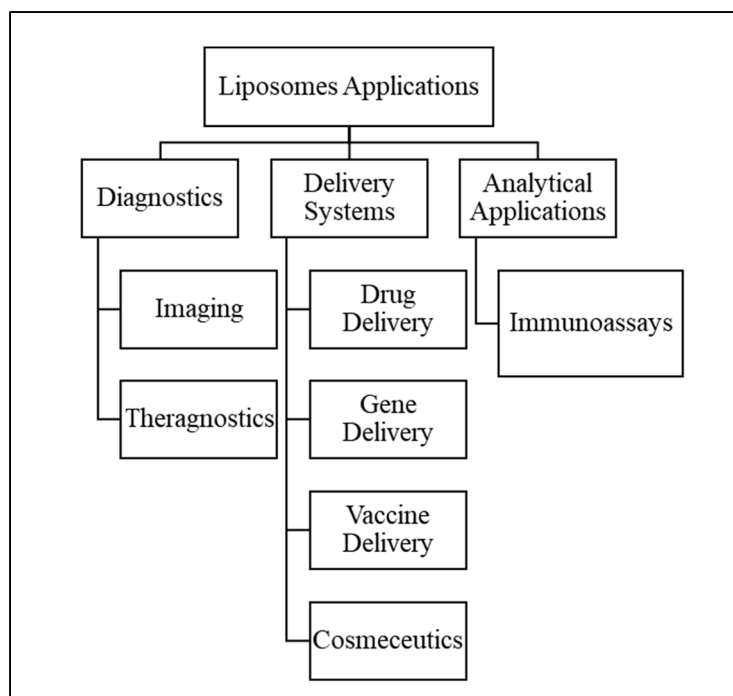


Figure 0.3 Liposome applications summary

NDS have the potential to add value to existing products, extending their product life as patented formulations as well as reducing toxicity. One example of this is the antibiotic field, where their indiscriminate use caused the resistance of bacteria, requiring increasing the level of dosage just below toxic values for effective treatment. Old formulations that right now are

not effective anymore could be reused through NDS. Currently, a few liposomal antibiotic formulations are under experimentation (Gao et al., 2014).

However, there are still challenges in the field of nanopharmaceuticals. Liposome based delivery systems are getting more sophisticated with new added bioactive molecules. At a laboratory-scale, this increased complexity translates into lengthy production processes that prevent innovative formulation production at the industrial scale. Moreover, these production methods must comply with good manufacturing practices (GMP), so they can be included in late clinical stages and commercialization (Hua et al., 2018). The nanopharmaceuticals industry looks for integrative liposome production systems with high reproducibility and scalability

Microfluidics devices, specifically micromixers, offer an approach that can produce liposomes in a continuous-flow production, improving reproducibility (Andreas Jahn et al., 2010). However, these microfluidic devices are not exempt from challenges. Low production yield and toxic solvent remains are still the main problems to be solved.

In this dissertation, a new microfluidic configuration is proposed to increase the production rate while keeping control over final liposome characteristics such as size, size distribution, and zeta potential. The mixing inside the proposed device is based on Dean flow dynamics. This device can produce liposomes of controlled size, and it can be useful for creating other types of NDS.

## **0.2 Problem statement**

Liposomes are used in medical imaging, general delivery, and analysis systems (Pattni et al., 2015). These vesicles encapsulate drug formulations, genes, imaging labels, and proteins. The biodegradable components of liposomes provide them with the capacity to interact safely with biological systems. Moreover, by adding surface moieties and controlling the size, it is possible to target distribution towards specific organs and tissues, increasing drug circulation time, and

improving drugs therapeutic window (Allen & Cullis, 2013; Gabizon et al., 1994; Matsumura & Maeda, 1986; Safra et al., 2000). Figure 0.4 shows a typical liposome with potential contents and surface ligands (Liu & Boyd, 2013).

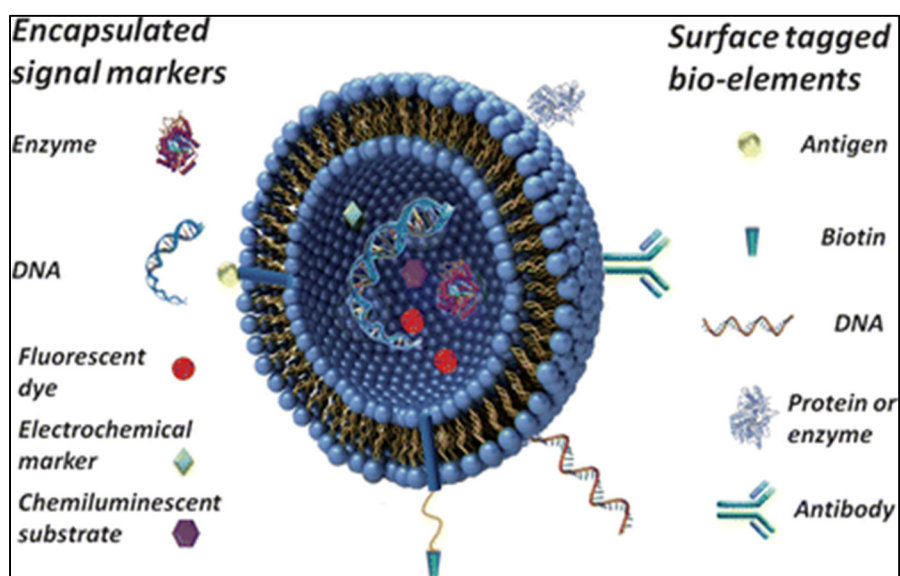


Figure 0.4 Structural liposome model, encapsulated, and surface elements  
Taken from Liu & Boyd (2013, p.392)

Liposomes physicochemical characteristics such as size, size distribution, and zeta potential are crucial for general delivery applications. Inside the human body, for example, large liposomes >2000 nm are rapidly filtered in liver and spleen, whereas vesicles with size from 100 to 200 nm escape to this filtration and accumulate in tumors. Particles < 5 nm are filtrated by kidneys (Blanco, Shen, & Ferrari, 2015; Hak Soo et al., 2007). The size, shape, and surface properties also play a crucial role in nanoparticle accumulation, as shown in Figure 0.5. Moreover, liposomes monodispersity is a determinant quality factor, defining if all the prepared particles will finish at the desired place. LNPs ranging between 150 to 200 nm are necessary because they accumulate in tumors due to the enhanced retention and permeability effect (EPR). This effect establishes that particles of specific sizes accumulate selectively in solid tumors. Particles pass through the large fenestrations in the endothelial cells caused by abnormal angiogenesis (Matsumura & Maeda, 1986). Current commercially available lipid-

based nanoparticles are in the size range between 45 and 180 nm (Sedighi et al., 2019). On the other hand, zeta potential determines how particles interact with the human body by controlling circulation time or particle entrapment by cells (P. L. Felgner et al., 1987; Khadke, Roces, Cameron, Devitt, & Perrie, 2019). Thus, controlling liposome physicochemical properties is crucial for delivering the right substance to the right place.

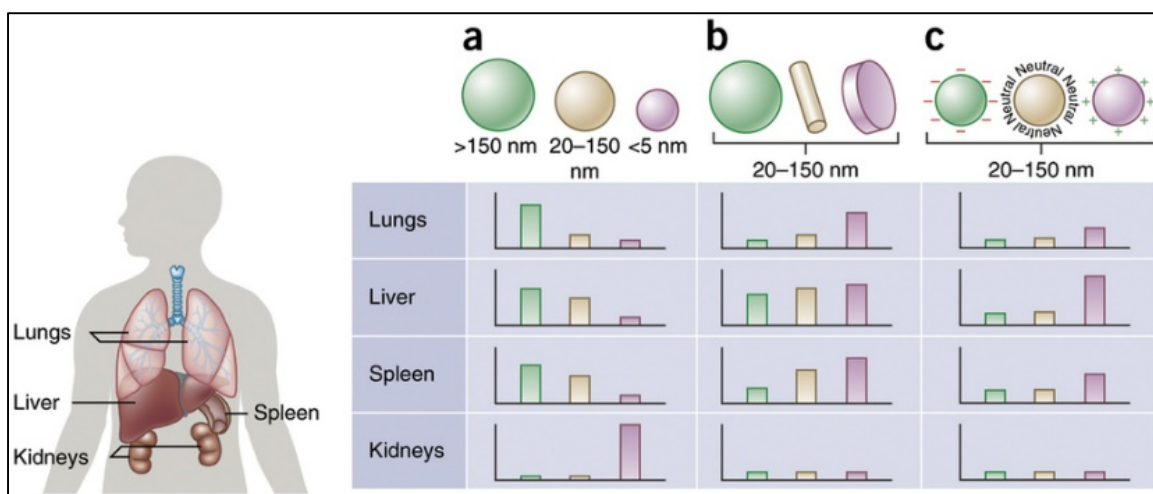


Figure 0.5 Nanoparticle accumulation  
Taken from Blanco et al. (2015, p.947)

The control of liposome characteristics requires systematic exploration of the factors influencing liposome properties in each new proposed micromixer. The relationship between these variables is complex. Statistical modeling can shine a light on this subject. For micromixers based on molecular diffusion and chaotic advection, this modeling has proved useful in identifying and controlling liposomes size, size distribution as well as transfection efficiency in gene delivery applications (Tiago A. Balbino et al., 2013; Kastner et al., 2014). However, for Dean flow dynamics-based micromixers, there are not reported results of such characterization.

Even though several liposome drug formulations have been approved, such as Doxil®, among others, production methods are still behind regarding industrial-scale purposes. The fragility of the production methods was proved in November 2011, when Doxil® production was

suspended due to manufacturing and quality problems. Patients were not able to access their vital medicine worldwide. In February 2013, the Food and Drug Administration (FDA) needed to approve a similar drug version called Lipodox to solve the shortage problem (Barenholz, 2012) partially. Production problems represent a latent risk that faces liposomal formulations if no action is taken to research better manufacturing approaches. At an industrial level, there are two significant problems: reproducibility and scalability.

First, the lack of reproducibility of commonly used batch methods makes new formulations challenging to manufacture at industrial-scale, while production methods require multiple steps that might further degrade nanoparticles quality (Stavis, Fagan, Stopa, & Liddle, 2018). The reproducibility is crucial for maintaining high-quality standards; it is decisive to meet the requirements of the regulatory agencies, such as the FDA or the European Medicines Agency (EMA) (Hafner, Lovrić, Lakoš, & Pepić, 2014).

Second, the scalability of the production methods is pivotal to ensure a reliable medication supply to patients. Current commercial production methods mostly rely on conventional laboratory-scale techniques such as thin-film hydration or ethanol injection assisted by sonication and membrane extrusion that require additional steps for cargo loading (Hua et al., 2018).

Microfluidics devices, specifically micromixers, are capable of producing size-controlled LNPs in continuous-flow. Liposome cargo can be added in a single step. Moreover, these devices can be parallelized for an increased production rate while keeping the same control over liposome properties resulting in process intensification as well as reducing waste and cost (Shallan & Priest, 2019).

Liposomes produced using micromixers have typically highly monodispersed to low polydispersed populations. However, lipid concentration remains too small for scaling-up. Usually, the initial lipid concentration in a typical micromixer based on molecular diffusion is of the order of 5 to 80 mM and, after passing through the micromixer, is diluted even more



from 10 to 50 times to achieve a liposome size below 100 nm. If we compare this value with commercial formulations such as Doxil® that is in the order of 8 mM, it becomes clear why novel micromixer approaches are not yet substituting available methods for industrial-scale productions.

Interesting solutions to overcome the liposome final dilution problem have been proposed. One is the Staggered Herringbone Micromixer (SHM), which reduces the dilution of lipid concentration required for small liposomes (Belliveau et al., 2012). Another is the vertical flow focusing (VFF) (R. R. Hood & DeVoe, 2015), which increments the flow in the device by increasing height in microchannels. These two devices can yield tens to hundreds of mg/h of liposomes. However, these micromixers are challenging to produce because they include 3D features in the case of SHM or high aspect ratio channels, as in the VFF. New devices with simpler geometries that increase liposome production rate are needed. Dean flow dynamics-based micromixers are in general, easy-to-fabricate. There are a few that have been used for liposome production (Kimura et al., 2018; Jisun Lee et al., 2013; Valencia et al., 2010; Y. Wu, Li, Mao, & Lee, 2012).

An essential part of liposome production using the principle of nanoprecipitation is mixing an organic solvent into an aqueous solvent, which causes a polarity change. It has been shown that a fast mixing produces small and uniformly-sized liposomes (Andreas Jahn et al., 2010). Numerical modeling provides the tools to better understand the mixing process. Current used numerical models for studying mixing in liposome production not always include variables that depend on the ethanol concentration (Amrani & Tabrizian, 2018; Kimura et al., 2018). In binary mixtures, density, viscosity, and the mutual diffusion coefficient change as concentration changes. Only a few authors have used models that include viscosity and mutual diffusion coefficient dependent on concentration (Renee R. Hood, DeVoe, Atencia, Vreeland, & Omiatek, 2014; Andreas Jahn et al., 2010). However, none has added density to numerical model calculations as far as the author knows it.

Finally, the solvent remains in liposome production using micromixers are inherent to the process itself. Lipids must be diluted first in an organic solvent, to later be mixed with an aqueous solvent to produce liposomes. Harmful leftovers can interact with the liposome cargo reducing their stability, capabilities, or in the worst-case scenario, they can damage the biological systems that they interact with. An inline filtration or the substitution of organic solvent with some other similar substances could improve the usability of produced liposomes. A better understanding of how organic-aqueous solvent mixtures affect liposome size, size distribution and zeta potential would be useful for controlling such characteristics. Only a few studies have tried to describe this influence in micromixers for liposome production (Webb et al., 2019).

In summary, controlling liposome physicochemical characteristics is crucial for their functionality. Thus, modeling which factors influence these properties is the first step towards liposome functionalization. Additionally, reliable liposome production methods that can be easily scalable from laboratories to commercial manufacture are required to ensure the supply chain to patients worldwide. Micromixers offer a solution; however, current devices are cumbersome to fabricate. Dean flow dynamic-based micromixers have the potential to produce controllable-size liposomes, with easy-to-fabricate devices. Finally, conventional organic solvents could be removed or replaced by substances capable of improving liposome therapeutic properties.

### **0.3 Research objectives**

The general objective of this research work is to investigate liposome production in Dean Flow dynamics-based micromixers. The research objectives include the evaluation of the factors influencing liposome properties to produce liposomes in a controllable way, with a final concentration and size comparable to commercially available formulations.

### 0.3.1 Specific objectives

1. Production of LNPs with controlled physicochemical characteristics such as size, size distribution, and zeta potential.
2. Preparing liposomes in the range of 50 to 200 nm as commercially available formulations with homogenous size.
3. The removal or substitution of the potentially harmful solvent remains.
4. Achieving liposome production yields in the order of tens to hundreds of mg/mL.

### 0.4 Research approach and main hypothesis

In this work, numerical modeling was used to investigate the mixing of two fluids in microfluidic devices. The **central hypothesis of this dissertation** is that a fast and uniform mixing or, in other words, changes in polarity, will result in smaller liposomes with homogeneous size populations. This hypothesis was further developed first by identifying which factors control liposome physicochemical characteristics. Later, flow-related factors were statistically modeled. Then, through confocal images and liposome characterization, the relationship between mixing and LNPs properties was further investigated.

Additionally, other molecular factors influencing liposome properties were considered, such as temperature, lipid type, and initial lipid concentration. Finally, by using different organic solvents, we extended the mixing hypothesis to investigate how by modulating the polarity change rate, average liposome size can be controlled too. All previously mentioned studies were focused on Dean flow dynamics-based micromixers.

## 0.5 Main contributions

The main contributions of this dissertation are the following:

1. **A method to fabricate micromixing channels with optical windows** using biocompatible materials and 3D printing. This fabrication method enables the production of microfluidic devices at low-cost with reduced steps compared with conventional soft lithography. At the same time, it allows optical access to the mixing channels to evaluate mixing performance. This method can be extended to produce different types of micromixers for applications, including liposome production, where materials need to be biocompatible. This contribution resulted in the following conference paper publication.

Lopez, R., Nerguizian, V., & Stiharu, I. (2018, 24-27 June 2018). *Low-Cost 3D-Printed PLA-COC Micro Hydrodynamic Focused Device*. Paper presented at the 2018 16th IEEE International New Circuits and Systems Conference (NEWCAS). (Presented and published)

2. **The identification of the most important factors controlling liposome characteristics in Dean flow dynamics-based micromixers.** A Plackett-Burman experimental design was used to evaluate in a reduced number of experimental runs what factors contributed to each of the liposome properties studied in this work (liposome size, size distribution, and zeta potential). This contribution resulted in the following conference poster presentation.

López Salazar, R. R., Ocampo, I., Bergeron, K.-F., Alazzam, A., Mounier, C., Stiharu, I., & Nerguizian, V. (2019). *Assessment of the Factors Influencing Liposome Size in Dean Forces Based  $\mu$ mixers*. Paper presented at the  $\mu$ TAS 2019 The 23rd International Conference on Miniaturized Systems for Chemistry and Life Sciences Basel, Switzerland. (Presented as poster).

3. **The design and fabrication of a micromixer based on Dean flow dynamics, capable of producing LNPs. The periodic disturbance mixer (PDM).** This micromixer uses semicircular structures to guide the flow inside the microchannels to a circular path that

produces centripetal forces. These forces change their vector direction and speed periodically. These two changes combined contribute to an improved mixing process. Later, we demonstrated the performance and utility of this new micromixer. The conception and design of this mixer were aided by numerical modeling and previous works in the field.

4. **A validated numerical model of binary mixtures mixing** with viscosity, density, and mutual diffusion coefficient in function of the organic solvent concentration. This model couples Navier-Stokes equations with convection-diffusion equations. The model was used to investigate the relationship between mixing efficiency with liposome properties. This model is useful in studying and evaluate mixing performances in different types of micromixers.
5. **The creation of a statistical model using design of experiments (DoE) and response surface methodology (RSM) for optimizing the factors that control liposome size and size distribution.** Once the factors that control liposome properties were identified, the evaluation of what levels resulted in which responses was required. The presented model was used for further contributions to locate an experimental region where nanosized liposomes were produced with a low polydispersity index. The same methodology can be used to create new models if liposome production conditions change (new lipids, concentrations, or microfluidic devices).
6. **The evaluation of the mixing efficiency and organic solvent concentration profile influence over liposomes properties in a PDM device.** Liposome production in micromixers depends on the polarity change rate caused by the mixing of the organic and aqueous solvent. This change rate controls liposome size and size distribution; it is unique for each micromixer type. We found out through numerical simulations and experiments this relationship for the PDM. This contribution, as well as previously mentioned 3,4,5, resulted in the following journal publication.

López, R. R., Ocampo, I., Sánchez, L.-M., Alazzam, A., Bergeron, K.-F., Camacho-León, S., Mounier, C., Stiharu, I., & Nerguizian, V. (2020). Surface Response Based Modeling of Liposome Characteristics in a Periodic Disturbance Mixer. *Micromachines*, 11(3), 235. (Published)

7. **The parametric evaluation of both flow and molecular related factors influencing liposome production in a PDM device.** Through numerical simulations, confocal imaging, and parametric experimentation, we evaluated other factors previously identified in the screening experiments such as concentration, temperature, and primary lipid type and their influence over liposome properties. With this extended set of experiments, the formulation of liposomes under various production conditions can be simplified.
8. **The demonstration of the fatty acid chain length role in liposome properties and its independence of the liposome zeta potential.** To investigate the effect of the fatty acid chain length in liposome properties, we substituted the primary lipid in our liposome forming mixture with a one with a longer fatty acid chain. This lipid has the same head terminal group. We found out that as a result of this change, liposomes size increased, and the size distribution was modified. Also, we found out that the zeta potential of liposomes was the same as the shorter acid chain length lipid. This result indicates that liposome zeta potential is only influenced by the lipid terminal head groups. This contribution resulted in the following conference paper.

López, R. R., G. Font de Rubinat, P., Sánchez, L.-M., Alazzam, A., Stiharu, I., & Nerguizian, V. (2020). *Lipid Fatty Acid Chain Influence over Liposome Physicochemical Characteristics Produced in a Periodically Disturbed Micromixer*. Paper presented at the IEEE Nano 2020, Montreal. (Accepted and to be presented as oral presentation).

9. **A model that related initial lipid concentration to liposome size.** An analytical model explaining the relationship between concentration and liposome size was presented. This model allows evaluating if intermediate-disk shaped lipid structures are disrupted while liposomes are in the process of being formed. This contribution and contributions 7 and 8 derived in the following submitted journal paper.

López, R. R., Ocampo, I., G. Font de Rubinat, P., Sánchez, L.-M., Alazzam, A., Tsering, T., Bergeron, K.-F., Camacho-León, S., Burnier, J. V., Mounier, C., Stiharu, I., & Nerguizian, V. (2020). *Parametric Study of the Factors Influencing Liposome Physicochemical Characteristics in a Periodic Disturbance Mixer*. Manuscript submitted.

10. **The replacement of conventional organic solvents with Transcutol® for liposome nanoparticle production in microfluidic devices.** The use of organic solvents for liposome production using micromixers requires to dilute the lipids as a part of the nanoprecipitation process. However, most of the conventional organic solvents are toxic at a certain level. Therefore, additional steps are required to filter these residues. By contrast, Transcutol® HP has a history of safe use in applications such as food, care products, and drug solubilizer in topical, transdermal oral and injectable human products. We demonstrated for the first time using micromixers that liposomes can be produced using Transcutol® as organic solvent. This solvent has reduced toxicity and enhanced transdermal drug delivery, saving filtration steps this contribution derived in the following conference poster presentation.

López, R. R., G. Font de Rubinat, P., Sánchez, L.-M., Ocampo, I., Alazzam, A., Bergeron, K.-F., Mounier, C., Stiharu, I., & Nerguizian, V. (2020). *Transcutol®: A promising drug solubilizer suitable for in continuous flow liposome production in a Periodic Disturbance  $\mu$ mixer*. Paper presented at the 7th FIP Pharmaceutical Sciences World Congress (PSWC2020), Montreal, Canada. (Accepted and to be presented as poster)

11. **The demonstration of the polarity change rate influence over liposome properties.** In micromixers, the liposome formation process is controlled by the polarity change rate caused by the mix of the order of milliseconds of the organic and the aqueous solvent. Another way of controlling this process is by selecting specific organic solvents. We investigated the influence of the organic solvents over liposome properties. We found out that the polarity gradient plays a crucial role in controlling liposome size. Moreover, we found out that this variable does not influence liposome zeta potential. We further investigate Transcutol® as a replacement for ethanol. It was demonstrated that

Transcutol® produced smaller liposomes over different concentrations and temperature conditions. This contribution and contribution 10 derived in the following journal paper.

López, R. R., G. Font de Rubinat, P., Sánchez, L.-M., Alazzam, A., Bergeron, K.-F., Mounier, C., Stiharu, I., & Nerguizian, V. (2020). *The Effect of Different Organic Solvents in Liposome Properties Produced in a Periodic Disturbance Mixer: Transcutol®, a potential organic solvent replacement*. Manuscript submitted

12. **The characterization of physicochemical properties of extracellular vesicles (EVs) derived from Uveal Melanoma cancer cells.** Liposomes and EVs share common characteristics such as lipidic membranes and the capacity to encapsulate biomolecules. As liposomes, EVs physicochemical characteristics play a key role in their interactions inside the human body. Additionally, EVs are studied as biomarkers and their potential link to cancer dissemination. Using the same methods to investigate liposome properties, we characterized EVs derived from healthy and UM cell lines. We found a difference in physicochemical properties between EVs derived from metastatic, primary, and non-cancerous cells. This characterization is the first step towards the use of EVs-like liposomes to investigate cancer dissemination and cell to cell communication. This work resulted in the following conference poster presentation.

López, R. R., Tsering, T., Bustamante, P., G. Font de Rubinat, P., Stiharu, I., Burnier, J. V., & Nerguizian, V. (2020). *Unraveling uveal melanoma-derived extracellular vesicles: a physicochemical characterization*. Paper presented at the Association for Research in Vision and Ophthalmology (ARVO 2020), Baltimore, USA. (Accepted and to be presented as poster).

## 0.6 Thesis organization

**Chapter 1** reviews literature, including an introduction to liposomes, their classification, and applications. Next, a detailed literature review of the micromixers used to produce these vesicles is presented divided by mixing principles.



**Chapter 2** deepens the theory of liposomes formation in micromixers using the nanoprecipitation method as well as mixing theory. This chapter also includes a general description of the methods and materials used in this work.

**Chapter 3** is divided into two parts. In the first one, it identifies the most important variables controlling liposome physicochemical characteristics in a PDM. In the second one, the most statistically significant variables are used to create an experimental design to produce a statistical model capable of predicting liposome size. This model is compared with experimental results. Finally, numerical simulations are introduced to understand better the role of mixing in liposome properties.

**Chapter 4** evaluates the relationship between mixing conditions and liposome physicochemical characteristics. In this chapter, we assess the PDM performance in liposomes production through confocal image microscopy, simulations, and experiments. We also add three additional variables related to molecular factors: temperature, concentration, and lipid fatty acid chain length. Finally, a model relating initial lipid concentration and liposome size is presented.

**Chapter 5** explores a way of modulating liposome size by using different organic solvents. We introduce a hypothesis of how polarity change rate control liposome size. Finally, in this chapter, it is proposed the substitution of the organic solvent ethanol, by Transcutol for the first time in liposome production using micromixers. This solvent has potential applications in transdermal drug delivery systems.

**Chapter 6** describes future work focused on translating this platform to applications in the medical field. The chapter includes innovative ways of producing devices at low-cost, geometry optimization for enhanced yield, pumpless liposome production approaches, EVs characterization, and gene delivery optimization.

**Appendix I** summarizes the works published during the Ph.D. studies. These publications include journal papers, conference presentations and popular science.

## CHAPTER 1

### LITERATURE REVIEW

#### 1.1 Introduction

Since the first description of phospholipid systems (Bangham, Standish et Watkins, 1965), liposomes have been used for a variety of applications, some of the most used are related to drug delivery systems (Allen & Cullis, 2013), medical imaging (Arrieta et al., 2014), and gene delivery (Buck, Grossen, Cullis, Huwyler, & Witzigmann, 2019). After more than 50 years of research, these vesicles have shown several advantages, such as their biodegradable and biocompatible components that allow them to safely interact with the human body as well as their capacity of encapsulating several formulations (Gregoriadis, 1973).

#### 1.2 Liposomes

In general, liposomes can be described as sphere-shaped vesicles structured in one or more lipid bilayers. Liposomes are formed by amphiphilic molecules called lipids, composed of a hydrophilic head and two hydrophobic tails. These amphiphilic molecules are insoluble in water except when they are assembled in lipid bilayers with polar heads of the outer layer pointing outwards and the polar heads of the inner layer pointing inwards. This configuration leaves space inside the inner bilayer for hydrophilic formulations and between the bilayers for hydrophobic formulations (Pattni et al., 2015). Figure 1.1a shows the general chemical structure of phospholipids. Figure 1.1b shows the size of a typical lipid bilayer and Figure 1.1c a liposome representation (van Swaay & deMello, 2013).

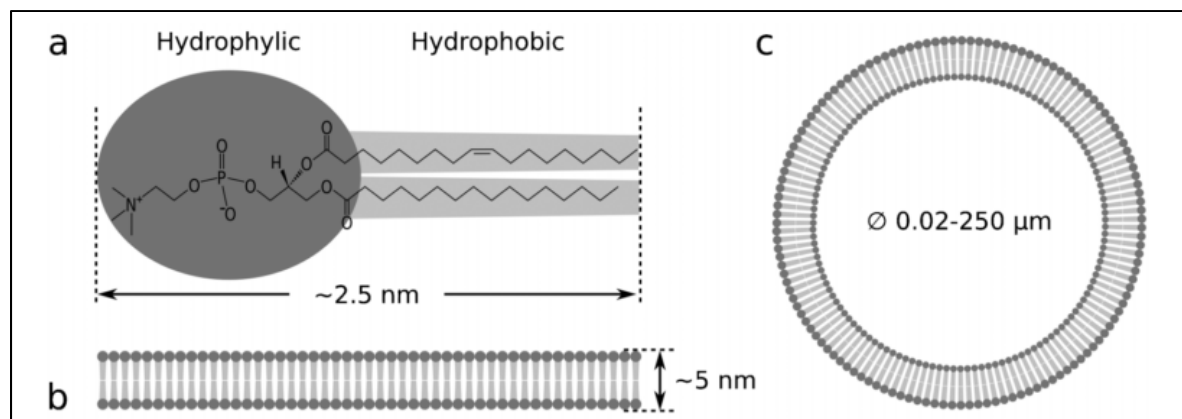


Figure 1.1 a Structure of POPC lipid molecule b Lipid bilayer thickness  
c Lipid vesicle

Taken from Van Swaay & deMello (2013, p.753)

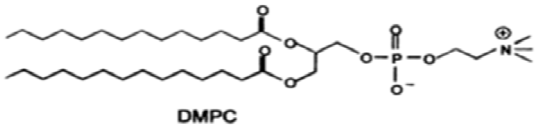
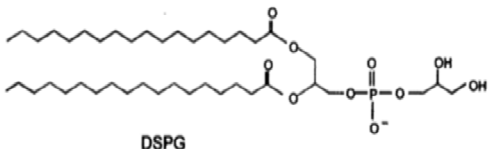
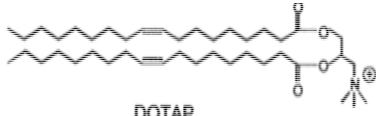
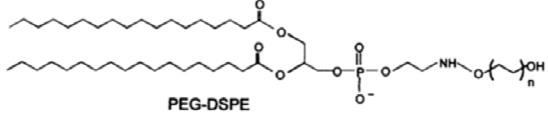
The lipids are commonly formed by two hydrocarbon chains esterified to a glycerol backbone or constituted from a ceramide. The hydrophobic part is connected to a polar head that might contain phosphate (“phospholipids”) or carbohydrate units (“glycolipids”).

There are head groups of the amphiphilic molecules that define the surface properties of liposomes formed from them. For instance, the phosphatidylcholine (PC) produces zwitterionic liposomes (Ulrich, 2002).

On the other hand, positively charged lipids such as Dioleoyl-3-trimethylammonium propane (DOTAP) are used to create lipoplexes (Tiago Albertini Albino, Azzoni, & de la Torre, 2013). These liposomes are capable of condensing DNA due to electrostatic interactions and interact with biological membranes. They are used to transfect cells.

Another example is the PEGylated liposomes, also known as stealth liposomes. The Polyethylene Glycol (PEG) in the head groups of the lipids masks them against opsonization and further destruction by the Mononuclear Phagocyte System (MPS). In this way, liposomes have longer circulation times inside the human body (Allen & Cullis, 2013). Table 1.1 shows examples of lipid head-groups and the chemical graphical representation of those examples.

Table 1.1 Headgroups classification with examples  
Adapted from Ulrich (2002, p.131)

Type of headgroup	Examples	Graphical Example
Zwitterionic	Phosphatidylcholine (PC), phosphatidylethanolamine (PE), sphingomyelin (SM)	 <p>DMPC</p>
Negatively Charged (Therapeutics)	Phosphatidic Acid (PA), phosphatidylglycerol (PG), phosphatidylserine (PS), phosphatidylinositol (PI), cardiolipin.	 <p>DSPG</p>
Positive charged (Transfection)	DOTAP, DOTMA, DODAC	 <p>DOTAP</p>
PEGylated (Stealth liposomes)	PEG-DSPE	 <p>PEG-DSPE</p>

### 1.2.1 Classification of liposomes

Liposomes can contain multiple bilayers; they are called multilamellar vesicles (MLV) or one single bilayer called unilamellar vesicles. Similarly, classification regarding size is accepted, such as large unilamellar vesicles (LUV), small unilamellar vesicles (SUV), and giant unilamellar vesicles (GUV) (van Swaay & deMello, 2013). Additionally, liposomes classification can also follow function or composition. Table 1.2 shows the common liposomes classifications.

Table 1.2 Liposome classification  
Adapted from Pattni et al. (2015, p.10940)

Based on lamellarity or size	Based on composition
Multilamellar vesicles (MLV) >500 nm	Conventional liposomes
Oligolamellar vesicles (OLV) 100-1000nm	Long-circulating liposomes (e.g. PEGylated)
Giant unilamellar vesicles (GUV) >1000nm	Cationic Liposomes (e.g. used for transfection)
Large unilamellar vesicles (LUV) >100nm	Stimuli-sensitive
Small unilamellar vesicles (SUV) 20-100 nm	Immunoliposomes
Liposome nanoparticles (LNPs) 20-100 nm unilamellar	Imaging Liposomes

### 1.2.2 Liposomes applications

The capability of liposomes to encapsulate multiple cargos makes them versatile delivery systems.

Drug delivery systems are one of the most prolific fields for liposomes applications. Since the beginning of the field, liposomes were viewed as potential carrier candidates for drugs (Gregoriadis & Ryman, 1971). The first-ever approved nanodrug approved by the FDA was a liposomal formulation composed of cholesterol and a lipid called phosphatidylcholine. It encapsulates Doxorubicin®, a chemotherapy that interferes with the DNA function of rapidly dividing cells (Barenholz, 2012). As opposed to its free form, the liposomal formulation Doxil® showed to accumulate in tumors due to the EPR, reducing side effects (Gabizon et al., 1994). Later, PEGylated liposomes helped to improve circulation time (Safra et al., 2000). PEGylation helps to avoid opsonization and further elimination by Mononuclear Phagocyte System (MPS). By contrast, in some cases, where the disease is affecting precisely the MPS such as leishmaniasis, PEGylation is not necessary because MPS uptake is desirable (New, Chance, Thomas, & Peters, 1978). Currently, liposomes drug delivery applications extend beyond cancer, in antibiotics (Campardelli, Trucillo, & Reverchon, 2018), vaccines (Kanra et

al., 2004), and antiviral applications (Croci et al., 2016). New applications include particles that encapsulate two different drugs in one carrier, opening the door to custom therapies (Joshi et al., 2016; Ma, Kohli, & Smith, 2013). Several liposome-based medications have developed and approved by regulatory agencies. Table 1.3 shows liposome approved formulations.

Table 1.3 Approved liposome formulations  
Adapted from Leung et al. (2019, p.12)

Approval Year	Trade Name	Active Agent	Lipid Composition	Indication
1993	Epaxal (Discontinued)	Inactivated hepatitis A virus.	DOPC:DOPE (75:25 molar ratio)	Hepatitis A
1995	Doxil	Doxorubicin	HSPC:Cholesterol: PEG 2000-DSPE (56:39:5 molar ratio)	Ovarian, breast cancer, Kaposi's sarcoma
1995	Abelcet	Amphotericin B	DMPC:DMPG (7:3 molar ratio)	Invasive fungal infections.
1996	DaunoXome	Daunorubicin	DSPC:Cholesterol (2:1 molar ratio)	AIDS-related Kaposi's sarcoma
1996	Amphotec	Amphotericin B	Cholesteryl sulphate: Amphotericin B (1:1 molar ratio)	Several fungal infections
1997	Ambisome	Amphotericin B	HSPC:DSPG:Cholesterol:Amphotericin B (2:0.8:1:0.4)	Presumed fungal infections
1997	Inflexal V (recalled)	Inactivated hemagglutinine of influenza virus strains A and B	DOPC:DOPE (75:25 molar ratio)	Influenza
1999	Depocyt (discontinued)	Cytarabine/Ara-C	Cholesterol:Triolein: DOPC:DPPG (11:1:7:1 molar ratio)	Neoplastic meningitis

<b>Approval Year</b>	<b>Trade Name</b>	<b>Active Agent</b>	<b>Lipid Composition</b>	<b>Indication</b>
2000	Myocet	Doxorubicin	EPC-Cholesterol (55:45 molar ratio)	Combination therapy with cyclophosphamide in metastatic breast cancer
2000	Visudyne	Verteporfin	EPG:DMPC (3:5 molar ratio)	Choroidal neo-vascularization
2004	DepoDur (discontinued)	Morphine sulfate	Cholesterol:Triolein: DOPC:DPPG (11:1:7:1 molar ratio)	Pain management
2009	Mepact	Mifamurtide	DOPS:POPC (3:7 molar ratio)	High-grade, resectable, non-metastatic osteosarcoma
2011	Exparel	Bupivacaine	DEPC,DPPG,CHOL, and Tricaprylin	Pain management
2012	Marqibo	Vincristine	SM: Cholesterol (55:45 molar ratio)	Acute lymphoblastic leukemia
2015	Onivyde	Irrotecan	DSPC:MPEG-2000: DSPE (3:2:0.015 molar ratio)	Combination therapy with fluorouracil and leucovorin in metastatic adenocarcinoma of the pancreas
2017	Vyxeos	Daunorubicin/Cytarabine	DSPC: DSPG:CHOL (7:2:1 molar ratio)	Therapy related acute myeloid leukemia (t-AML) or AML with myelodysplasia-related changes (AML-MRC)
2018	Onpattro	Patisiran	Dlin-MC3-DMA-PEG200-C-DMG	Hereditary transthyretin-mediated amyloidosis.



On the other hand, liposomes can deliver genetic materials inside the cells. Liposomes offer protection against DNase, RNase digestion, as well as improved gene “infectivity” of at least 100 times compared with naked DNA (Fraley, 1980). These liposomes usually include cationic lipids such as DOTAP that allow them to have a positively charged surface (J. H. Felgner et al., 1994; P. L. Felgner et al., 1987). It also helps them to interact with negatively charged cell membranes. Electrostatic interactions allow the genetic material to attach to liposomes and facilitate the intake by cells (Tiago Albertini Albino et al., 2013). The combination of the genetic material and liposomes is called lipoplex. Liposomes also encapsulate small interfering ribonucleic acid (siRNA) (Belliveau et al., 2012) for therapeutic purposes. Recently, Onpattro® a gene delivery liposomal formulation was approved. This therapy encapsulates siRNA that partially silences the production of a protein that otherwise accumulates, causing peripheral neuropathy. As far as the author understands, this is the only approved therapeutic in its class (Hoy, 2018).

Considering the ability of liposomes to reach specific sites by passive and active targeting, they are suitable for delivering labeling substances. The accumulation of these substances improves the signal intensity required to image particular organs or tissues (Pattni et al., 2015).

By using liposomes, even some typically difficult to access spaces such as retina can be attainable by controlling liposomes size and surface characteristics. This approach is used for imaging purposes as well as for drug delivery applications, as shown in Figure 1.2. Liposomes with different surface properties were loaded with Dil red dye to investigate their penetration into the retina (Junsung Lee et al., 2017).

Complex imaging liposomes incorporate moieties for long circulation time, active targeting, and radiolabeling. The PEGylated liposomes include in the membranes a polychelating amphiphilic polymer heavily loaded with gadolinium as well as a specific antibody for active targeting. These sophisticated liposomes allow the enhancement of magnetic resonance (MR) imaging (Erdogan, Medarova, Roby, Moore, & Torchilin, 2008).

Theragnostic includes in a single liposome, both imaging and therapeutic agents. One example of these combined therapies is the use of  $^{99m}\text{Tc}$  and liposomal DOX to treat pleural mesothelioma. An increased uptake measured by the radiolabel and enhanced efficacy of chemotherapy was observed (Arrieta et al., 2014).

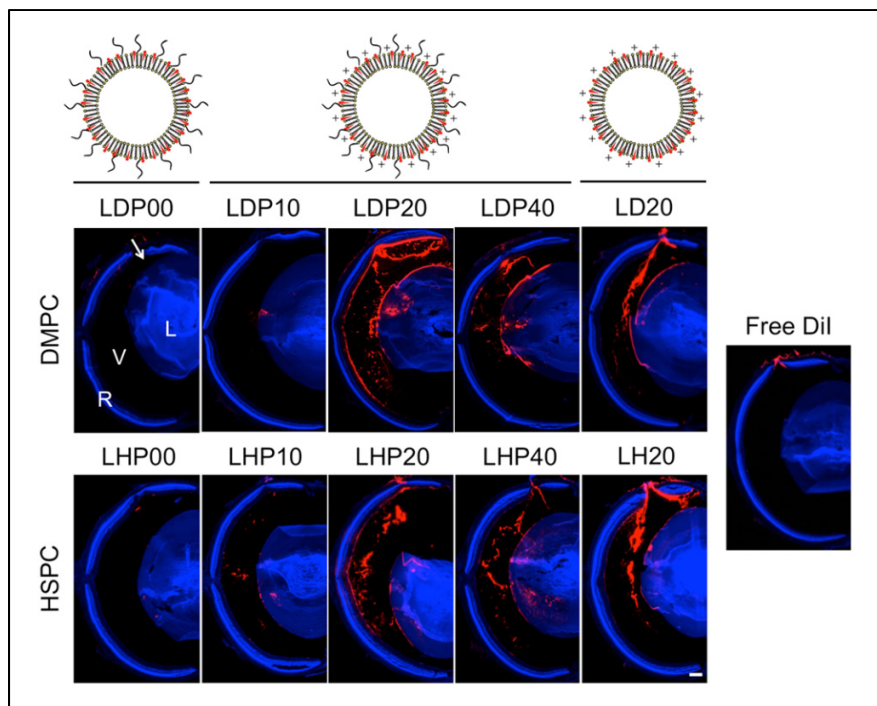


Figure 1.2 Liposomes loaded with Dil red dye in the retina space  
Taken from Junsung Lee et al. (2017, p. 425)

Finally, liposomes have applications in the field cosmeceutics, food industry, nutraceuticals, and synthetic biology. In cosmeceutics, liposomes have emerged as suitable carriers; their lipid components enable liposomes to function as transdermal delivery systems as well as improving skin hydration (Rahimpour & Hamishehkar, 2012). Moreover, hydrophilic and hydrophobic antioxidants (AO) encapsulated into liposomes penetrate deep into the skin as well as enhancing AO stability (Van Tran et al., 2019). Alternatively, liposomes can carry nutritive value ingredients such as vitamins, antioxidants, among others. These components might change food flavor when they are introduced into the food in their free form. However, with liposome encapsulation, these taste distortions can be prevented (Khorasani, Danaei, &

Mozafari, 2018), facilitating food fortification. Liposomes membranes and cell membranes are quite similar; for that reason, liposomes are also used to produce synthetic cells (Stano, 2018).

In brief, liposome applications are growing every day. The availability of suitable production means is crucial to keeping the momentum of this field.

### **1.3 Liposomes production methods**

There are several liposome preparation techniques at the laboratory scale. For instance, the Bangham method begins with lipid dissolved in an organic solvent, then the mixture is dried and finally dispersed in aqueous media under agitation leading to liposome formation (Bangham, De Gier, & Greville, 1967). Most of the conventional methods use batch approaches, such as reverse-evaporation method (Szoka & Papahadjopoulos, 1978), electroformation (Angelova & Dimitrov, 1988), ethanol injection (Batzri & Korn, 1973), freeze-thaw (Costa, Xu, & Burgess, 2014), and cross-flow injection (Wagner, Vorauer-Uhl, Kreismayr, & Katinger, 2002). Generally, conventional methods lead to polydispersed vesicle populations that required further treatment for reducing the size and lamellarity by breaking them using mechanical methods, such as sonication, extrusion, handshaking, or freeze-thaw method.

On the other hand, in-line mixing methods revolve around the injection of a lipid diluted in ethanol into water stirred under a pressure of 10 lb/in<sup>2</sup> using N<sub>2</sub>. Liposomes are formed by convective-diffusive mixing (Batzri & Korn, 1973). Mixing could be improved by joining the aqueous media and lipids in ethanol streams into a special mixing compartment. Industrial-scale in-line static mixers are available for multiple applications (Thakur, Vial, Nigam, Nauman, & Djelveh, 2003), and some of them are used for liposome preparation (Baker & Heriot, 2005).

More recently, novel liposome preparation methods focus on solving problems related to conventional approaches. For example, avoiding organic solvent remains as in the supercritical

fluids method (Castor, 1996; Magnan, Badens, Commenges, & Charbit, 2000; Otake, Imura, Sakai, & Abe, 2001), improving encapsulation efficiency as in the freeze-thaw method (Costa et al., 2014) and homogenization of liposome preparation conditions as in dual asymmetric centrifugation (Massing, Cicko, & Zirolì, 2008). Some other approaches use active external energy forces to homogenize size as in adaptative focused acoustics (AFA) (Shen, Kakumanu, Beckett, & Laugharn Jr, 2015).

On the other hand, microfluidic devices are used to produce liposomes. These bottom-up based production methods such as the pulse jet flow method (Funakoshi, Suzuki, & Takeuchi, 2007) focus on improving the control over liposome size, one liposome at the time production or multiple at the time as in the membrane contactor method (Jaafar-Maalej, Charcosset, & Fessi, 2011). Finally, micromixers offer not only precise control over liposome size, but also reproducibility and scalability by parallelization means (Andreas Jahn, Vreeland, Gaitan, & Locascio, 2004).

Remarkably, micromixers have proven to be suitable for controlling the bottom-up process of liposome synthesis in a continuous-flow way improving reproducibility with precise control over liposome size and size distribution. Moreover, these devices can easily be parallelized to increase the production rate even more. Of all the universe of micromixers, only a few have been studied for liposome manufacturing.

#### **1.4 Liposome production using micromixers**

Micromixers offer an alternative to improve control over liposomes production variables such as size and size distribution. Typically, an organic solvent, where the lipids are initially diluted in, is mixed with an aqueous solvent. The rapid replacement of the organic solvent by the aqueous solvent (polar) produces an increase in the medium polarity, causing liposomes to self-assemble (Andreas Jahn, Lucas, Wepf, & Dittrich, 2013). This process is similar to the ethanol injection method; however, the mixing process is better controlled. Typically, microfluidic devices operate under laminar flow conditions enabling stable fluid interfaces.

Micromixers use microchannels with width sizes ranging from 10 to 500 $\mu\text{m}$ . At this scale, viscous forces are dominant over inertial forces, and laminar flow is common, leading to uniform mixing conditions and mixing time in the order of milliseconds (Nguyen & Wu, 2005). The main transport phenomena in micromixers are molecular diffusion (B. Knight, Vishwanath, Brody, & Austin, 1998), chaotic-advection (M. G. Lee, Choi, & Park, 2009; Stroock et al., 2002; Thiermann et al., 2012), and Taylor dispersion (Nguyen, 2012a). The last two principles can be combined in micromixers that produce folding and lamination.

Micromixers are classified as active and passive. Active mixers regularly rely on forces other than fluid pumping for perturbing the flow in the microchannels such as surface acoustic waves (SAW) (M. C. Jo & Guldiken, 2013). By contrast, passive micromixers rely only on the pumping energy and geometry to produce flow perturbations to enhance mixing. Usually, passive micromixers are relatively easy to fabricate because they do not require active elements as opposed to active micromixers (Lin & Basuray, 2011). Considering that liposome production tends to move towards simplicity, most of the micromixers used for liposome preparation have taken the passive approach pondering the relatively good results in liposomes size control and reproducibility.

#### **1.4.1 Molecular diffusion-based micromixers for liposome production**

Molecular diffusion is a physical phenomenon produced by Brownian motion. This phenomenon explains the net movement of particles from a high concentration to a low concentration region. The first micromixer used to produce liposomes in continuous-flow was the microfluidic hydrodynamic focusing mixer (MHF) (Andreas Jahn et al., 2004). This micromixer was based on pure molecular diffusion.

MHF provides laminar flows combined with relatively homogenous physical properties along with the mixing fluid interfaces, producing highly monodisperse liposome populations. A typical MHF device is a cross junction, with a continuous phase flowing from lateral inlets and

a dispersed phase flowing from the internal channel-focused by external flow (Carugo, Bottaro, Owen, Stride, & Nastruzzi, 2016). The dispersed flow is typically a lipid dissolved in an organic solvent, and the continuous phase is an aqueous solvent. The diffusion of the organic solvent in the aqueous solvent creates zones of low organic solvent concentration (or high polarity), forcing liposomes to self-assemble.

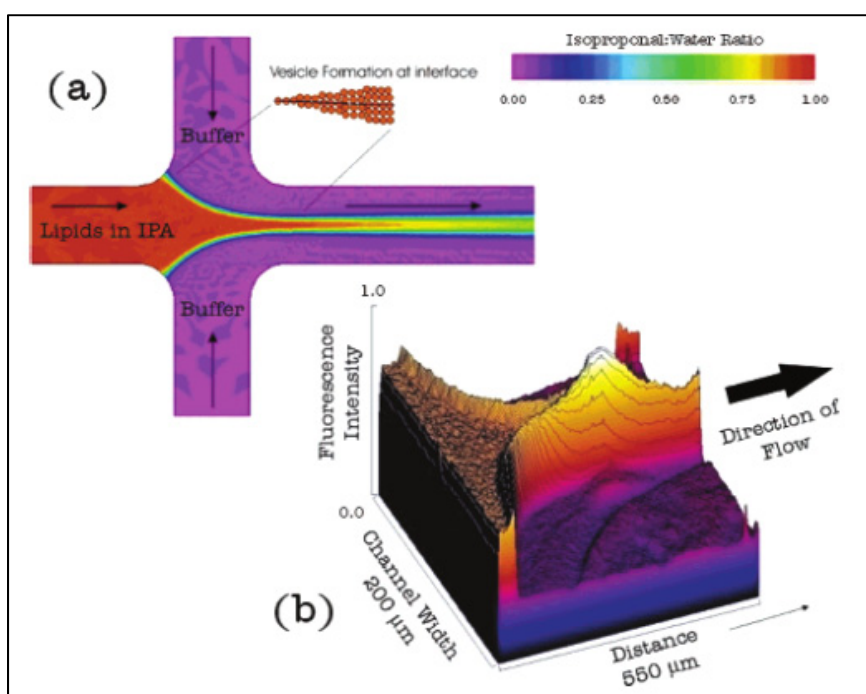


Figure 1.3 Flow focusing production method (a) Numerical model  
(b) DiIC<sub>18</sub> fluorescence intensity during liposome formation  
Taken from Jahn et al. (2004, p.2674)

One of the firsts vesicle formation studies using MHF introduced a fluorescent dye 1,1'-Diiodo-3,3',3',3'-Tetramethylindocarbocyanine Perchlorate (DiIC<sub>18</sub>) to study liposome formation. This dye increases its quantum efficiency when it is trapped inside a lipid membrane so that this dye can be used as a marker of liposome formation. In the study, Jahn *et al.* used this dye jointly with lipid in isopropyl alcohol (IPA) solution to mark liposomes self-assembly. Using MHF, the authors showed the location where the liposomes were formed, and they compared these results with a numerical model. The liposomes were formed in the areas where

IPA concentration is critically diluted (40 wt %), as is shown in Figure 1.3 (Andreas Jahn et al., 2004).

There is a relationship between the flow rate ratio (FRR) (aqueous/organic solvent) and the size of resulting liposomes (Andreas Jahn, Vreeland, DeVoe, Locascio, & Gaitan, 2007). Vesicles are smaller at higher ratios. For example, at a 30:1 ratio, liposomes had a diameter of 30 nm. When the FRR is 10:1, the size is approximately 70 nm (Carugo et al., 2016). The relation is non-linear, and it does not extend much above 70:1 ratio. By contrast, the relationship between lipid concentration in the initial solution and particle is non-proportional. Finally, the total flow rate (TFR), which is the sum of all the flows in the device, has shown little influence over particle size for this type of device. The control over FRR leads to relatively easy size tuning and monodispersed populations with less than 10% of standard deviation. Moreover, no additional steps are required for liposome homogenization. However, some organic solvent residues remain inside the vesicles, and extra purification steps are needed, such as dialysis (Andreas Jahn et al., 2010). Finally, the FRR required to achieve small liposomes is high, resulting in highly diluted liposomes.

Active approaches, together with MHF for liposome production, have been explored. Such as submerging the microfluidic device in a water bath, to later be subjected to sonication. This approach was able to reduce liposome size from 150 nm to 50 nm under constant flow conditions (Huang et al., 2010). Another method involved the use of SAW, where the power of the waves was related to a liposome size decrease. The lipoplexes created using this method yield liposomes with a size of 20 nm (Westerhausen et al., 2016).

One logical approach to increase mixing performance in the MHF using only molecular diffusion is increasing the focused area using three-dimensional microfluidic hydrodynamic focusing (3D- MHF). Typically, the synthesis of LNPs occurs in rectangular microchannels that are costly to produce because the fabrication process involves a soft lithography process which requires a clean room to prepare masks and molds. Instead, 3D-MHF is realized using a commercially available annular array of capillarity tubes, as shown in Figure 1.4. The central

stream is focused on all directions leading to an increased area of contact. This approach improved diffusion and increasing the size uniformity of liposomes. Liposomes produced under similar conditions in the 3D-MHF showed a reduced polydispersity index<sup>1</sup>(PDI) two times smaller compared with a traditional MHF device (0.044 vs. 0.083). As expected, a reduction in the size of the orifice led to smaller liposomes populations (Renee R. Hood et al., 2014). However, the resulting liposomes were highly diluted.

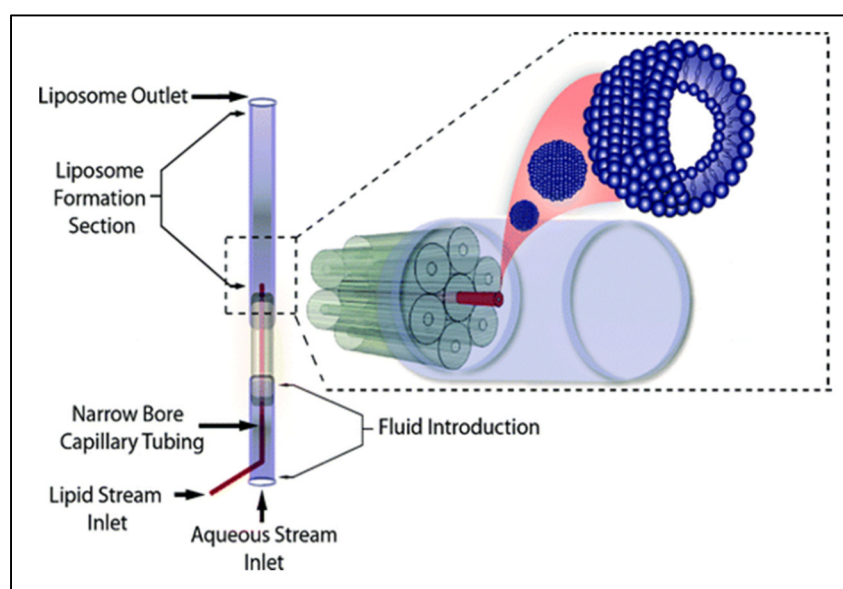


Figure 1.4 Schematic of 3D-MHF liposome formation device  
Taken from Hood et al. (2014, p. 2405)

Additionally, the coaxial turbulent Jet in Co-Flow method was introduced as a modification of the ethanol injection method. This method is similar to the 3D-MHF in its mixing strategy. By contrast, authors explored larger volume flows up to 50mL/min compared with 1.5 mL/ min for the 3D-MHF creating turbulent flow inside the channels. Channels were much larger compared with the 3D-MHF (63 to 255  $\mu\text{m}$  vs.  $\sim 500$  to 3000  $\mu\text{m}$ ). An interesting result was the relationship between the Reynolds number  $Re$  of the mixture and liposome size, showing

---

<sup>1</sup> Liposome average size homogeneity. A low PDI value means more homogenous liposome populations.



that monodispersed and small particles are highly related to increase Re numbers, and it is independent of flow velocity ratios (Costa, Xu, Khan, & Burgess, 2016).

In a separate study, the influence of the temperature in liposome size in MHF devices relating lipid bilayer membrane flexibility to variations in size was addressed. It was found that for most of the lipids, liposome size decreased with temperature (Zook & Vreeland, 2010). Afterward, this relationship appeared once again in a publication related to transfection (Wi, Oh, Chae, & Kim, 2012), where only two different temperatures were studied with similar results.

Liposome formulations that are already in the market, such as Doxil<sup>®</sup>, have a final concentration of around 8 mM (Carugo et al., 2016). Usually, MHF mixers start with a lipid concentration between 5 mM to 80 mM. This initial concentration is further diluted to achieve LNPs in the order of 10-40 times resulting in extremely low final lipid concentrations, thus low productivity.

The next research efforts were focused on overcoming the low final lipid concentration by considering a way to increase the diffusion area of the diluted phase as well as the liposomes production yield. The VFF approach addresses the problem by creating high aspect ratio channels (100:1). This strategy keeps the monodispersity and control over the size of LNPs. The diffusion contact area is increased even more than 3D-MHF. The increased flow capacity of the high-aspect-ratio channels improves the micromixer liposomes throughput. At the same time, this microfluidic device keeps the well-known characteristics of MHF micromixers, such as laminar flows, short diffusion scale, and uniform mixing conditions. The demonstrated production rate of VFF is as high as 95 mg/h, improving liposomes yield by almost three orders of magnitude compared with normal MHF. Unfortunately, at a liposome size of 70 nm, the device reaches an asymptotic behavior, where even by increasing FRR, the liposome size remains the same. This behavior prevents liposome size from decreasing more (R. R. Hood & DeVoe, 2015). Figure 1.5 contrasts the planar MHF and VFF.

Dimensional considerations, including the aspect-ratio, were later studied, supporting what was reported earlier by *Hood et al.* Liposome size increases with the aspect ratio of MHF devices (Michelon, Oliveira, de Figueiredo Furtado, Gaziola de la Torre, & Cunha, 2017). Also, an integrated method that included liposome production and active drug loading was presented (R. R. Hood, Vreeland, & DeVoe, 2014). Recently novel fabrication approaches such as stereolithography (SLA) 3D printing have been investigated together with high aspect ratio devices from 1 to 4 that are complicated to realize with standard soft lithography. The study resulted in devices capable of controlling liposome size easily as in a normal MHF, with the advantage that device fabrication is greatly simplified (Chen, Han, Shumate, Fedak, & DeVoe, 2019).

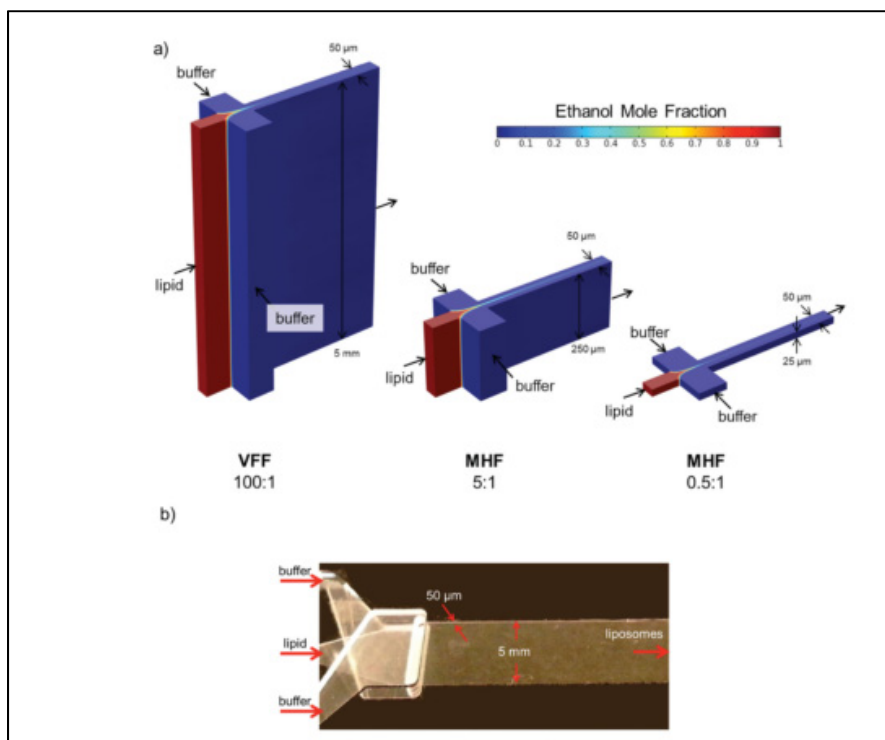


Figure 1.5 a) Numerical models comparing the ethanol concentration profiles for VFF and MHF devices  
 b) Photograph of multilayer VFF with an aspect ratio of 100:1  
 Taken from Hood & DeVoe (2015, p.5792)

The original MHF device was used for transfection and gene functionalization (Tiago A. Balbino et al., 2013; Tiago A. Balbino, Serafin, Radaic, de Jesus, & de la Torre, 2017), bacteriophages encapsulation (Cinquerrui, Mancuso, Vladislavljević, Bakker, & Malik, 2018), drug encapsulation (Amrani & Tabrizian, 2018; Zizzari et al., 2017) and even for functionalizing other liposomes (Jia et al., 2016).

In summary, MHF is a well-established device for liposome production. The uniformity of physical and chemical conditions along the channel enables these passive mixers to prepare highly monodisperse liposomes with controlled size by varying FRR. Moreover, flow laminarity plays a crucial role in liposome size control that requires more in-depth studies. Unfortunately, liposome production rate and lipid concentration for most of the devices remain below commercially available product standards limiting the translation of the technology from clinical to industrial scale. Additionally, solvent remains are not discussed or investigated in detail for their possible replacement or filtration. There are still opportunities and questions to solve. For example, recent studies using this micromixer found that the ionic strength of the aqueous solvent is directly related to liposomes size (Perli, Pessoa, Balbino, & de la Torre, 2019).

#### **1.4.2 Chaotic advection-based micromixers for liposome production**

Previously presented devices are designed to increase the diffusion surface area and reduce the diffusion path length. By contrast, chaotic advection micromixers add obstacles in the fluid main advection direction to produce flow patterns.(Capreto, Cheng, Hill, & Zhang, 2011) This type of micromixer is discussed in depth in the next paragraphs.

The staggered herringbone micromixer (SHM) and similar micromixers, use small asymmetric depression in the floor channels to create chaotic advection in a short length, increasing the diffuse mixing by “rotating the flow” (Stroock et al., 2002) as shown in Figure 1.6. Laminar streams of lipids in ethanol and aqueous buffers are injected in different inlets of SHM. Herringbone structures induce chaotic advection causing at a critical polarity point the

formation of LNPs (Zhigaltsev et al., 2012). A typical SHM is shown in Figure 1.7. The SHM enables more effective diffusional mixing and the ability to create “limit size” liposomes in the range of 20 nm, which means that they are the smallest possible particles considering molecular constraints. The device achieves a mixing time of 3 ms (Belliveau et al., 2012). The authors argue that a parallelize ensemble using 6 SHM micromixers with a TFR of 72 mL/min, can produce 580 mg/h of lipids compared to 95 mg/h for VFF (Belliveau et al., 2012).

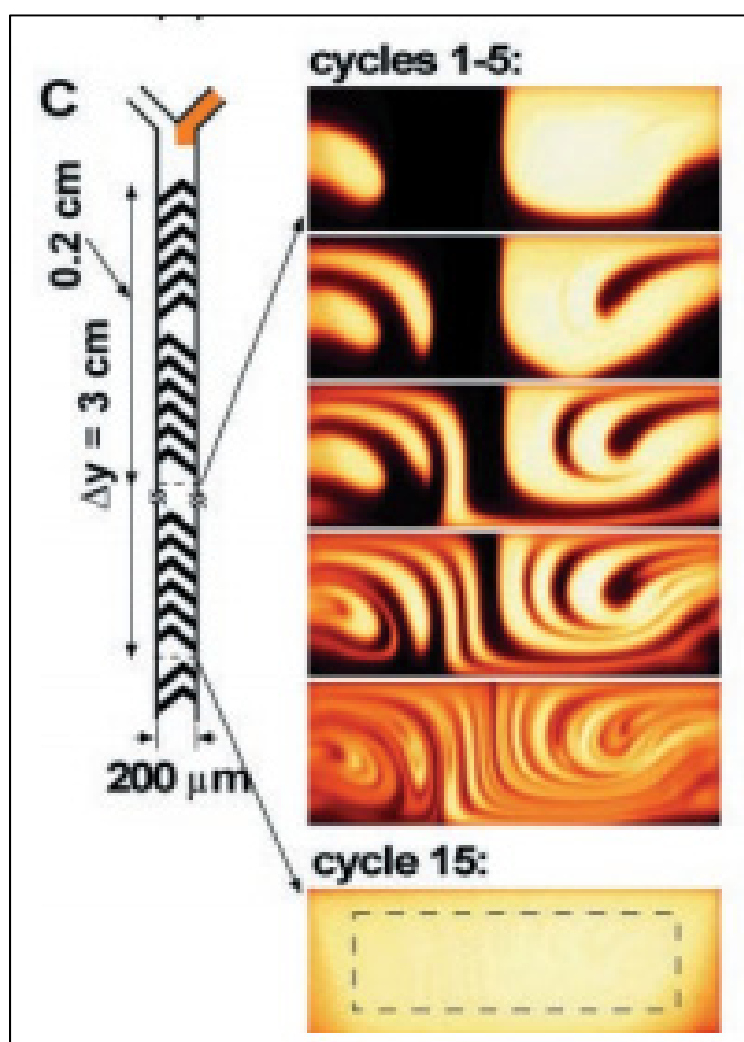


Figure 1.6 Mixing inside a SHM. The micrographs are a cross-section view at different distances from the beginning of the channel  
Taken from Stroock et al. (2002, p.649)

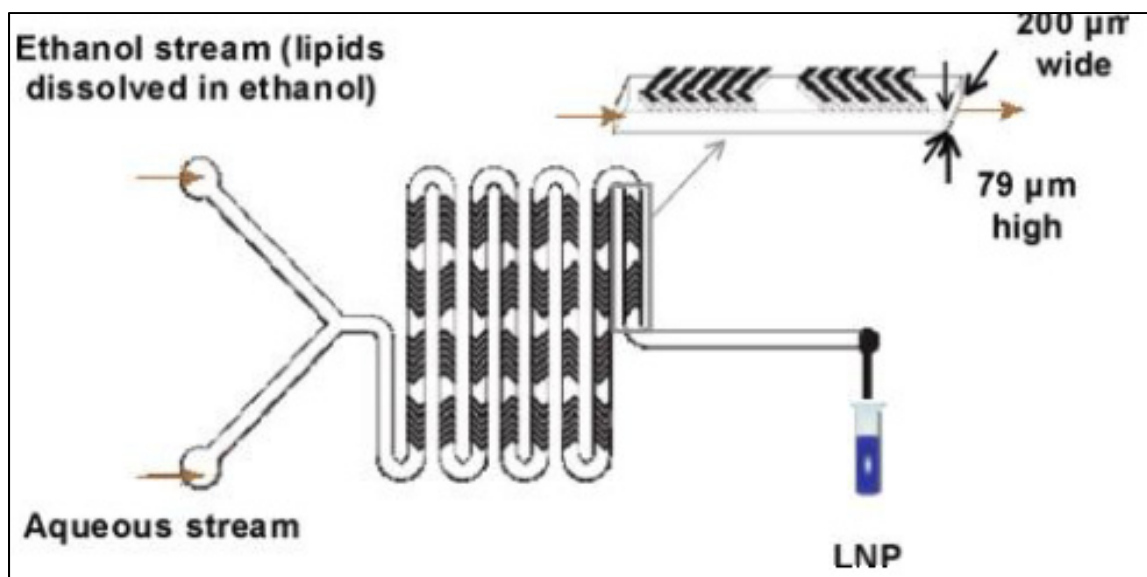


Figure 1.7 Herringbone structures induce chaotic advection of the laminar streams. Dimensions of the mixing channel are  $200\mu\text{m} \times 79\mu\text{m}$ , and herringbone structure is  $31\mu\text{m}$  high and  $50\mu\text{m}$  thick  
Taken from Zhigaltsev et al. (2012, p.3634)

After the introduction of a commercially available nanoparticle production system called the NanoAssemblr® by Precision Nanosystems, the publications using this system have increased dramatically (Hamano et al., 2019; Khadke et al., 2019). The liposome formation investigation in the SHM translated to more clinical and correlational studies of variables, except for a few works in the area (Maeki et al., 2017). For instance, transfection effectivity was optimized based on TFR and FRR using as a control a commercially available Lipofectamine® from ThermoFisher. The results showed that FRR is highly related to transfection effectivity as opposed to TFR, which controls only the device's productivity (Kastner et al., 2014). Later the same group investigated the encapsulation of poorly soluble drugs (propofol) by introducing them directly with lipids in the organic solvent. They compared the encapsulation efficiency among other parameters with the thin hydration method. The results showed an encapsulation efficiency above 50% for the microfluidic method and 20% for the conventional hydration method (Kastner, Verma, Lowry, & Perrie, 2015). More recently, the DoE was used to control and optimize liposome size (Sedighi et al., 2019) of therapeutic liposome formulations.

Furthermore, with the same microfluidic platform, the encapsulation of two drugs at the same time, in a single step process, was achieved (metformin and glipizide), one hydrophobic, and the other hydrophilic. In the same work, four different binary mixtures and four different lipids were tested to investigate their influence in liposome size. It was found that the smallest liposomes were produced with a binary mixture of methanol and phosphate buffer saline solution (PBS) using 1,2-distearoyl-sn-glycero-3-phosphocholine (DSPC) lipids (Joshi et al., 2016).

Recently, with the help of NanoAssemblr<sup>®</sup>, conventional analysis of SHM liposome characteristics was performed, confirming previous results about the relation of FRR, liposome size. TFR demonstrated to be an almost independent variable. The research group investigated the drug release profiles of different liposomes formulations and their relationship with lipid composition, size, and type of drug encapsulated (Guimarães Sá Correia, Briuglia, Niosi, & Lamprou, 2017). The approach can be applied to other kinds of micromixers.

On the other hand, the removal of the organic solvent and the non-incorporated drug remnants has been one of the challenges of liposome production using micromixers. Recently, using a SHM, online purification, and characterization were accomplished (Forbes et al., 2019). This filtration is done by connecting the device directly to a tangential flow filtration (TFF) device, leaving only 1% of the non-incorporated drug leftovers (Dimov, Kastner, Hussain, Perrie, & Szita, 2017). However, these approaches require additional steps or are not integrated into the same microfluidic chip.

More recently, a flow-focusing device with staggered herringbone structures was presented as chaotic advection-based microfluidic device (CA-MD), as shown in Figure 1.8. The CA-MD device influence over liposome properties was contrasted with an MHF-like device. This assessment was made to compare molecular diffusion with chaotic advection mixing approaches and their result in liposome properties. Cationic liposomes (CL), as well as stealth liposomes (SL) liposomes, were produced under the same conditions. The flow conditions used were a FRR = 10 and a variable TFR from 100 to 1500  $\mu\text{L}/\text{min}$ , for the CA-MD. Liposome

diameter showed multiple particle populations indicating agglomerations. This result is an indication of disorganized aggregation caused by chaotic advection. Consequently, PDI values were from 0.4 and up to 0.8 for both CLs and SLs as opposed to the MHF-like device, which showed monomodal liposome populations. The CA-MD showed better results when the FRR was reduced to 1 at different TFRs resulting in a PDI around 0.2. Due to the high ethanol content derived from this approach, a centrifugal vacuum concentrator was used to remove ethanol from the final liposome mix (Eş et al., 2020). These results show that the mixing approach selected has a crucial influence over liposome physicochemical properties.

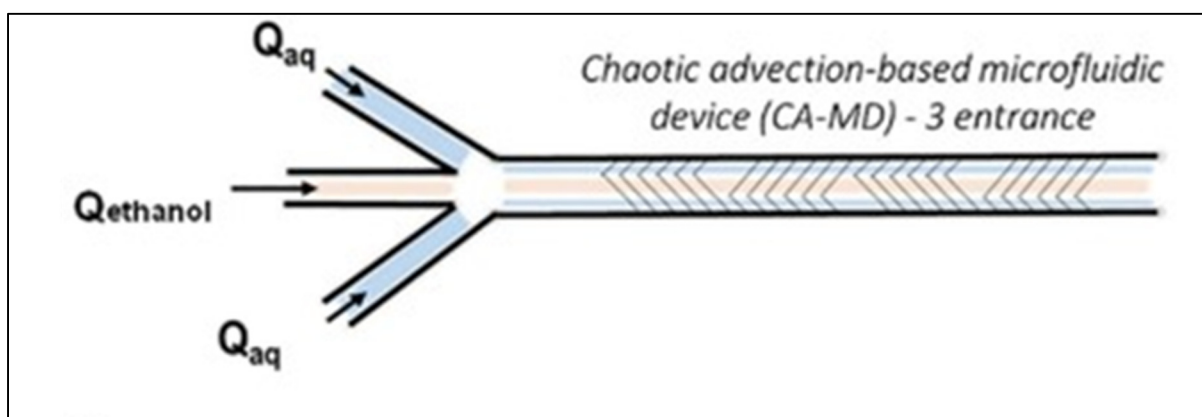


Figure 1.8 Chaotic advection-based microfluidic Device (CA-MD)  
Taken from Es et al. (2020, p.4)

In conclusion, SHM, compared with MHF, has an increased liposome production rate due to the smaller FRR required for LNPs synthesis, an increased flow rate, and the ability to produce limit size liposomes. Chaotic advection micromixers have shown promising results. Recent works have established a connection between mixing and liposome size in this type of micromixer. A fast mixing result in smaller liposomes, which self-assembly under specific organic solvent concentrations (Maeki et al., 2017). However, this approach not always results in monomodal liposome populations. Unfortunately, SHM devices also suffer from clogging (Kimura et al., 2018), and are laborious to produce because of their 3D features. Finally, more research is needed to find innovative mixing strategies that could lead to more effective and fast mixing with easy to fabricate devices.

### 1.4.3 Fluid lamination and folding

Lamination refers to the strategy of separating a single streamline into multiple zones to increase the diffusion area, enhancing the mixing process (Löb et al., 2004). On the other hand, these laminae can be folded and even make them collide with each other to further increase mixing performance. The use of circular paths creates centripetal forces that, under certain circumstances, can produce chaotic advection. Only a few of these types of micromixers have been explored in liposome production.

The Tesla valve is a geometry-based check valve, which allows the fluid to move in one direction only. This geometry also laminates and recombine the flow inside it. Using this geometry, lipid-based nanoparticles were synthesized. A mixture of poly lactic-co-glycolic acid (PLGA) and 1, 2-distearoyl-sn-glycero-3-phosphoethanolamine-poly (ethylene glycol) (DSPE- PEG) lipids were used to produce nanoparticles from 40 to 250 nm. The surface of the nanoparticles was modified with different functional groups such as COOH connected to the amphiphilic molecules to study its effects on zeta potential and liposomes size. These particles encapsulated quantum dots for imaging purposes (Valencia et al., 2010). Further exploration of temperature or geometry influence of this structure is not discussed.

To reduce organic solvent remains and improve the control over the size of theragnostic lipoplexes, a split and recombine device was investigated together with electrospraying. First, reagents were mixed as usual, but at the outlet, an electrospray nozzle broke the liquid in tiny droplets to rapidly evaporate the organic solvent. Liposomes were trapped using PBS (Y. Wu et al., 2012). However, the final concentration of produced liposomes is in the order of 1.5 mg/mL, with a size of 195 nm.

Furthermore, the semicircular contraction expansion array (CEA) based micromixers was implemented successfully to produce liposomes. The CEA structures induce Dean Vortices by splitting and redirecting the flow, creating multiple laminae. The results showed a 90% mixing



efficiency for channels with 30 semicircular structures producing liposomes with a mean size of 150 nm. The lipid concentration remained constant for the entire experiment (10 mM), so no discussion is provided about its influence over liposome size, or temperature (Jisun Lee et al., 2013).

Recently, liposome size modulation in steps of 10 nm has been demonstrated for a range from 20 to 100 nm using a baffle structure. This structure has a squared shape serpentine. Liposome size decreased as FRR and TFR were increased; however, after  $TFR = 30 \text{ mL/h}$  vortices start to appear according to presented numerical models at the same time, liposome size reduction starts plateauing. Liposomes produced using the invasive lipid nanoparticle production device (iLiNP) were used as gene carriers.

More recently, an active mixing device which uses SAW to acoustically excite bubbles and sharp edges create vortices that enhance mixing. The minimum size liposome produced was around 65 nm, with a maximum production rate of 2 mg/ mL, which is comparable to the first MHF device (Rasouli & Tabrizian, 2019).

Additionally, the analysis of the diffusion process using a pH indicator has been performed in structures with curvilinear paths to validate numerical models. These results were contrasted with MHF devices. Different FRR and TFR were evaluated. The authors concluded that adding curvilinear paths improve the mixing performance (Bottaro, Mosayyebi, Carugo, & Nastruzzi, 2017).

2D-dimensional mixer devices based on Dean flow dynamics combine multiple principles to mix lipids and produce liposomes. They are easier to fabricate compared with structures such as the SHM. However, these micromixers have not been in-depth investigated as the ones based on molecular diffusion and chaotic advection micromixers on liposome production. There is a lack of understanding of how these micromixers produce liposomes. Additionally, there are no available statistical models for these devices regarding liposome production. Finally, it is not known how different organic mixtures will influence liposome properties.

#### 1.4.4 Micromixers for liposome production evolution

In summary, micromixers improve the control over liposome size and size distribution by creating uniform conditions for liposomes self-assembly; however, several parameters are still to be improved before translating all the benefits of micromixing to commercial use. Since the beginning of the 2000's, a significant growing trend was recorded in the research of micromixers. The use of micromixers for liposome preparation was reported in 2004 (Andreas Jahn et al., 2004) based on previous mixing studies (B. Knight et al., 1998). There is a gap of six years between the first investigations in just mixing and the research of liposome preparation using a specific micromixer. At the time, the results were encouraging, and some significant improvements have been made since then. The same applies to the SHM, a highly successful micromixer that was first introduced by Stroock in 2002 and in-depth studied for liposome preparation in 2012 by Belliveau and others, which occurred ten years after. The research was performed by the group, which produced the NanoAssemblr<sup>®</sup> Platform, a successful device commercially available for pharmaceutical and biology research.

However, there are still many potential micromixers that need to be studied and evaluated from a liposome manufacturing perspective as well as how critical production factors relate to liposome properties. For example, the crisscross micromixer (CM) can theoretically mix at a faster rate than the SHM (Wang, Yang, & Lyu, 2007). This micromixer has never used for liposomes production.

Figure 1.9 summarizes liposome production evolution using micromixers. The arrows represent shared fundamental principles. The micromixers investigated before for liposome production are colored in green. In brown are the ones that need more research. Finally, in red, there are examples of micromixers which have never been used in liposome production.

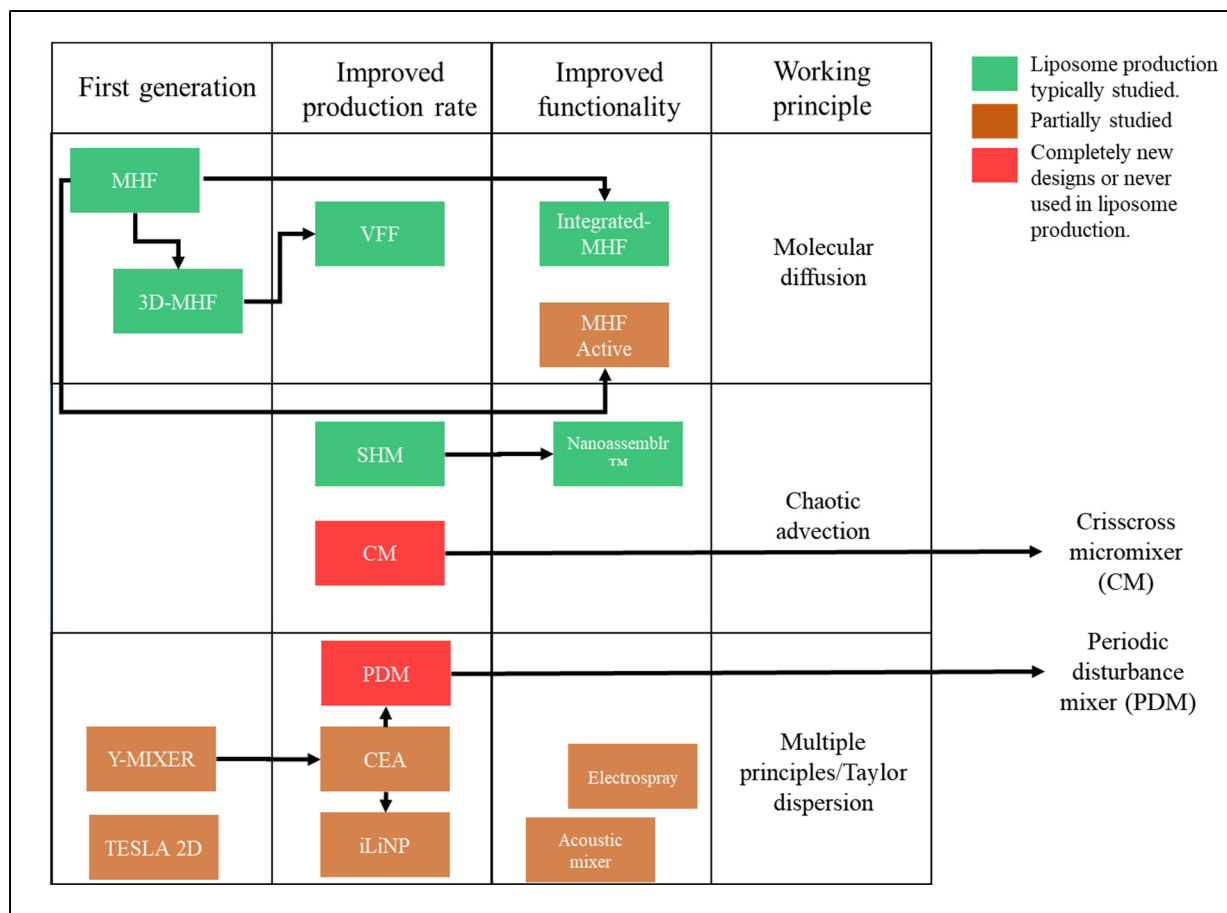


Figure 1.9 Liposome production using micromixers evolution

In this work, we proposed a new micromixer based on Dean flow dynamics to produce both chaotic advection and Taylor dispersion by alternatively changing centripetal forces vector direction and speed. The PDM, which will be presented in the following chapters, was never used for liposome production. This dissertation work focuses on the investigation of liposome production in this device.

## 1.5 Patents and companies working on the field

This section's objective is to give the reader a general overview of the patents related to liposome production as well as key market players, supplementary to the thesis body, and by no means an exhaustive market assessment.

There are several liposome patents granted for specific production methods such as supercritical fluids (Castor, 1996; Castor & Chu, 1998). These patents are currently expired as well as others using technologies from the early 90s and 2000s (Baker & Heriot, 2005). Newly developed methods, such as focused acoustics, have been recently patented (Beckett, Laugharn, & Kakumanu, 2017).

On the other hand, there are active patents for creating liposomes using micromixers, expressly the MHF device patent was granted in 2015, and it will expire until 2030 (A. Jahn, Vreeland, Locascio, & Gaitan, 2015). From the same group, a previously discussed device capable of actively loading drugs into liposomes was patented recently (R. Hood & Devoe, 2019). A patent related to the SHM production of liposomes was tried but abandoned later, by the University of British Columbia.

Lately, researchers and companies have focused their efforts on patenting liposomes formulations themselves for specific applications such as transfection (Ramsay et al., 2019) and drug delivery (Richter, Zelig, Elmalak, & Eyal, 2018), or with general functions such as encapsulating two drugs in the same shell (Tardi, Harasym, Webb, & Shew, 2010). The field is moving from research towards commercially available solutions, thus securing intellectual property is fundamental in this area of research.

Regarding the liposome production market, a key player is Precision Nanosystems. It is a company based in Vancouver. This company, like many others, originated from Pieter Cullis' laboratory or Nanomedicines Research group. This business has patented different parts of its nanoparticle production system, such as the micromixers cartridges (Fang et al., 2017) for their platform called the NanoAssemblr™. Another company with a commercial liposome production system is Dolomite, with its Liposome Synthesis Systems (Dolomite, 2020), which uses an MHF that can be connected in parallel. The field is growing momentum as more researchers rely on micromixers to produce liposomes, so more liposome formulations are expected to reach the market soon.

## **1.6 Chapter 1 conclusions**

So far, we have presented different strategies for producing liposomes. We mainly focused on those based on micromixers. Some micromixers rely on improving molecular diffusion by increasing the interface area and reducing the diffusive path. Others involve complicated geometries to produce chaotic advection.

New alternatives combining multiple mixing principles and new micromixers designs tailored to liposome production nuances might help to improve the production rate and the usability of micromixers. This evolution, at the same time, must preserve what makes micromixers an excellent option to produce liposomes, size control, reproducibility, and scalability by parallelization means. Dean flow dynamics-based micromixers have shown the same control over liposome size than previously characterized micromixers, but they are easier to fabricate.

Research is required to model both mixing and liposomes physiochemical properties as well as clearing or substituting harmful organic solvents. Currently, research facilities involved in liposome production are moving these technologies to the market. It is expected that the liposome applications will significantly grow in the near future.

In the next chapter, the principles of mixing and liposome formation are detailed, as well as the materials and methods used in this work.



## **CHAPTER 2**

### **LIPOSOME FORMATION IN DEAN DYNAMICS FLOW BASED MICROMIXERS DEVICES: THEORY, MATERIALS, AND METHODS**

In this chapter, the basic concepts of liposome formation theory are introduced. Additionally, the nanoprecipitation method is explained and generalized for other nanoparticles and connected with the relevance of the mixing process. Furthermore, the relevant principles of mixing at microscale are discussed for Dean Dynamics Flow-based micromixers. Finally, materials and methods are described in general; more specific explanations are found in the following chapters.

#### **2.1 Liposome formation theory**

The liposome formation process can be explained from an energy point of view, as stated in previous works (Lasic, 1988; Lasič, 1987). This model states that first, lipids will aggregate in a transitional disk-shaped lipid bilayer structure with an energy-related to its edge caused by hydrophobic tails exposition to the aqueous media and proportional to the disk perimeter. At this stage, new lipids may add to the disk structure or break into smaller fragments if structures are destabilized; this could be achieved by electrical fields, also known as electroformation (Angelova & Dimitrov, 1988). The energy related to the edges can be reduced by closing the disks into spheres, but this at the same time involves an energy penalty associated with the bending energy. The system total energy increases as the disk-shaped structures bend. When vesicles are closed, the overall energy decreases trapping liposomes in a high energy level state (Patil & Jadhav, 2014) as shown in Figure 2.1A. The energy additions to the system in micromixers come from the change in medium polarity. This change is caused by the rapid mixing result of pumping the fluid into the microchannels for passive micromixers.

On hydration methods, the deposited stack of lipid bilayers could be slowly separated by high-shear forces leading to MLV liposomes. On the other hand, the fast separation aided by electric

fields with no shear forces will lead to unilamellar liposomes (Patil & Jadhav, 2014). Figure 2.1B shows both processes.

The lipid bilayer elastic bending energy is influenced by temperature, lipid type, and fatty acid chain length. Furthermore, the addition of different components to the main lipid mixture, such as cholesterol, further change this parameter by making the lipid bilayer membrane stiffer, thus affecting liposome properties (Zook & Vreeland, 2010).

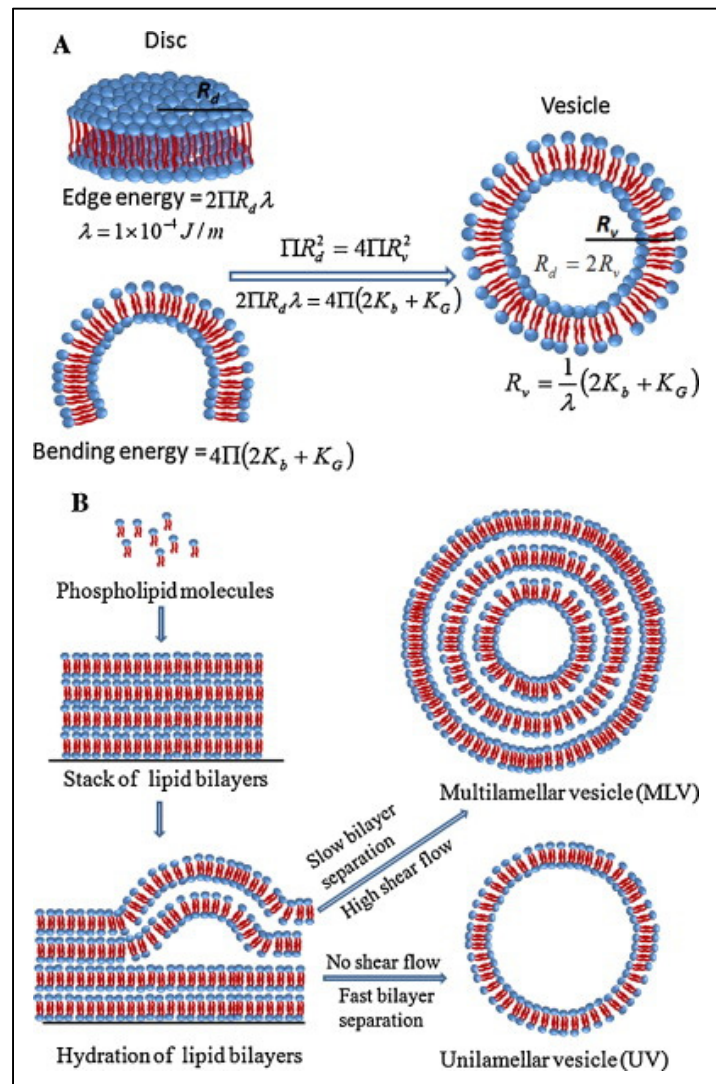


Figure 2.1 Schematic showing the liposome formation process explained by energetic considerations  
 Taken from Patil & Jadhav (2014, p.9)



Considering free energy, the lipid stacks or lipid aggregates have the lowest energy, followed by MLVs. To achieve LUVs and SUVs, more energy needs to be added to the system. The higher free energy level SUVs will agglomerate into LUVs and MLVs after some weeks (Lasic, 1988). Figure 2.2 shows this energy transitions. This agglomeration can be delayed or prevented if liposomes zeta potential values are above or below  $\pm 30$  mV (Kumar & Dixit, 2017), or if particles are sterically stabilized (Cheung & Al-Jamal, 2019).

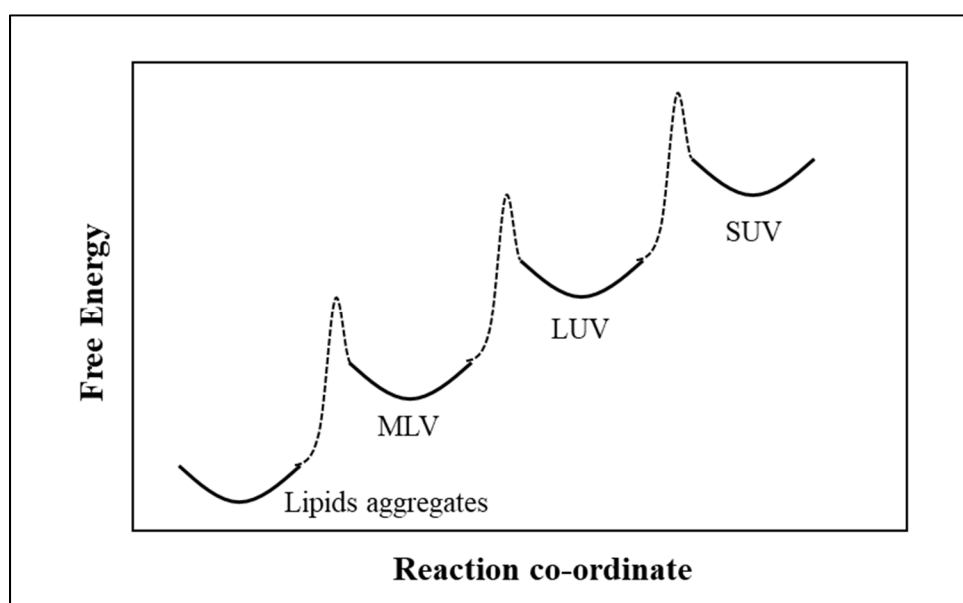


Figure 2.2 Energy diagram of lipid aggregates as they move from phospholipid aggregates to SUVs  
Adapted from Lasic (1988, p.2)

## 2.2 Nanoprecipitation method and mixing

The nanoprecipitation method, also known as the solvent displacement method, is the base principle of several nanoparticle preparation approaches such as the ethanol injection and micromixers. The first reported nanoparticles created using the nanoprecipitation method were made of poly-(D,L-lactide) encapsulating indomethacin drugs (Fessi, Puisieux, Devissaguet, Ammoury, & Benita, 1989). In general, the method consisted of diluting the shell or capsule

reagents first into a suitable solvent (in this case, acetone), then pouring this solution into an aqueous solvent (water) where nanocapsules are formed.

Nanoprecipitation, in its simplest form, mixes two different phases. One phase contains a film-forming material of amphiphilic nature (e.g. lipids) diluted into an organic solvent (e.g. ethanol) where lipophilic substances such as drugs or surfactants could be added. The second phase contains an aqueous solvent (e.g. water) where additional hydrophilic components could be diluted in. As these two phases mix under stirring, nanoparticles are self-assembled (Martinez Paino, Santos, & Zucolotto, 2017).

Mixing proved to be crucial for controlling liposome characteristics. In the ethanol injection method, mixing is controlled by the stirring speed. An increase in the mixing rate avoids the formation of large vesicles (Batzri & Korn, 1973).

Another critical aspect to consider in the liposome formation process is the medium in which liposomes are formed. In these organic-aqueous solvent mixtures, also known as binary mixtures, properties, such as density, viscosity, polarity, and mutual diffusion coefficient, directly depend on the concentration of binary mixture components affecting the mixing process. In a few experimental works, the authors have calculated these properties at several different ratios between organic and aqueous solvents (González, Calvar, Gómez, & Domínguez, 2007; Pratt & Wakeham, 1974).

For liposome formation in micromixers, mixing means the change in polarity at which lipids are exposed, as the mixing occurs, polarity increases. How fast polarity changes reduce the time for intermediate disk-structures to increase their size, resulting in smaller liposomes. In this work, previous models and experimental results will be used to discuss such influence (Bosch & Rosés, 1992; Langhals, 1982).

### 2.3 Mixing theory

In the context of this work, mixing is the transport of diluted species to increase homogeneity. Mixing, in the case of nanoprecipitation, results in a change of lipids into liposomes by mixing a low polarity organic solvent with high polarity aqueous solvent. Micromixers are governed exactly by the same physics as their macro counterparts; however, there are dimensional scaling consequences. For example, the surface area-to-volume ratio, surface tension, and diffusion do not scale linearly.

Microfluidic devices typically operate under laminar flow as a direct consequence of their dimensions. Meaning that fluid flows smoothly. Viscous forces dominate over inertial forces, the velocity at any location inside the liquid is invariant with time when boundary conditions are constant. Mixing at this scale only occurs by molecular diffusion, chaotic advection, and Taylor Dispersion (Nguyen, 2012a). On the other hand, turbulent flow is characterized by the dominance of inertial forces over viscous forces; the motion is random in space and time; mass transport occurs in all directions. Reynolds number defines if a flow is laminar or turbulent and is described by Equation (2.1).

$$Re = \frac{\rho u D_H}{\mu} = \frac{u D_H}{\nu} \quad (2.1)$$

Where  $u$  is the flow velocity  $\rho$  is the fluid density,  $\mu$  is dynamic viscosity,  $\nu$  is kinematic viscosity and  $D_H$  is a hydraulic diameter. The latter depends on the dimensions and shape of the channels.

Because of laminar flow, most of the mixing in microfluidics occurs by passive molecular diffusion and advection. Molecular diffusion is the Brownian motion of molecules from a region of high concentration to one with a low concentration; it depends on temperature, the viscosity of the fluid, and the size of particles, and it is defined by Fick's first law shown in Equation (2.2).

$$j = -D \frac{dc}{dx} \quad (2.2)$$

Where  $j$  is the diffusion flux,  $D$  is the diffusion coefficient,  $c$  is the concentration of the species, and  $x$  is the position of the species. For spherical particles,  $D$  can be calculated from the Einstein-Stokes equation shown next.

$$D = \frac{kT}{6\pi\mu R} \quad (2.3)$$

Where  $k$  is the Boltzmann's constant,  $T$  is the absolute temperature,  $R$  is the radius of the particles, and  $\mu$  is the viscosity of the medium. The time required for a species to diffuse scales quadratically with the distance covered.

Taylor dispersion arises in fluids where a distributed velocity field is present. For example, in a Poiseuille flow. The pipe walls are considered to have a non-slip condition resulting in a parabolic profile (Senturia, 2001). When two miscible liquids are mixed, it appears that the diluted species is stretching in the advection direction in the middle of the pipe (Nguyen, 2012b). This diffusion  $D^*$  is characterized by the next equation.

$$D^* = D + \frac{2h^2\bar{u}^2}{105D} \quad (2.4)$$

Where  $D$  is the original diffusion coefficient, and  $2h$  represents the gap between the pipes and  $\bar{u}$  is the average velocity in the advection direction.

Chaotic advection is defined as a phenomenon in which a pure Eulerian velocity leads to a chaotic response. It is essential to mention that a fluid can be chaotic and laminar at the same time; this must not be confused with turbulence. At any given point, the velocity components stay constant in laminar flow, while for turbulent flow, they change randomly. Under chaotic

advection, diluted species diverge exponentially, enhancing the mixing process. (Nguyen, 2012b). This chaotic advection could be created by adding obstacles in the path of laminar flow or by adding curvilinear paths that create centripetal forces that induce the formation of vortices, also known as Dean Vortices.

The Dean Number characterizes the formation of Dean Vortices. It is the ratio between centrifugal forces and inertial forces (Nguyen, 2012b). It is calculated using (2.5)

$$De = Re \sqrt{\frac{D_H}{2R_c}} \quad (2.5)$$

Where  $D_H$  is the hydraulic diameter,  $Re$  is the Reynolds number, and  $R_c$  is the ratio of curvature. It has been shown that at a  $De$  of 10, Dean vortices are created for certain types of micromixers (M. G. Lee et al., 2009).

Ideally, a micromixer tailored for liposomes production using Dean flow dynamics should have the following properties and conditions:

1. A Reynolds number as small as possible that guarantees a laminar flow regime inside the microchannels, thus stable fluid flow interfaces that, in theory, result in homogenous liposome populations.
2. A fluid flow speed capable of generating Dean Vortices ( $De \geq 10$ ) to enhance the mixing process (M. G. Lee et al., 2009).
3. Feature sizes compatible with the soft lithography process constraints.
4. A channel cross-section area as large as possible to increase production yield and, at the same time, operate according to pressure and flow constraints given by the microfluidic device, including operating temperatures.

5. Controllable mixing times in the order of milliseconds to modulate the medium polarity change rate and thus the liposome self-assembly process.

A hypothetical Dean Flow Dynamics-based micromixer combines the use of curvilinear paths to induce Dean Vortices and, at the same time, uses microchannel size reductions to change the flow speed producing Taylor dispersion. This microfluidic device's more critical variables would be the TFR, the radius, and direction of the curvilinear paths, as well as the aspect ratio considering that Taylor dispersion is proportional to the square of the velocity and the Dean number, is directly proportional to velocity, as shown in Equation (2.4) and Equation (2.5). In the next chapters, we will present a micromixer design that includes previously mentioned characteristics.

## 2.4 Mixing and liposome production relationship

Liposomes formation, in micromixers, is a kinetic phenomenon driven by the speed at which intermediate disk structures close into sphere vesicles. This speed is controlled by the medium polarity change rate consequence of the aqueous-organic solvent mix (Andreas Jahn et al., 2010). Thus, mixing time, which is governed by the Navier-Stokes and Convection-Diffusion equations as well as the polarity of the binary mixture, controls liposome characteristics such as size and size distribution. Additionally, the uniformity of this mixing influences the size distribution of particles (R. R. Hood & DeVoe, 2015).

Mixing time is defined as the time required to achieve a given level of homogeneity, which in most of the works is from 90 to 95% of mixing efficiency. For this work, the mixing efficiency was calculated based on the intensity of segregation ( $I_s$ ), (Danckwerts, 1952) defined by the next equation.

$$I_s = \frac{\sigma^2}{\sigma_{max}^2} \quad (2.6)$$

Where  $\sigma_{max}^2$  is the maximum variance of concentration, and  $\sigma^2$  is the variance of current concentration. The mixing efficiency (ME) is defined by:

$$ME = \left[ 1 - \sqrt{\frac{\sigma^2}{\sigma_0^2}} \right] \times 100\% \quad (2.7)$$

Where  $\sigma^2$  is the variance of the concentration in the tested cross-section,  $\sigma_0^2$  is the variance of the concentration in no mixing condition, generally at the beginning of the mixing channel. ME is also referred to as a mixing index (MI). The latter is represented in decimal form as opposed to ME that is described in percentages. The cross-sections in the numerical models were divided into a grid of 50 x 50 elements from where variances were calculated.

While mixers such as SHM create liposomes in the order of tens of nanometers with mixing times of 3 ms (Zhigaltsev et al., 2012), liposomes of 500 nm are formed under static conditions, with an estimated assembly time of 50 ms (Phapal, Has, & Sunthar, 2017). These results give an operational order of magnitude of the mixing times required to produce LNPs as well as a design objective for new micromixers tailored to LNPs production.

## 2.5 Numerical modeling

Numerical models are a powerful way to investigate fluid flow behavior inside microfluidic channels. These models solve partial differential equations that describe flow physics using computational methods based on well-defined boundaries and initial conditions. These models are useful when those physics equations do not have analytical solutions. While in the case of Navier-Stokes equations, certain assumptions can be taken so analytical solutions can be derived, this can be done only under particular conditions as well as taking advantage of systems symmetries. In the case of Micro Hydrodynamic Focused (MHF) mixers, which geometries are relatively simple, extended analytical solutions have been found (Sadeghi, 2019; Z. Wu & Nguyen, 2005b). However, for other types of micromixers, such as the chaotic

advection based mixers, numerical models are required to obtain a glance at the mixing process (Du, Zhang, Yim, Lin, & Cao, 2010; Rhoades, Kothapalli, & Fodor, 2020).

The typical length scales of the simulations are in the order of tens of micrometers with Knudsen number way above 1; thus, the continuum assumption is acceptable. The self-assembly process of the liposome cannot be simulated using the continuum assumption because the representative length scale is in the order of nanometers. In this case, a statistical mechanics approach is more suitable (Bernardes, 1996; Tamai et al., 2016). This approach is out of the scope of this work.

In this work, the micromixing phenomenon is numerically modeled using Navier-Stokes equations coupled with the convection-diffusion equation, considering a single-phase flow using the software COMSOL Multiphysics 5.5. The numerical model includes an organic solvent concentration-dependent density, viscosity, and mutual isotropic diffusion in 3 dimensions unless stated differently. The Navier-Stokes conservation of momentum Equation (2.8), as well as the continuity equation, Equation (3.9), were solved until a steady state was reached.

$$\rho(\mathbf{u} \cdot \nabla)\mathbf{u} = \nabla \cdot [-p\mathbf{I} + \mu(\nabla\mathbf{u} + (\nabla\mathbf{u})^T)] + \mathbf{F} \quad (2.8)$$

$$\rho \nabla \cdot (\mathbf{u}) = 0 \quad (2.9)$$

Where  $\rho$  is the fluid density,  $\mathbf{u}$  is the flow velocity,  $p$  is the pressure,  $\mu$  is the dynamic viscosity, and  $\mathbf{F}$  represents outer forces. The boundary conditions for the walls were set to no-slip condition. The velocity field that resulted from previous equations was used to solve the Convection Equation (2.10) and the Diffusion Equation (2.11).

$$\mathbf{N} = -D\nabla\mathbf{c} + \mathbf{u}\mathbf{c} \quad (2.10)$$

$$\nabla \cdot (-D\nabla\mathbf{c}) + \mathbf{u} \cdot \nabla\mathbf{c} = \mathbf{R} \quad (2.11)$$



Where  $c$  is the diluted species concentration,  $D$  is the mutual diffusion coefficient between water and ethanol,  $R$  is the net volumetric source for the species, and  $N$  is the molar flux.

In this model,  $D$ ,  $\rho$ , and  $\mu$  are in function of the organic solvent concentration  $c$  in the aqueous media. This approach enables to model more realistically, the mixing conditions. Unfortunately, the relationship between the concentration and the previously mentioned variables has not been analytically established. However, in literature, one can find experimental values based on the molar concentration of the organic solvent for binary mixtures such as ethanol-water. To introduce these values into the model, one can take two approaches; the first one, introduce the experimental values and use COMSOL Multiphysics 5.5 interpolation function for complex variables relationships. Second, use the experimental results and fit them into a function that closely resembles the experimental data. For the mutual diffusion coefficient, a polynomial data fit was appropriate, as shown in previous works (Renee R. Hood et al., 2014).

The equations approximating the mutual diffusion coefficient are described in the model by a polynomial fitting experimental data from binary mixture ethanol-water (González et al., 2007; Pratt & Wakeham, 1974). This approach enables to introduce a mutual diffusion coefficient that is dependent on concentration. Figure 2.3 shows the comparison between the experimental data and the adjusted fifth-order polynomial described in Equation (2.12).

$$D(c) = [-7.008c^5 + 25.01 c^4 - 36.65 c^3 + 26.74c^2 - 8.298c + 1.249] 1 \times 10^{-9} \frac{\text{m}^2}{\text{s}} \quad (2.12)$$

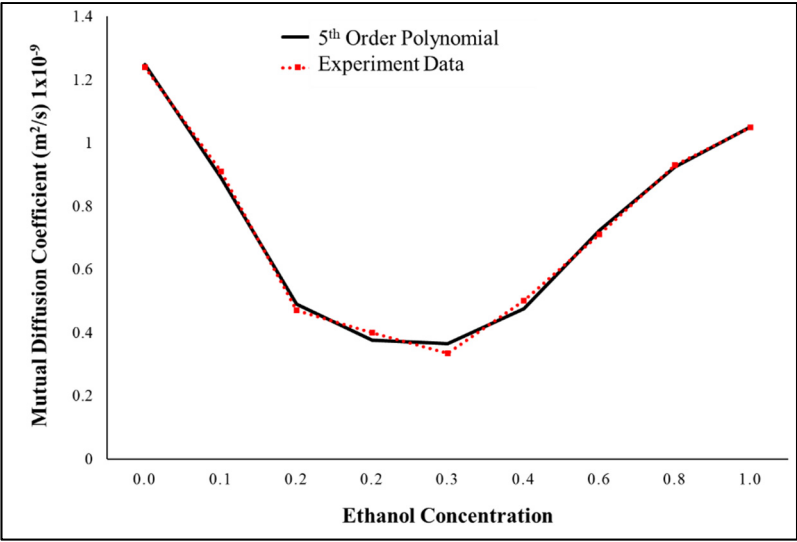


Figure 2.3 Mutual diffusion coefficient for the binary mixture ethanol-water dependent on concentration. In black, the experimental data, in red, the 5th order polynomial

Density and dynamic viscosity were fitted using COMSOL Multiphysics 5.5 interpolation function and the experimental data of the binary mixture ethanol-water (González et al., 2007).

The boundary conditions include the no-slip condition for the walls, the inlets with defined flow rates, and an outlet with no pressure. For the transport of diluted species, the walls represented no flux condition, with a defined initial concentration 1 of the diluted species for the inlet in which ethanol is injected and a concentration of 0 for the inlet where water is injected. The summary of boundary conditions is presented in Table 2.1.

Table 2.1 Summary of boundary conditions and domains in numerical models

Boundary Condition	Domains
Navier Stokes/Convection Diffusion	
No-slip/No Flux	Walls
Inlet Defined Flow/Defined Concentration	Inlets
Outlet with no pressure	Outlet

The previously described numerical model was compared with the results presented in the literature as well as validated through experimentation. Figure 2.4 shows on the left, the experimental results where ethanol is dyed in red and water in blue, on the right their numerical simulations counterparts. The mixing profiles are similar.

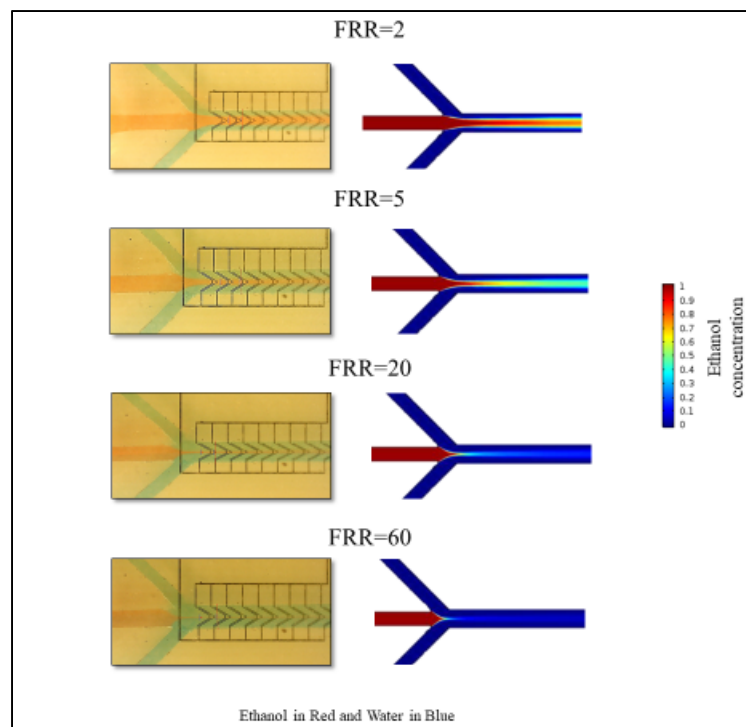


Figure 2.4 Mixing of ethanol and water in a microfluidic device. Experimental vs. numerical modeling

## 2.6 Micromixer design and fabrication

To investigate liposome formation in a Dean Flow Dynamics-based micromixer, we designed and fabricated PDM micromixers with different aspect ratios (AR) and semicircular structures. All micromixers have two inlets in one extremity and one outlet in the other. The inlets are connected to the mixing channel in a Y-shape cross. The goal of the channels connecting the inlets with the mixing channel is to ensure that a stable parabolic profile is obtained (Durst, Ray, Ünsal, & Bayoumi, 2005). The mixing channel consisted of semicircular structures, which centers pointed in alternative directions along the channel. All semicircular structures

have a radius of  $260\ \mu\text{m}$ . The maximum channel width is  $300\ \mu\text{m}$  given as a result that the narrowest part of the channel was  $40\ \mu\text{m}$ . The radius of the inlets and outlets was  $1\ \text{mm}$ . Figure 2.5 shows the dimensions of the PDM. As explained in the next chapters, these dimensions enable the mixing of ethanol and water in the order of milliseconds under laminar flow conditions with a varied range of De numbers as further detailed. For most of this work, the maximum microchannel height was designed to be as large as possible to increase liposome production yield. Furthermore, it considered the aspect ratio soft lithography microfabrication constraint, which in practice is typically up to 1:10.

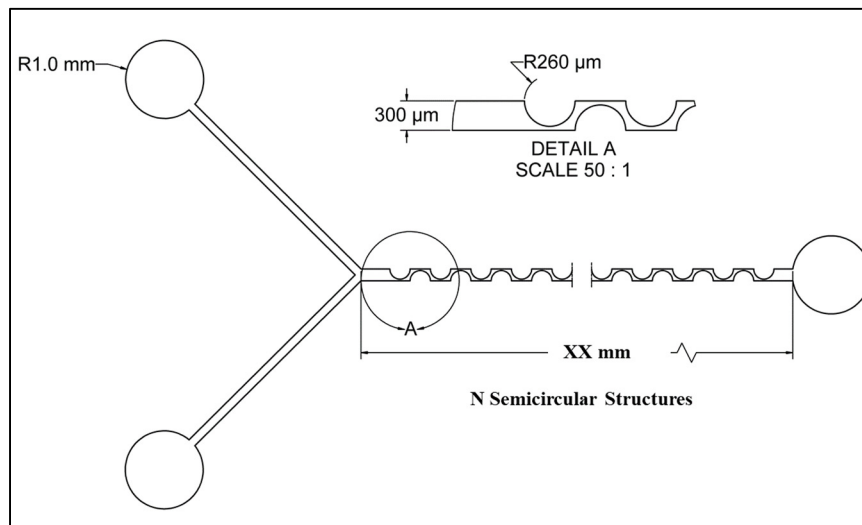


Figure 2.5 PDM. The micromixer consists of two inlets a micromixing channel and an outlet

This design was first realized in AutoCAD 2019 and used for both performing numerical modeling in COMSOL 5.5 and to fabricate a mask using the Dilase 650 multifunction photolithography system (KLOÉ, Montpellier, OCC, France). Substrate with 8 epoxy (SU-8) negative photoresist (MicroChem Co. Westborough, MA, USA) was poured on a 4" silicon wafer, spin-coated, baked, exposed to UV light through a photomask and developed to create a master mold. The microfluidic device was fabricated using Sylgard 184 polydimethylsiloxane (PDMS) (Ellsworth Adhesives Canada, Stoney Creek, ON, Canada). First, the PDMS base and the curing agent were mixed at a 10:1 weight ratio. The mix was

first degassed under vacuum conditions and poured on the top of the SU-8 mold. The PDMS was degassed again to remove remaining bubbles. Then it was cured at 65 °C for four hours. The PDMS device was carefully peeled off from the mold, and the inlets and outlets were punched using a biopunch. Finally, the PDMS element was bonded to a 75 x 25 mm microscope slide (Globe Scientific Inc., Mahwah, NJ, USA) after treating both parts with oxygen plasma (Glow Research, Tempe, AZ, USA). Tygon® Tubing (Cole-Parmer, Montreal, QC, Canada) and stainless-steel fitters were used to connect the device ports to the syringes. The microfabrication process is shown in Figure 2.6.

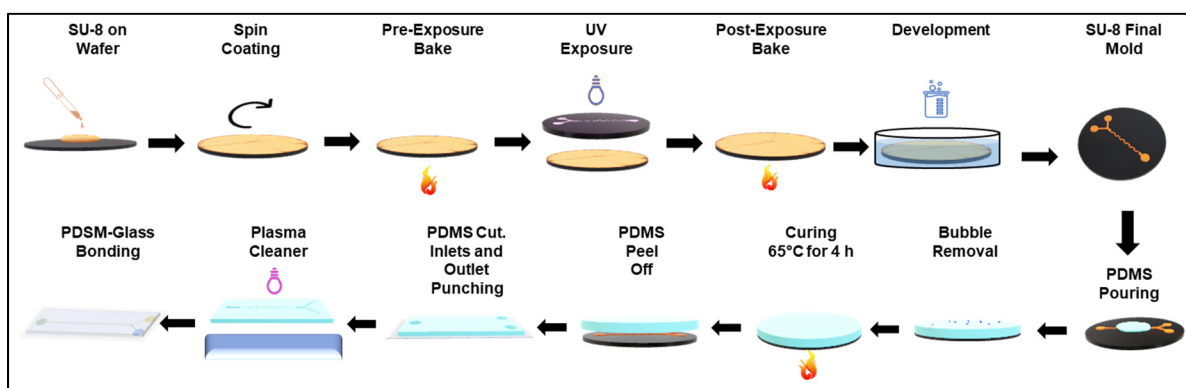


Figure 2.6 Micromixer fabrication process

## 2.7 Mixing imaging

The mixing process inside the microchannels was imaged by staining fluid flows using either food dyes or fluorescence dyes such as TP-3900 (Tracer Products, Westbury, NY, USA). The imaging is carried out at different times. Images were taken after the flow has reached a steady state. Since the flow inside the micromixer is laminar, thus time-invariant, we could stitch multiple pictures taken at different times under the same flow conditions. This imaging technique would not be possible for turbulent flows.

For the food dyes imaging, an AmScope™ (AmScope, Irvine, CA, USA) inverted microscope was used. Images were taken with a 5 MP camera. Figure 2.7A shows the mixing process imaging using food dyes.

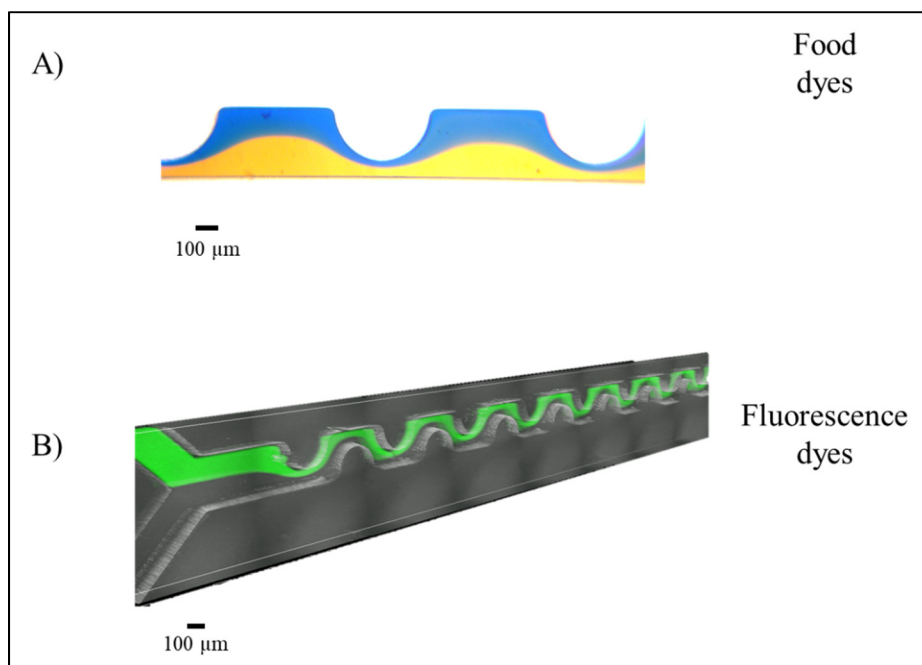


Figure 2.7 Micromixing imaging A) Food dyes imaging in two dimensions. In blue-stained water and in orange ethanol  
B) Fluorescence dyes imaging in three dimensions

TP-3900 dye is excited by UV light. For fluorescence dye experiments, a laser scanning confocal microscope Nikon Eclipse Ti (Nikon Instruments Inc., Melville, NY, USA) was used. This microscope takes several images of the z-planes of the studied subject to reconstruct a 3D image or visualize transversal planes using NIS-Elements software as shown in Figure 2.7B

The experimental setup consisted of two syringes containing water (one dyed with TP-3900), connected through 0.22  $\mu\text{m}$  filters to the PDM devices. The liquid was collected at the outlet. Two syringe pumps Harvard Apparatus 11 plus 70-2212 (Harvard Apparatus Canada, Montreal, QC, Canada), as shown in Figure 2.8.

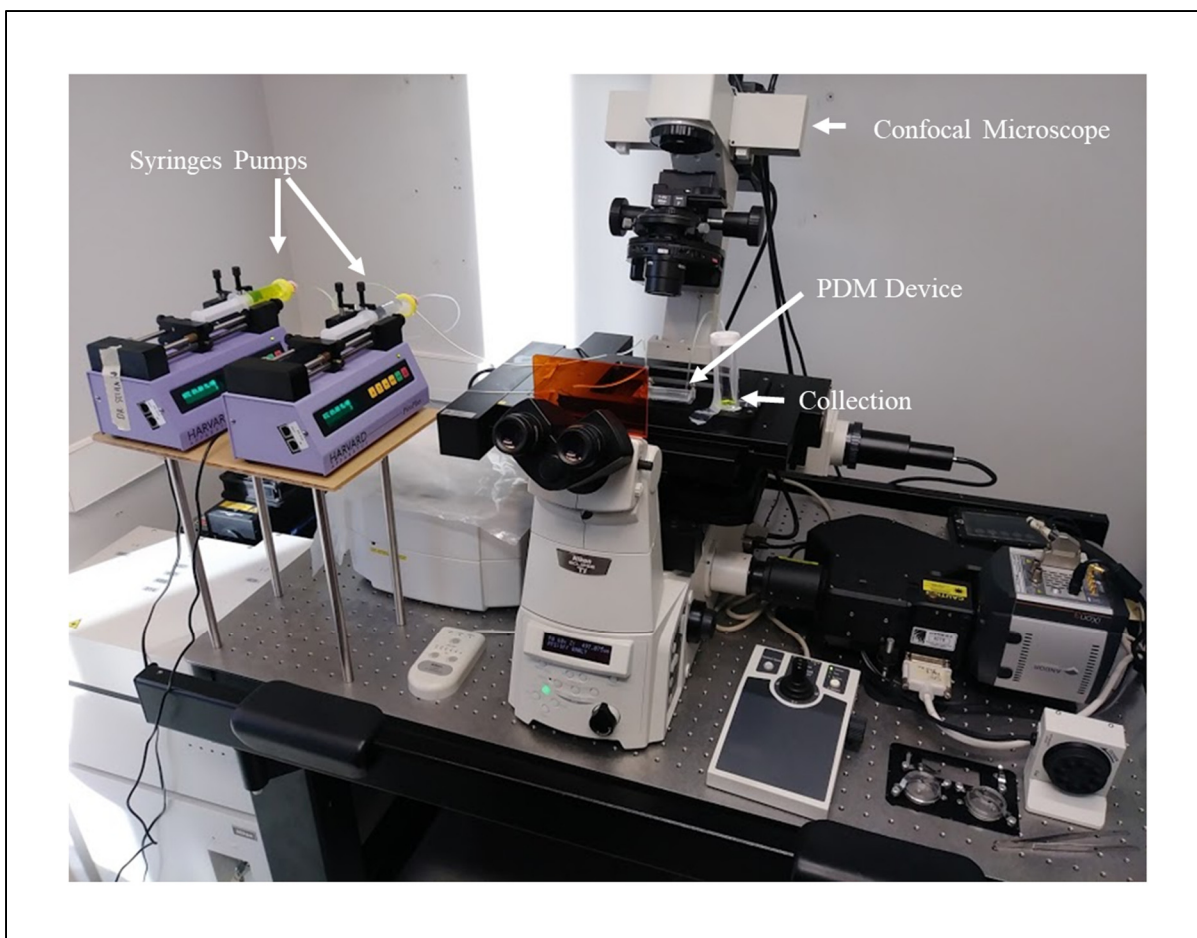


Figure 2.8 Mixing imaging experimental setup

## 2.8 Lipid preparation

Lipids were acquired from Sigma Aldrich (Sigma-Aldrich, Oakville, ON, Canada). Lipids come in two different presentations; one is in a powder form, the second diluted in chloroform. In both cases, lipids were aliquoted to a given final concentration (20 mM) in chloroform. These aliquots were the base for preparing the lipid mixtures presented in this work. Since all aliquots have the same molar concentration, it facilitated the calculation of the molar ratios.

Once the molar mix was prepared, the chloroform was evaporated under a free of oxygen atmosphere. This procedure was accomplished by using filtered nitrogen. To remove any chloroform residues, the mixture was exposed to a vacuum for 24 hours. Finally, lipids were

dissolved in an organic solvent to a predetermined final concentration (Andreas Jahn et al., 2010). Before using the lipids for liposome preparation, they were warmed-up at 70 °C and vortexed for 3 minutes to ensure a complete dilution. Figure 2.9 shows step by step the process to produce a typical lipid mixture consisting of 1,2-dimyristoyl-sn-glycero-3-phosphocholine (DMPC), cholesterol (CHOL) and dicetyl phosphate (DHP) with a molar ratio 5:4:1, a final concentration of 5 mM, and a volume of 5 mL.

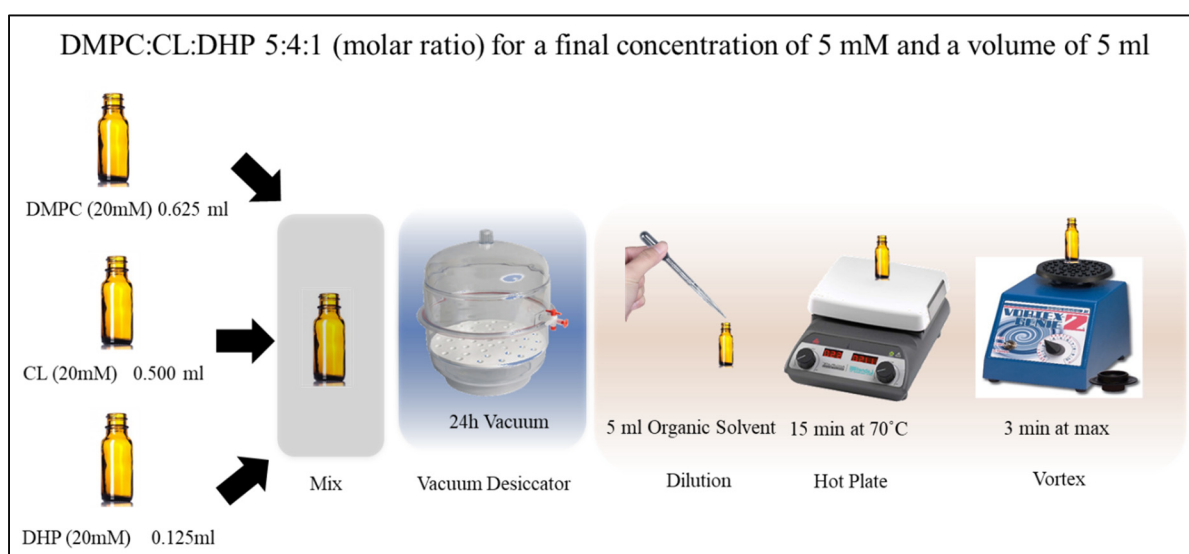


Figure 2.9 Lipid preparation process. From left to right, lipid mixture, chloroform removal, and organic solvent dilution  
Courtesy of Ixchel Ocampo

## 2.9 Liposomes production using micromixers

In this work, liposomes were produced using previously described PDM. A syringe (Norm-Ject 10 mL) was filled with the lipids diluted in an organic solvent. A second syringe was filled with an aqueous solvent. These syringes were connected separately to an inlet in the PDM through 0.22  $\mu$ m filters and Tygoon® tubing. The PDM was placed on the top of a hot plate as well as a collection vial. The temperature was set according to experimental parameters. Two syringe pumps Harvard Apparatus 11 plus 70-2212 controlled the flow (Harvard Apparatus Canada, Montreal, QC, Canada). A tube connected to the outlet directed the



liposomes to a 4 mL scintillation vial, where liposomes were further diluted to a suitable concentration for liposome characterization. After, samples were cooled down for 15 minutes, then stored at 4 °C. Figure 2.10 shows the main components of the experimental setup.

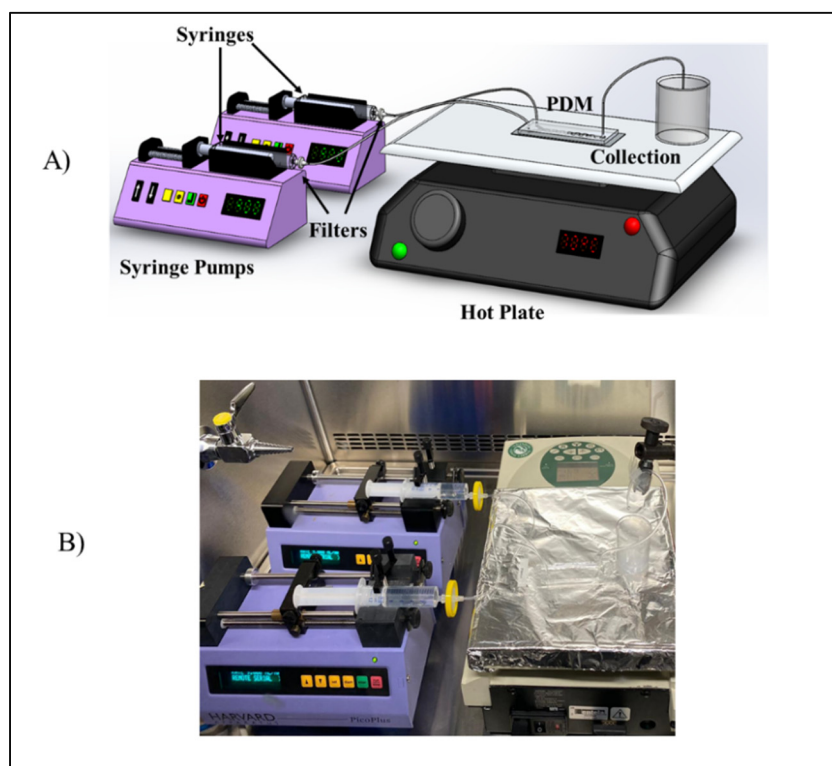


Figure 2.10 Liposome production experimental setup  
A) Schematic B) Photography of the functional experimental setup  
Courtesy of Ixchel Ocampo

The aqueous solvent flow rate  $Q_{as}$  and the organic solvent flow rate  $Q_{os}$  were calculated using Equation (2.13) and Equation (2.14).

$$Q_{as} = \frac{FRR \cdot TFR}{(1 + FRR)} \quad (2.13)$$

$$Q_{os} = \frac{TFR}{(1 + FRR)} \quad (2.14)$$

Where FRR is the flow rate ratio, and TFR is the total flow rate.

The total liposome production rate  $P$  was calculated based on Equation (2.15) as presented elsewhere (R. R. Hood & DeVoe, 2015).

$$P = \frac{TFR \cdot c N_A a}{4\pi[(r_h)^2 + (r_h - e)^2]} \quad (2.15)$$

Where  $P$  is the liposome production rate per hour, TFR is the total flow rate in  $\text{m}^3/\text{s}$ ,  $c$  is the final lipid concentration in  $\text{mol}/\text{m}^3$ ,  $N_A$  is the Avogadro's Number,  $a$  is the cross-section area of the lipid head group,  $r_h$  is the hydrodynamic radius of the liposome and  $e$  is the lipid bilayer thickness.

This equation is based on the hypothesis that all lipids at the outlet are transformed into liposomes. It considers a total lipid bilayer area divided by the area of an unilamellar liposome with a define radius  $r_h$ .

## 2.10 Liposome characterization

After production, liposomes physicochemical characteristics such as size, size distribution, and zeta potential were measured. The Z-average (intensity-based size mean) was measured using dynamic light scattering (DLS) principle as well as average particle size homogeneity related to the PDI.

If stated, additionally mean size measurements were performed using nanoparticle tracking analysis (NTA). Finally, the zeta potential was measured using the principle of electrophoretic mobility.

The measurement procedures and principles of liposome characterization are detailed in the next sections.

### 2.10.1 Dynamic light scattering

Also known as photon correlation spectroscopy (PCS), DLS measures Brownian motion and translates it to the hydrodynamic diameter ( $d_h$ ), which is an equivalent sphere of the same average diffusion coefficient. This translation from the diffusion coefficient to size is made using the Stokes-Einstein Equation (2.3). Small particles diffuse quicker than large particles.

When a coherent light source illuminates a particle, the particle scatters light in all directions. This light can be captured by a receptor that produces a signal. This signal fluctuates because of the random movement of particles suspended in the liquid (Brownian Motion). The Zetasizer Nano uses a digital correlator that compares the signal at a given time and shortly after. The time scale between the two signals is in the order of nanoseconds to milliseconds. The correlation between these two signals is used to measure the size of the particles. It is expected that for the same delta time, large size particle's correlation function value will be higher than for small particles. Small particles diffuse faster, causing a rapid decay in the correlation function.

Once the correlation function is measured, the Zetasizer uses algorithms to convert this decay rates into an intensity (scattered light) base size distribution. So, the native result of this equipment is intensity-based. This measurement can be converted to volume-based size distribution using Mie's and Rayleigh's theory of light scattering (S. Bhattacharjee, 2016; Mie, 1908; Rayleigh, 1899); furthermore, this can be converted to a number-based size distribution. To complete these conversions, it is crucial to know the refractive index of the particles as well as their absorption index. Nevertheless, these conversions are not free of errors; small errors in the intensity size distribution can cause significant errors in the number size distribution (Manual, 2013).

For this reason, it is essential to report intensity-based size distributions or properly validated number size-based distributions. This validation could be performed by doing other measurements in which the native results are number-based such as NTA or counting from

images such as in transmission electron microscopy (TEM). Another way to avoid errors is to repeat the measurement multiple times.

Scattered incident light is proportional to the  $d^6$  where  $d$  is the diameter of the particle (S. Bhattacharjee, 2016). From left to right, the scaled results for  $d$  (number),  $d^3$  (volume), and  $d^6$  (intensity) for a multimodal population where there are as many particles of 5 nm as of 50 nm. The difference in size distributions by number, volume, and intensity are shown in Figure 2.11.

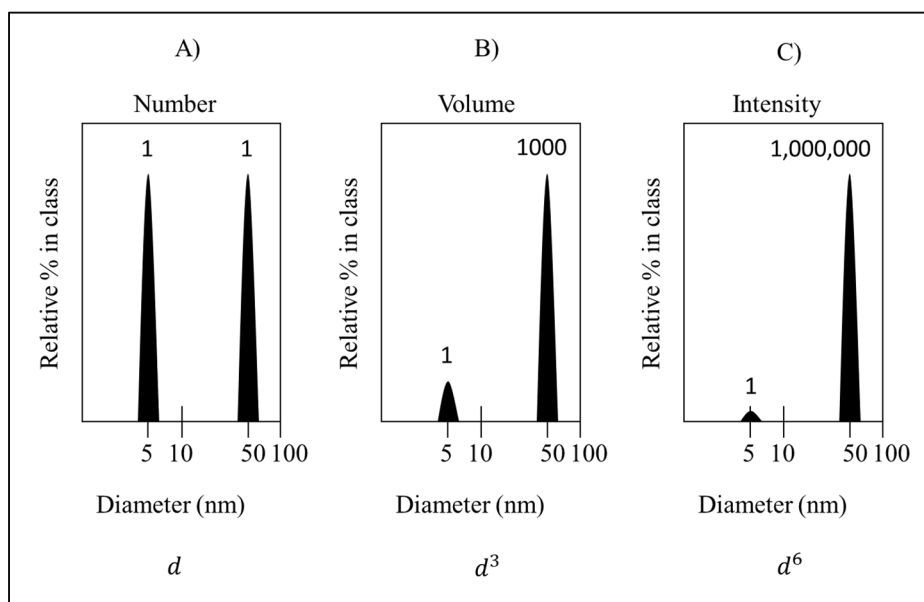


Figure 2.11 Particle size distribution A) By number

B) By volume C) By intensity

Adapted from Malvern (2013 p.11-5)

The main results of DLS measurements are Z-Average (diameter or size) and PDI. The Z-average, also known as the cumulants mean, is an intensity mean. This value is taken from the cumulant analysis that is a polynomial fit from the correlation function  $G1$  (Manual, 2013).

$$\ln[G1] = a + bt + ct^2 + dt^3 + et^4 \dots \quad (2.16)$$

The value of  $b$  is converted to size using the viscosity of the dispersant and other equipment parameters,  $c$  is scaled using  $2c/b^2$ , and it is known as PDI. The calculation of these parameters is defined in the ISO 13321:1996 (ISO, 1996), which was reviewed recently and changed by ISO 22412:2017 (ISO, 2017).

Z-average is only directly comparable with other types of measurements when the population is monomodal and monodisperse ( $PDI < 0.1$ ).

The lower PDI is, the more homogeneous a particle population is. A  $PDI < 0.1$  is typically considered as monodispersed, while  $PDI < 0.2$  is related to low polydispersity (R. R. Hood & DeVoe, 2015).

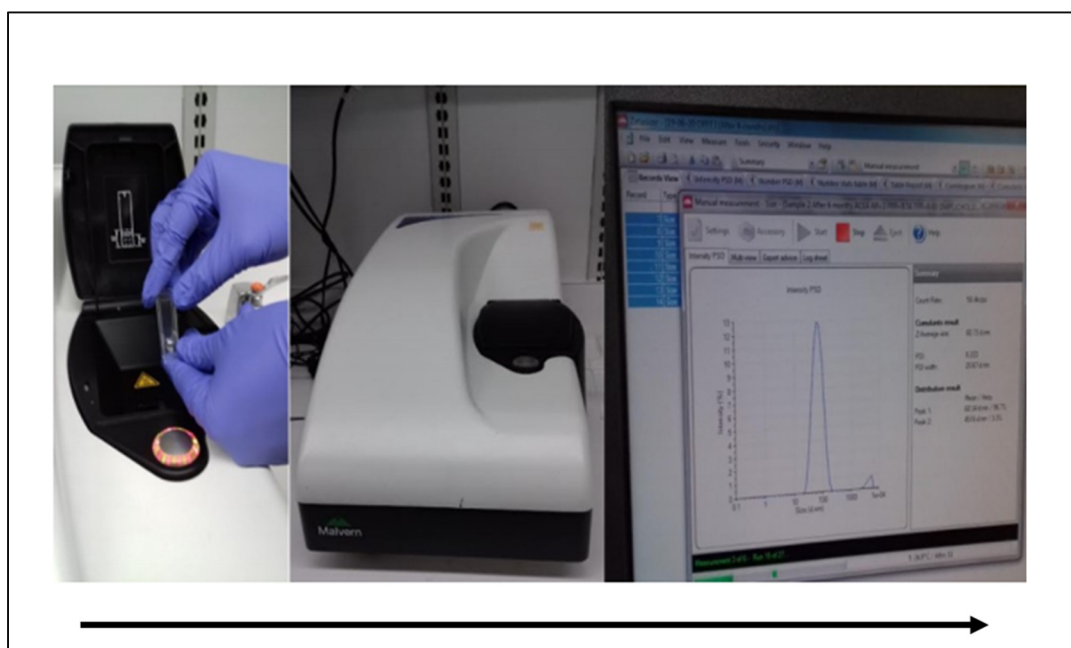


Figure 2.12 Zetasizer S90 workflow. From left to right, inserting the sample, equipment, and results  
Courtesy of Luz Maria Sanchez

The equipment used in liposome characterization was Zetasizer S90. It uses a He/Ne laser with an emission at 632.8 nm, a power of 4 mW, and a 90° angle scattering detector. All

measurements were performed at 25 °C unless stated differently. At least three measurement replicates were performed per sample. The software used to analyze and transform size distributions was Zetasizer Software 7.11. Usually, the liposomes in suspension are placed inside a cuvette that is inserted in the Zetasizer Nano. Figure 2.12 shows the Zetasizer S90 workflow.

### **2.10.2 Nanoparticle tracking analysis**

As mentioned before, particle size measurements based on DLS are intensity-based, meaning that a transformation to a size distribution by number might contain errors depending on the sample monodispersity and PDI. Additional measurement methods that give native number-based results can help to validate and confirm DLS measurements and transformations.

NTA is similar to DLS because both of them use Brownian motion, light scattering, and Stokes-Einstein equation to calculate particle size. However, NTA tracks single particles on a view field. By monitoring each particle movement, the size is calculated for each particle, giving a number-based result.

Particles are first pumped to a microfluidic device that is under a microscope with a proprietary optical element. A laser beam is lit on the microfluidic device, and the scattered light of particles is captured in a video. The software tracks the scattered light and the tracks of each visualized particle, then the mobility of the particles is related to their size using as in DLS. The mean size, the mode, and standard deviation are calculated.

Additionally, to size measurements, NTA can estimate the particle concentration. Since the volume visualized in the microscope is known, as well as the number of particles per field, the number of particles/mL can be calculated.

As opposed to DLS, NTA requires less particle concentration, it has a higher resolution, it can detect individual populations with more precision, and it gives a number-based result.

Additionally, one can “see” the particles; however, this is not a resolved image. Another problem is that these measurements are not performed according to an ISO standard, and the equipment is slightly more complex to operate.

Typically, NTA requires first to flush the microfluidic device and position the sample in the microscope viewing field by operating peristaltic pumps, as shown in Figure 2.13A. The results that come from the NTA include a detailed size distribution by number, as shown in Figure 2.13B. The software captures videos of the light scattered by the particles, and then these videos are processed in software that tracks each of the particle’s movement. Figure 2.13C is a snapshot example taken from NTA videos.

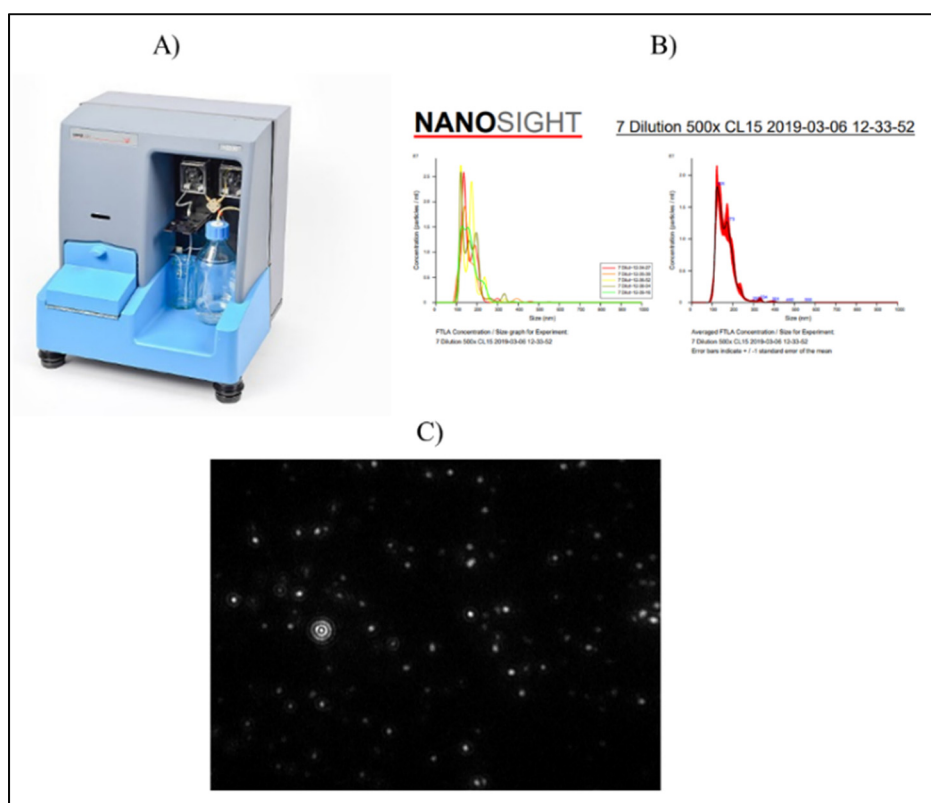


Figure 2.13 NTA Measurements A) Nanosight NS500  
B) Sample results are taken from NS500 C) Image of the  
scattered light of nanoparticles

### 2.10.3 Zeta potential (electrokinetic potential)

Zeta potential, also known as Electrokinetic Potential, in colloidal dispersions is the electric potential at the edge of the double layer. Particles have two layers of opposite charged ions. One layer is just beside the surface of the particle called the stern layer, and the second one called double layer, as it is shown in Figure 2.14. Thus, zeta potential values depend on the chemistry of the particle's surface and the dispersant. Zeta potential is affected by the pH, and ionic strength.

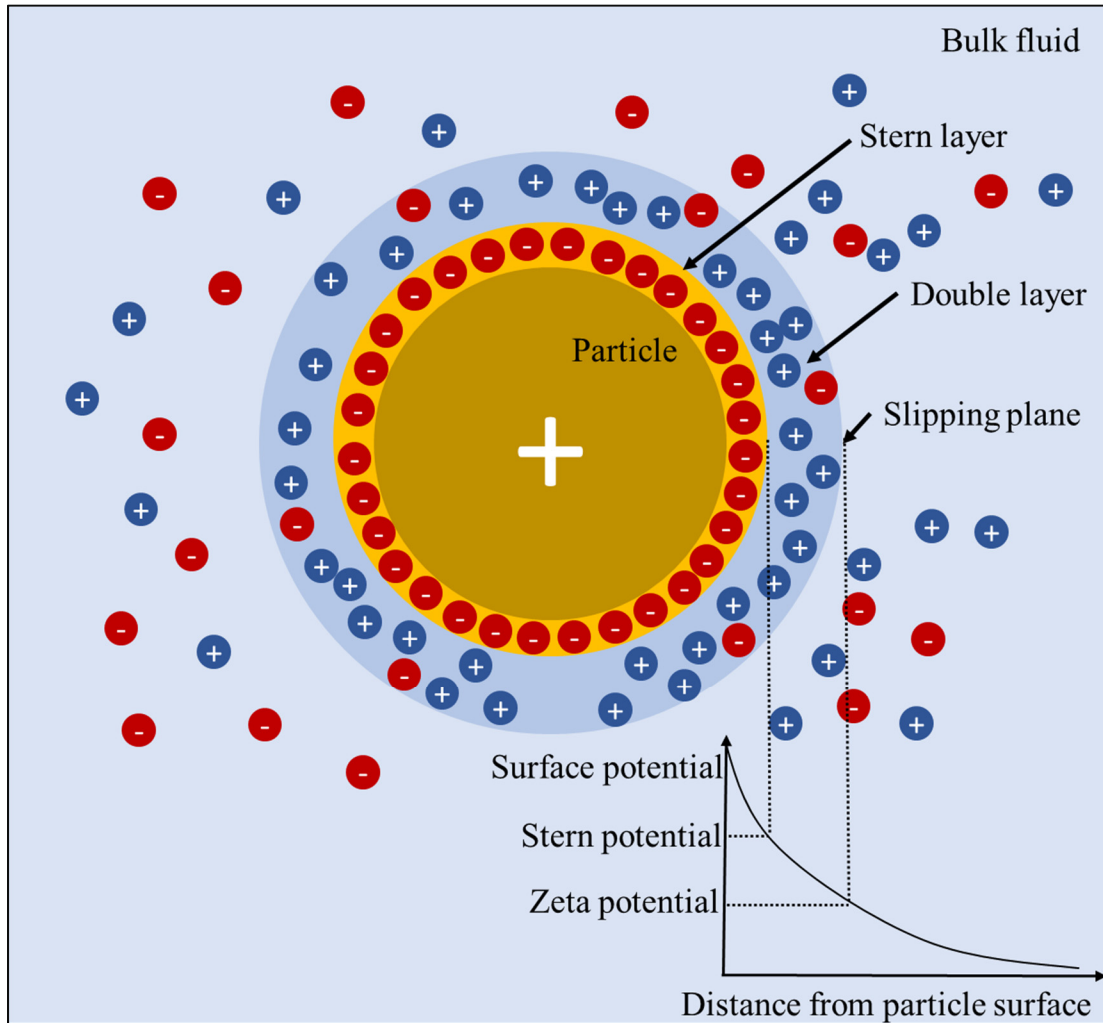


Figure 2.14 Diagram showing the potential as a function of the distance from the particle's surface in a colloidal dispersion



The zeta potential is calculated based on the electrophoretic mobility of particles suspended in a dispersant. Electrodes are in contact with the bulk material in which particles are diluted. An electric field is applied, and the average drift velocity is measured. This measurement is performed using a laser beam that passes through the sample, by measuring the frequency shift, the velocity of particles is calculated. By measuring this velocity, the electrokinetic potential in the slipping plane can be calculated, thus the zeta potential. In the experiments presented in this work, the equipment ZetaPlus (Brookhaven Instrument Corp.) was used. Measurements were performed at 25 °C unless differently stated.

#### **2.10.4 Transmission electron microscopy**

To image LNPs directly, TEM was used (Philips Tecnai T12 BioTwin electron microscope) (FEIT Technologies, USA), as shown in Figure 2.15. The microscope is equipped with a LaB6 filament and at 120 kV.



Figure 2.15 Philips Tecnai T12 electron microscope

First, liposomes were fixed in 2.5% Glutaraldehyde fixative solution. Then particles are absorbed into a carbon grid, which is surrounded by uranyl acetate stain (4%), which is quickly air-dried embedding the liposomes in the process. Liposomes appear bright in the electron microscope. Carbons grids were first glow discharged, so the hydrophilicity is increased. Samples were imaged at a magnification of 50 000x.

## **2.11 Chapter 2 conclusions**

In this chapter, liposome formation, general theory was presented using the nanoprecipitation method in micromixers. Liposomes are synthesized when lipids diluted initially in an organic solvent, self-assemble due to the polarity change caused by the replacement of this organic solvent by an aqueous solvent. The speed of the mix and uniformity influences the liposome size and size distribution. Micromixers generally provide laminar flow conditions which allow a controlled mixing interface and mixing times in the order of milliseconds. Micromixers that use multiple mixing strategies such as chaotic advection and Taylor dispersion have the potential to mix in the order of milliseconds without diluting too much the concentration of the reagents.

In general, this work methodology can be described as follows. First, the mixing principles used in micromixers were investigated, promising approaches were identified and further explored. To assess the mixing performance and operational conditions, we created state-of-the-art numerical models that enabled the evaluation of our proposed device. Later, this device was fabricated using soft lithography techniques, and further analysis was performed using mixing imaging techniques. Then liposomes were produced under various conditions using the PDM and characterized. Finally, the most critical factors controlling liposome properties were identified, model, and investigated in the PDM. Figure 2.16 shows the general methodology followed in this work.

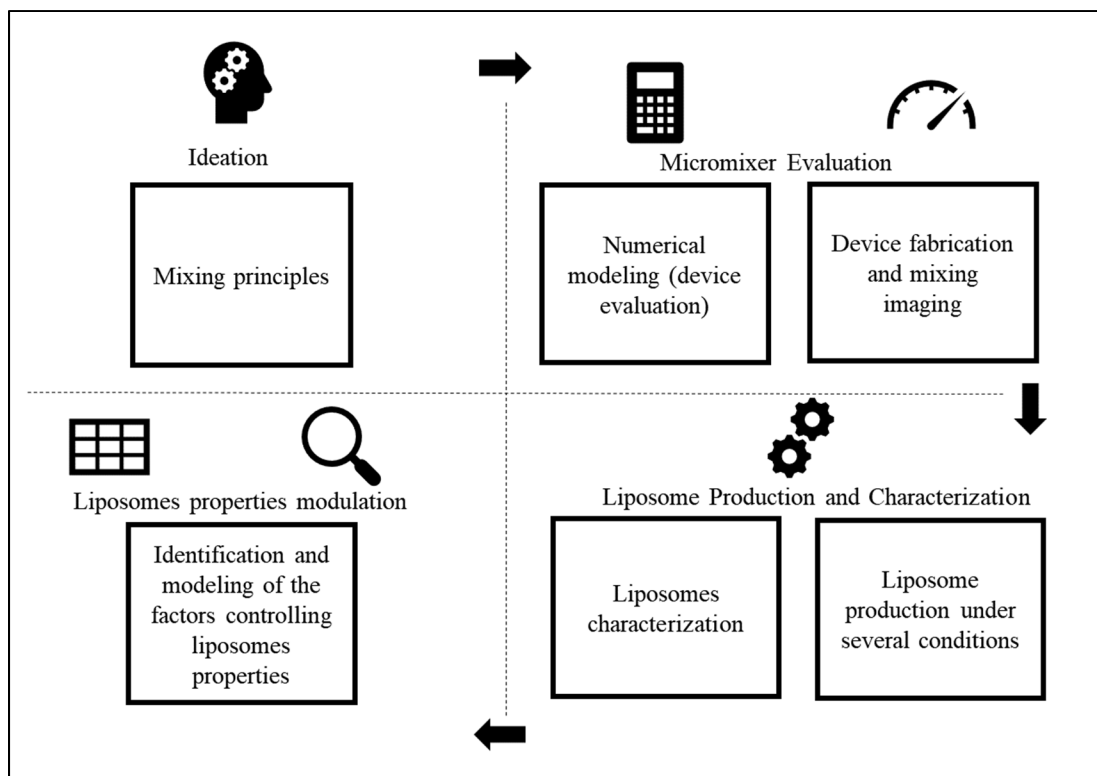


Figure 2.16 General methodology for investigating the liposome formation process in Dean Flow Dynamics based micromixers



## CHAPTER 3

### LIPOSOME PHYSICOCHEMICAL CHARACTERISTICS MODELING

Liposomes formation in micromixers is based on the general principle of nanoprecipitation. Each micromixer uses a specific set of principles, such as molecular diffusion, chaotic advection, and Taylor dispersion. These mixing principles determine liposome production conditions inside microfluidic devices and thus liposome physicochemical characteristics. Different factors might influence liposome properties such as TFR, FRR, temperature, mixing device, lipid mixture, concentration, among others. The most relevant factors, as well as the relationships between these variables, are unique to each micromixer. For example, the FRR is critical in controlling liposome size in MHF, because it modulates the disperse phase width and thus mixing diffusion path length. However, this variable is not so critical in the SHM, where TFR is closely related to liposome size. On top of that, the operational range conditions are determined by the geometry and microfabrication process.

In this chapter, Dean flow dynamics based micromixers are presented, especially the Periodic Disturbance Mixer. In section 3.1, we determined what are the most significant factors controlling liposome size, size distribution, and zeta potential, using screening experiments. In section 3.2, based on the screening experiments and available literature, the most critical factors controlling liposome properties were studied using design of experiments (DoE) and response surface methodology (RSM). The resulting model allowed us to find the levels of the factors required to produce liposomes from 50 to 200 nm, which is the size range of liposome formulations currently in the market (Sedighi et al., 2019). Moreover, a numerical model was used to explore the mixing influence over liposome properties.

Section 3.1 was partially presented in MicroTAS 2019, Basel Switzerland conference, as a poster, while Section 3.2 was published in Micromachines Journal.

### 3.1 Identifying the most significant factors.

Dean flow dynamics based micromixers create through curvilinear paths centrifugal forces. At a critical flow velocity values, these forces create vortices perpendicular to the main fluid advection direction, such as in the CEA (Jisun Lee et al., 2013), and our proposed device, the PDM (López et al., 2020). In the following section, we explore which factors are more important in controlling liposome properties for these two mixers.

#### 3.1.1 Screening experiments

Previously mentioned devices were fabricated using soft lithography, as described in Chapter 2.6. Both devices channels have a height of  $150\text{ }\mu\text{m}$ , a maximum mixing channel width of  $300\text{ }\mu\text{m}$  for an  $AR = 0.5$ . The semicircular structures have a radius of  $260\text{ }\mu\text{m}$ , while the CEA device has an expansion length of  $520\text{ }\mu\text{m}$  (space between semicircular structures). The PDM does not have one, to increase the density of semicircular structures, as shown in Figure 3.1.

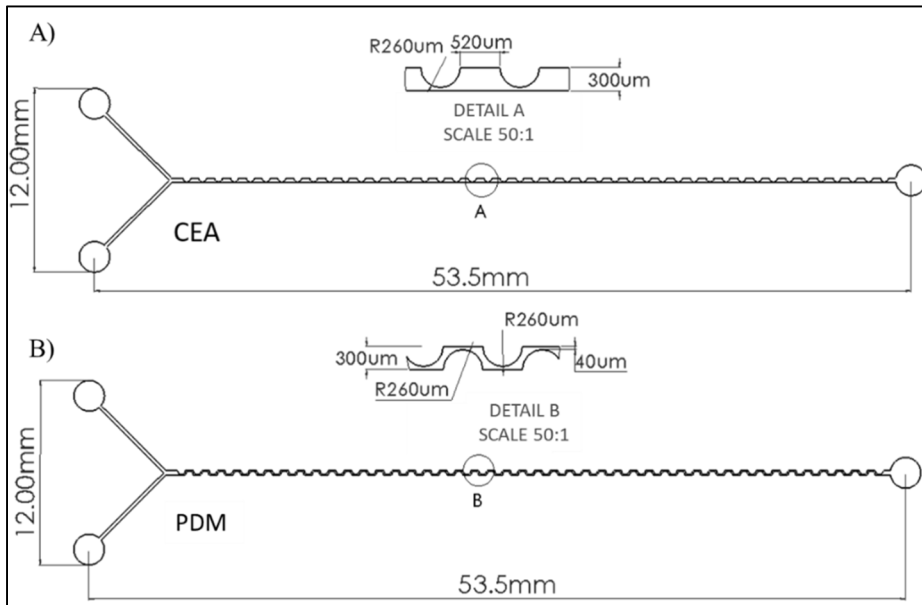


Figure 3.1 Dean Forces-based micromixers A) CEA based on flow lamination B) PDM, based on alternatively shifting centripetal forces

The most significant factors influencing liposome physicochemical characteristics were explored through a screening experiment. From the literature, we gather the factors that influence the performances of other types of micromixers. A Plackett-Burman (Plackett & Burman, 1946) experimental design was created using Minitab® 19, resulting in 12 experimental runs. This type of design objective is to remove the factors that do not significantly contribute to a given response. For the design, four continuous and two categorical factors were selected based on variables that can be tuned, each one at two different levels, as is shown in Table 3.1. FRR refers to the ratio between the flow of the PBS (aqueous solvent) and the lipids in ethanol (organic solvent). PBS was selected because of its extensive use in liposome production experiments. TFR refers to the combined flow of PBS and ethanol. Two different lipid mixtures were tested one containing DMPC, cholesterol, DHP in a molar ratio of 5:4:1; the second was a 1:1 molar ratio between DMPC and CHOL. The continuous factors range were chosen considering operational constraints

Table 3.1 Factors and levels tested in the experimental screening design

Name	Type	Low	High
<b>FRR</b>	Continuous	1	5
<b>TFR</b>	Continuous	6 mL/h	21 mL/h
<b>Lipid Type (<i>Lipid T</i>)</b>	Categorical	DMPC: CHOL 1 :1	DMPC: CHOL: DHP 5 :4 :1
<b>Initial Lipid Concentration (<i>IC</i>)</b>	Continuous	10 mM	40 mM
<b>Mixer Type (<i>MType</i>)</b>	Categorical	CEA	PDM
<b>Temperature</b>	Continuous	30 °C	70°C

The experimental screening design has 80% of changes in detecting effects of 1.68 standard deviations; its objective is to set a group of variables with a high probability of being significant to final liposome properties (see Figure 3.2 ) as a starting point for more detailed experiments.

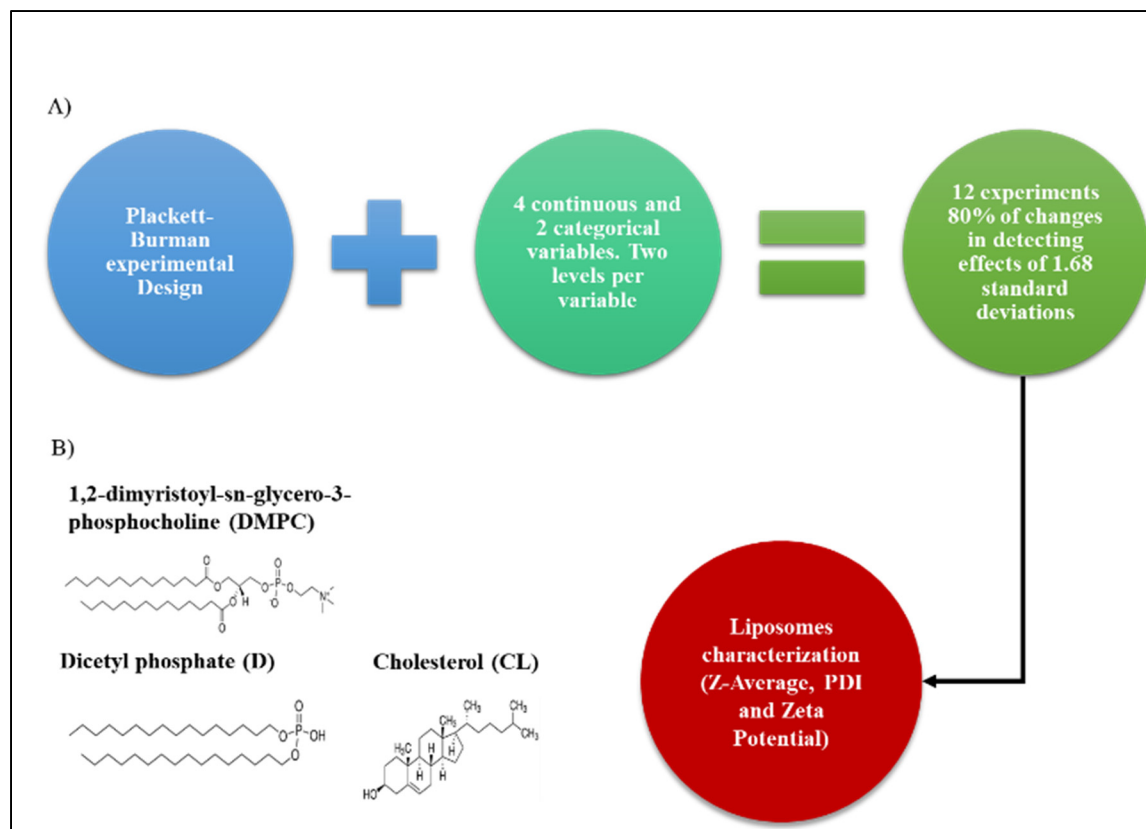


Figure 3.2 A) Screening experiments steps  
B) Lipids used in the screening experiments

Lipid and liposome production followed similar steps, as described in Chapter 2.8 and Chapter 2.9, except for the fact that no filters were used in the syringes, as shown in Figure 3.3. Liposomes were collected at the outlet without any further dilution. Liposomes characterization was performed using similar steps, as described in Chapter 2.10.1 and Chapter 2.10.3. The Z-average, PDI, and zeta potential of at least three independent measurements were taken. Samples with debris were filtered before characterization.



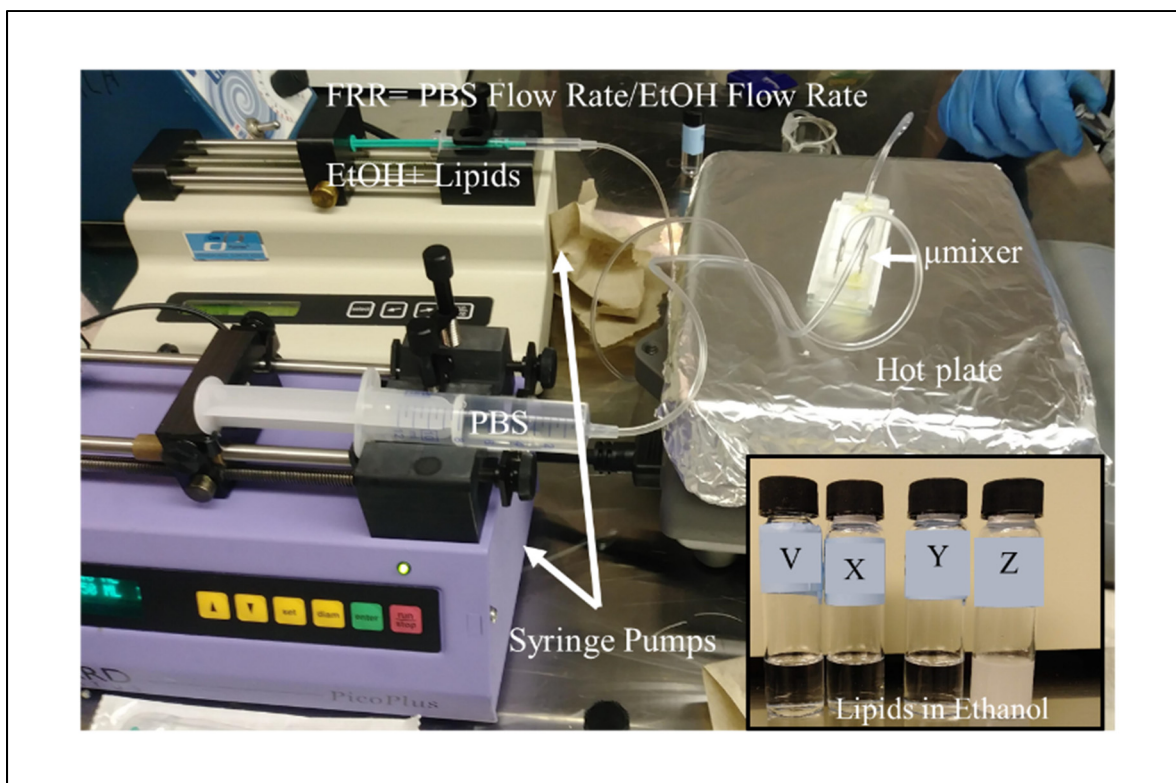


Figure 3.3 Experimental setup V) DMPC:CHOL:D 5:4:1 10 mM  
 X) DMPC:CHOL 1:1 40 mM Y) DMPC: CHOL 1:1 10 mM  
 Z) DMPC: CHOL: DHP 5:4:1 40 mM

### 3.1.2 Liposome size significant factors

The most significant factor in liposome Z-average (size) is the FRR, as is shown in Figure 3.4 in accordance with other works using micromixers such as the MHF (Andreas Jahn et al., 2007) and CEA (Jisun Lee et al., 2013) for this specific set of experiments. While the other factors are not statistically significant in this context, temperature, TFR, and concentration showed an inverse relationship to size. Additionally, the lipid mixture with a charged lipid produces slightly larger liposomes. Finally, the PDM produced smaller liposomes than CEA; however, this difference is not statistically significant.

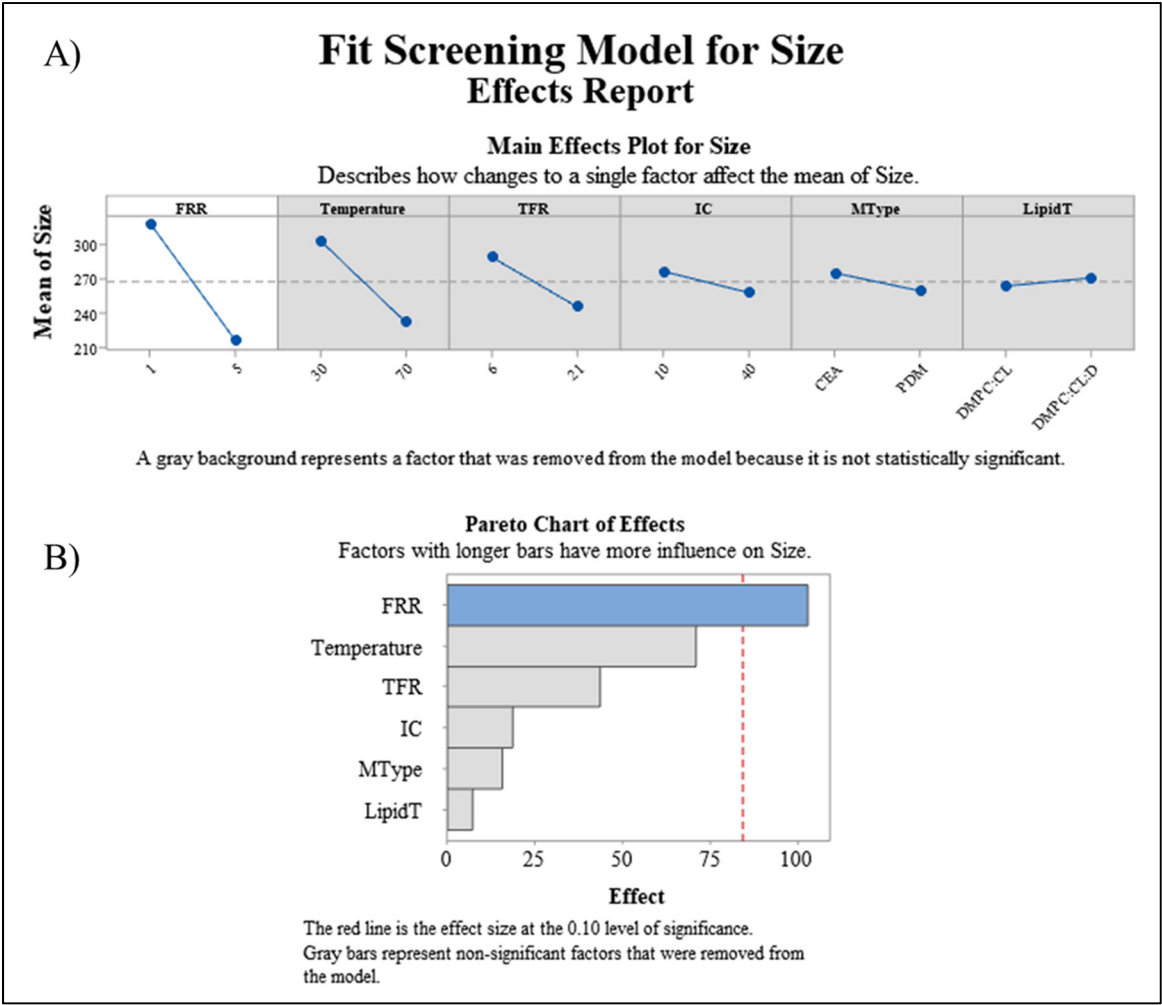


Figure 3.4 Fit screening model for size A) Main effects plots for size  
B) Pareto chart of effects

Figure 3.5 shows how FRR strongly affects liposome size. A higher FRR means a lower final concentration, thus smaller liposome size if we consider that fewer lipids are available to form liposomes.

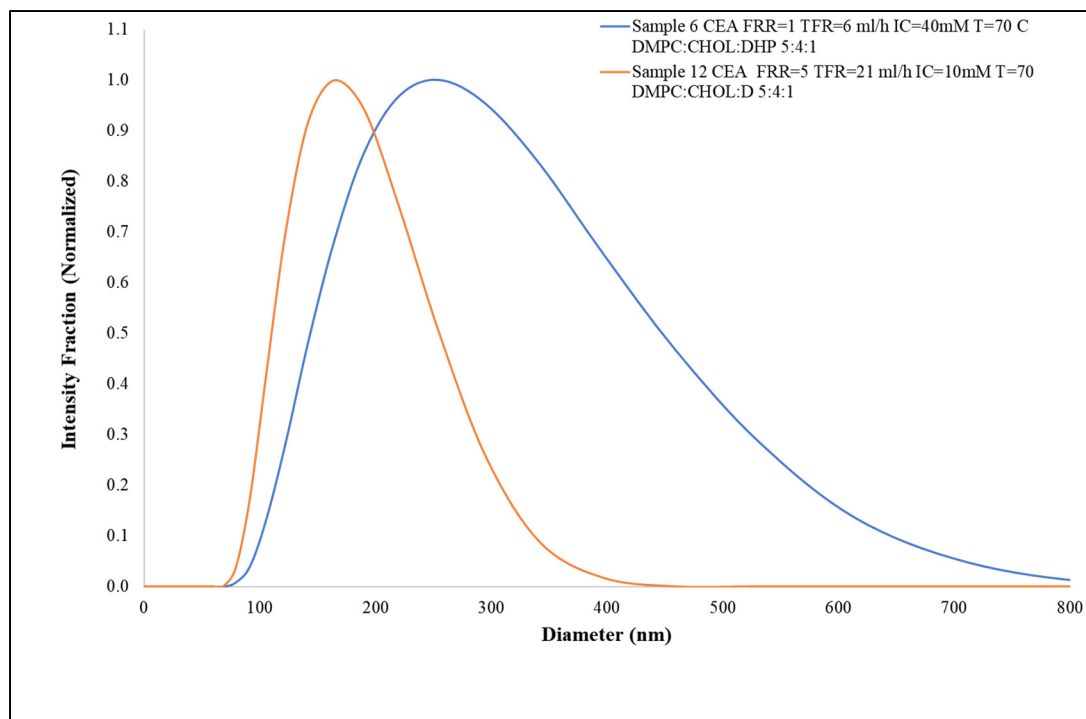


Figure 3.5 Normalized size distribution by intensity of two samples, produced by a CEA micromixer, in blue a Z-Average of 236.6 nm and in orange 160.7 nm for a FRR of 1 and 5

### 3.1.3 Liposome PDI significant factors

None of the studied factors shown to be statistically significant for the response PDI. However, this does not discard that the studied factors influence this response. Experiments presented in section 3.2.3.7, revealed a relationship with FRR.

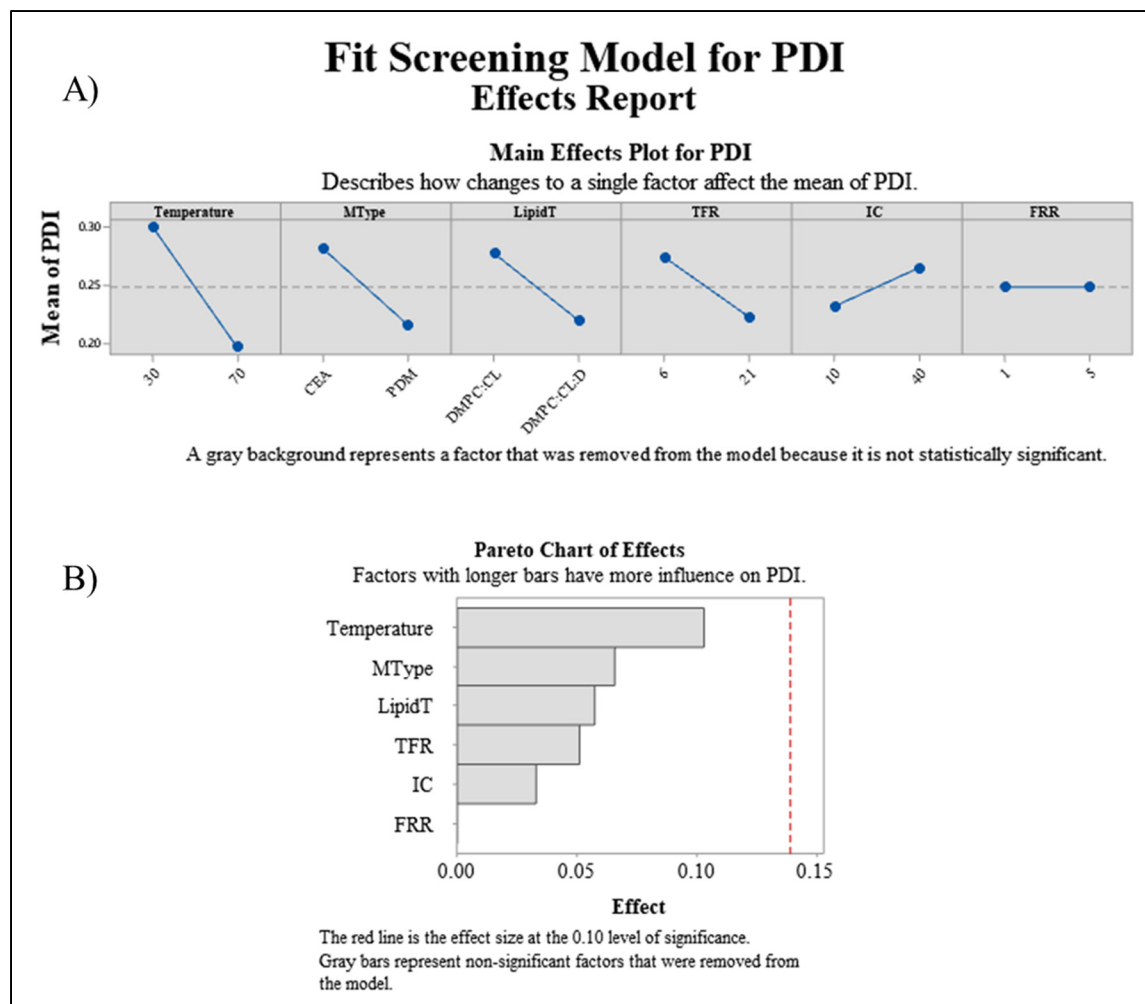


Figure 3.6 Fit screening model for PDI A) Main effects plots for PDI  
B) Pareto chart of effects

### 3.1.4 Liposome zeta potential significant factors

Three factors were shown to be statistically significant for the response zeta potential (ZP). The first one by far the most notable is the lipid mixture LipidT. In this set of experiments, we tested two similar mixtures. The first one contained only DMPC and Cholesterol, while the second also contained DHP, a negatively charged lipid. This charged lipid addition resulted in a clear difference between these two levels of the factor LipidT.

Additionally, TFR and Temperature showed a statistically significant influence over zeta potential for this set of experiments. However, this change in zeta potential was small. In subsequent experiments through this work, this hypothesis was tested.

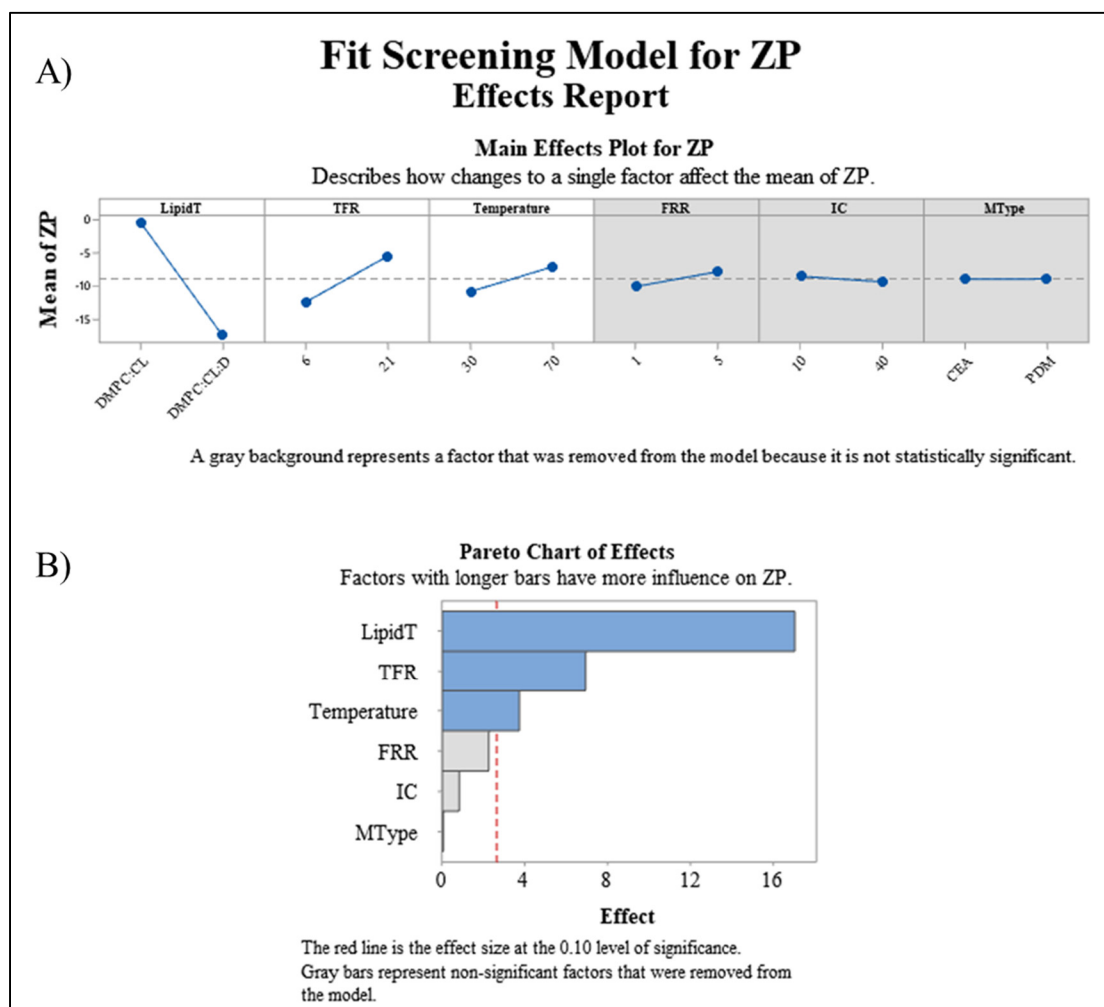


Figure 3.7 Fit screening model for zeta potential  
A) Main effects plots for PDI B) Pareto chart of effects

### 3.1.5 Conclusions on the most significant factors

The screening experiments, together with previous works in literature, pointed in the direction of the significant factors controlling liposome physicochemical properties in the PDM and

CEA, FRR, TFR, Temperature, and Lipid Mixture showed to influence the physicochemical properties of liposomes. In the next section, we investigated the first two variables, while in subsequent chapters, the other variables are explored.

### **3.2 Surface response-based modeling of liposome characteristics in a periodic disturbance mixer**

In this section, we used our own designed and fabricated PDM to produce liposomes. We used DoE and RSM to statistically model the relationship between the TFR and the FRR with the resulting liposome physicochemical characteristics.

#### **3.2.1 Introduction**

The modeling and optimization of the produced liposome characteristics using advanced statistical tools have proved to be useful for finding the suitable flow conditions under which LNPs can be synthesized in micromixers such as the SHM for drug delivery systems (Kastner et al., 2014; Sedighi et al., 2019) and the MHF for gene delivery applications (Tiago A. Balbino et al., 2013). This statistical characterization is necessary, given the complicated relationship between the factors controlling liposome properties. These properties vary from one micromixer to another, depending on their mixing principles, as well as other factors encountered at a molecular level (Bleul, Thiermann, & Maskos, 2015).

Previously presented results in Section 3.1 and published elsewhere (López Salazar et al., 2019) were used as a guide for exploring the factors controlling liposome physicochemical properties.

In this section, we used a Dean flow dynamics-based micromixer with a novel design using a curvilinear mixing channel to induce an alternatively changing force vector, called PDM. DoE and RSM were used to model and optimize liposome size, size distribution, and zeta potential. This methodology enables us to rapidly screen, optimize, and predict final liposome characteristics that otherwise would be time-consuming, e.g., study one factor at the time. We

demonstrated that our model was able to predict an experimental region where size-controlled liposomes ranging from 52 nm to 200 nm were produced. Finally, through numerical modeling, our work offers a glance at the relationship between the mixing performance of the proposed device and the properties of liposomes.

### 3.2.2 Materials and methods

While the general materials and methods are described in Chapter 2, in the following sections, the specific details for this section experiments are described.

#### 3.2.2.1.1 Micromixer device fabrication and design

The PDM used for the following experiments was fabricated, as described in Chapter 2.6. The AR of this device mixing channel in its widest part is one. It consists of two inlets in one extremity that convey fluid from a Y-shape into a mixing channel with 90 semicircular structures and an outlet at the other extremity, as shown in Figure 3.8A. Figure 3.8B shows a microscopy image of the device first mixing structures.

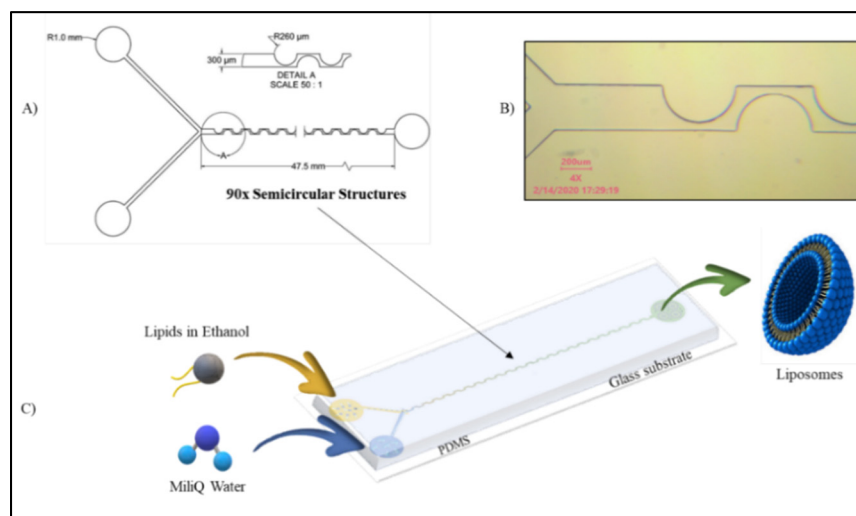


Figure 3.8 Periodic disturbance micromixer A) Microchannel dimensions B) Microscope image of the PDM C) Schematic representation of the liposome formation process

#### **3.2.2.1.2 Lipid and Liposome Preparation**

Lipids and liposomes were prepared according to Section 2.8 and Section 2.9 methods. 1,2-DMPC, cholesterol, and DHP (Sigma-Aldrich, Oakville, Canada) were mixed in a molar ratio 5:4:1. The mixture was then re-dissolved in ethanol to a final concentration of 5 mM. All previously described liquids were filtered using 0.22  $\mu\text{m}$  filters. The syringes were connected separately to each of the inlets in the previously described microfluidic device (Figure 3.8C) through 0.22  $\mu\text{m}$  filters to avoid bubble generation and debris. The process temperature was set to 70 °C, this value considered the lipids transition temperature, and, at the same time, it was set below ethanol's boiling point, which is 78 °C. Another reason to choose this temperature was that previous studies have shown that increasing temperature reduces liposome size (Zook & Vreeland, 2010). The flows were defined according to Equation (2.13) and Equation (2.14)

#### **3.2.2.1.3 Liposome Characterization**

Liposomes characterization was performed according to Section 2.10.3 and Section 2.10.1. Five hundred microliters of each sample was placed in a low-volume disposable cuvette. The average hydrodynamic diameter (Z-Average) and PDI of at least three independent measurements were recorded per sample. Liposomes collected from the outlet were further diluted for a final lipid concentration of 0.04 mg/mL. This concentration proved to yield high-quality measurement results. Liposome zeta potential was measured by placing each sample in a disposable cuvette (1850  $\mu\text{L}$ ). Zeta potential average is a result of 2 stable cycles and ten measurement repetitions.

#### **3.2.2.1.4 Design of Experiments**

Liposome final characteristics such as size, size distribution, and zeta potential relationship with flow conditions were modeled using RSM and DoE. RSM enables the evaluation of multiple factors or variables and their interactions influence on one or more responses, using



regression analysis. This methodology allows us to predict and optimize process responses (Silva, 2018). The use of DoE as opposed to One Factor At the Time (OFAT) allows interpreting interactions of two variables at the same time, as well as reducing the number of required experiments to model the liposome production process and time. In this work, TFR and FRR are considered factors independent process variables, while Z-Average (liposome diameter), PDI (size distribution), and zeta potential are considered responses.

The region of interest for the variables was delimited, considering the micromixer operational integrity and conditions under which a stable flow regime could be achieved. Table 3.2 shows the initial low and high values for each factor.

Table 3.2 Initial low and high experimental levels per variable

Name	Type	Low (Coded Value)	High (Coded Value)
<b>FRR</b>	Continuous	1.0 (−1)	12.0 (1)
<b>TFR</b>	Continuous	3.0 mL/h (−1)	18.0 mL/h (1)

A two-variable central composite circumscribed rotatable (CCCR) Design was created using the software Minitab® 19, considering the values in Table 3.2. This experimental design predicted that the variance is only dependent on the distance from the center point. This design is used for quadratic models.

The optimized experimental design resulted in 29 experimental points, 4 axial points with 3 repetitions each that are the extreme values above and below the low and high settings, 4 cube points with 3 repetitions each that are the initial low and high values, and one center point with 5 repetitions that are in the middle between the cube points. The value  $\alpha$ , which represents the distance between the center point and an axial point in coded units. The value was calculated as follows:

$$\alpha = [2^k]^{\frac{1}{4}} \quad (3.1)$$

Where  $k$  is the number of factors, in this case, 2 for a final  $\alpha = 1.41$ . The order of experimental runs was randomized. The continuous value for each experimental point was calculated by converting the coded value scale to the continuous value. Due to pumps resolution, values were rounded to 1 decimal position. Figure 3.9 shows the graphical representation of the experimental space and points for the two factors TFR and FRR.

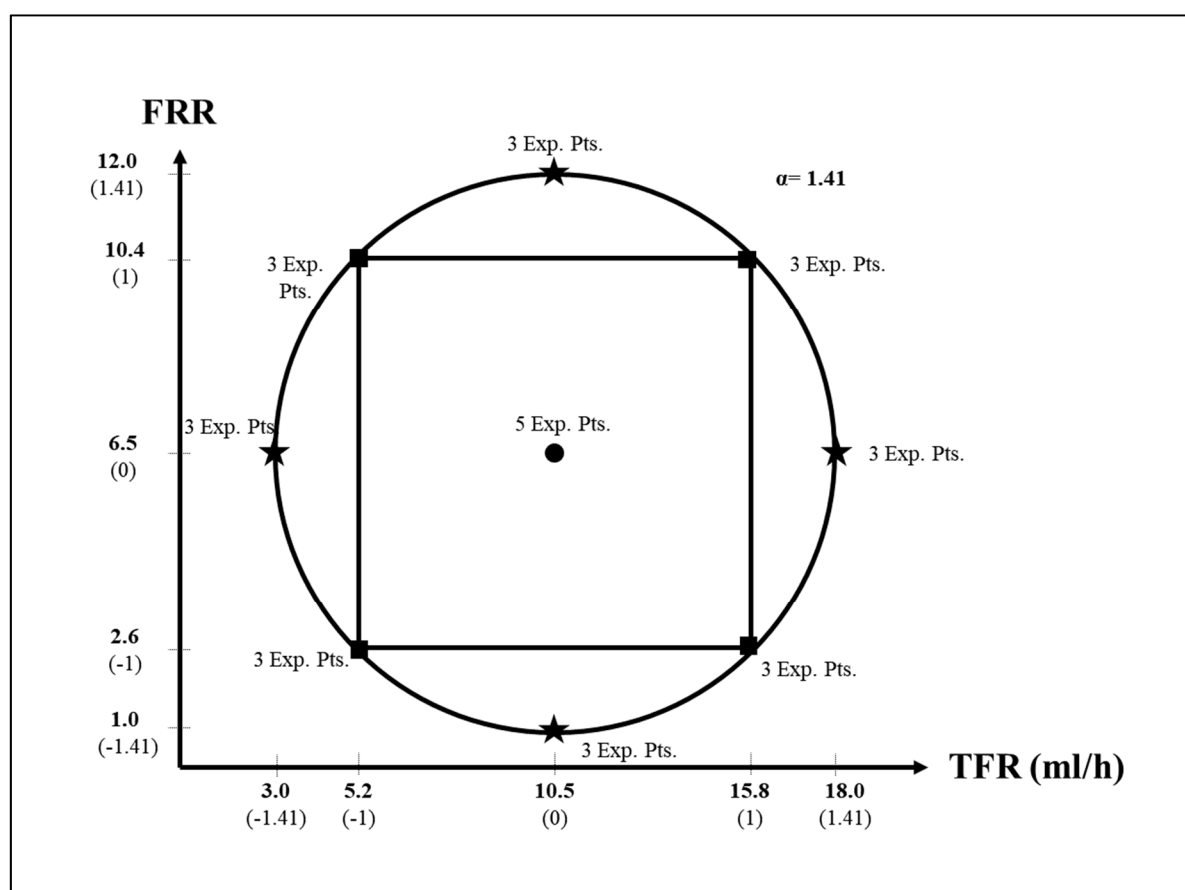


Figure 3.9 CCCR design graphical representation

Finally, a surface response model of second order with interactions was fitted for Z-average and PDI. Later, the model was assessed using analysis of variance (ANOVA) to identify the goodness of fit of  $R^2$ ,  $R^2$  (predicted), and model significance as well as each of the terms predicting liposome size and PDI ( $p = 0.05$ ). The best model, among them, was chosen

considering the statistics results. A post hoc Tukey test  $p = 0.05$  was used to evaluate PDI and zeta potential groups. A paired t-test was used to assess liposome stability statistically. All previously described tests were performed using the software Minitab® 19.

### 3.2.2.1.5 Mixing Efficiency Calculation using Numerical Modeling

The micromixing phenomenon was numerically modeled using Navier-Stokes equations coupled with the convection–diffusion equation as shown in Section 2.5 and the ME was calculated using Equation (2.7).

## 3.2.3 Results and discussion

The liposome characterization results from the CCCR experimental design were used to create through response surface methodology, a model capable of predicting Z-average, PDI, and zeta potential. Finally, model predictions were compared with an experimental validation run. These results were discussed and related to mixing efficiencies in the PDM.

### 3.2.3.1 Liposome properties DOE results

We investigated the influence of FRR and TFR using the experimental design shown in Table 3.3 . The coded values are in parenthesis. The resulting responses: i.e., liposome size (Z-average), PDI, and Zeta Potential, are given on the right side of the same table.

Table 3.3 CCCR design results for the 29 runs

Run Order	Factors		Responses		
	FRR	TFR (mL/h)	Z-Average (nm)	PDI	Zeta Potential (mV)
1	6.5 (0)	3.0 (−1.41)	133.50	0.185	−31.6
2	1.0 (−1.41)	10.5 (0)	190.70	0.060	−38.8
3	10.4 (1)	15.8 (1)	67.52	0.202	−23.1
4	6.5 (0)	18.0 (1.41)	66.63	0.185	−29.8

Run Order	Factors		Responses		
	FRR	TFR (mL/h)	Z-Average (nm)	PDI	Zeta Potential (mV)
5	12.0 (1.41)	10.5 (0)	75.09	0.232	-37.9
6	10.4 (1)	5.2 (-1)	133.5	0.174	-32.1
7	2.6 (-1)	5.2 (-1)	119.40	0.223	-35.2
8	2.6 (-1)	15.8 (1)	86.48	0.217	-29.9
9	6.5 (0)	10.5 (0)	81.81	0.207	-32.3
10	6.5 (0)	3.0 (-1.41)	120.70	0.179	-24.6
11	1.0 (-1.41)	10.5 (0)	197.00	0.072	-28.5
12	10.4 (1)	15.8 (1)	62.10	0.270	-28.8
13	10.4 (1)	5.2 (-1)	120.20	0.170	-33.9
14	6.5 (0)	18.0 (1.41)	57.14	0.238	-33.8
15	12.0 (1.41)	10.5 (0)	74.14	0.245	-30.7
16	2.6 (-1)	5.2 (-1)	122.4	0.207	-31.5
17	2.6 (-1)	15.8 (1)	88.74	0.221	-36.3
18	6.5 (0)	10.5 (0)	72.23	0.230	-37.7
19	6.5 (0)	10.5 (0)	73.81	0.235	-27.6
20	6.5 (0)	3.0 (-1.41)	116.00	0.189	-26.9
21	1.0 (-1.41)	10.5 (0)	199.70	0.064	-29.6
22	10.4 (1)	15.8 (1)	52.71	0.228	-28.2
23	10.4 (1)	5.2 (-1)	110.4.	0.184	-37.7
24	6.5 (0)	18.0 (1.41)	52.14	0.265	-34.4
25	12.0 (1.41)	10.5 (0)	73.80	0.247	32.4
26	2.6 (-1)	5.2 (-1)	131.60	0.206	-36.5
27	2.6 (-1)	15.8 (1)	90.27	0.241	-30.2
28	6.5 (0)	10.5 (0)	77.18	0.223	-27.6
29	6.5 (0)	10.5 (0)	77.24	0.262	-30.1

Liposome size ranged from 52 nm to 200 nm for the tested experimental conditions. PDI oscillated between 0.060 (highly monodisperse populations) to a maximum of 0.270 (low

polydispersed populations). Lastly, zeta potential varied in a range from  $-37.7$  mV to  $-24.6$  mV.

Liposomes produced under the same experimental conditions showed a maximum standard deviation of  $11.48$  nm in size and a minimum of  $0.43$  nm. These variations might have been caused by batch to batch lipid preparation variations and unpredicted bubbles generated inside mixing channels that can disturb the stability of the flow's interface.

### 3.2.3.2 Liposome Size (Z-Average) Modeling

First, a full quadratic surface response model was fitted using FRR and TFR as independent factors and Z-average (size) as a response. A one-way ANOVA analysis was performed for each term in the model. Then the model was reduced, considering the level of significance of each term. All terms with a  $p > 0.05$  were ignored. A new surface response model was run to increase the prediction precision or  $R^2$ -predicted. Equation (3.2) shows the final surface response model. Note that  $TFR^2$  and  $TFR \cdot FRR$  were removed because they yielded a  $p > 0.05$ .

$$Z_{average} = 236.3 - 26.95 FRR - 4.437 TFR + 1.573(FRR)^2 \quad (3.2)$$

Figure 3.10 shows the surface response model derived from the data, as well as the  $R^2$ ,  $R^2$ -adjusted, and  $R^2$ -predicted. The linear factors TFR and FRR reduce liposome size; on the other hand,  $FRR^2$  avoids further liposome size reduction for a value above  $8.56$ .

The factors FRR and TFR showed a considerable influence over the final liposome size, this in accordance with previous works in the field for other types of mixers such as the MHF micromixer (A. Jahn et al., 2015), the Staggered Herringbone Micromixer (Belliveau et al., 2012), and Dean Forces based micromixers (Kimura et al., 2018; Jisun Lee et al., 2013). Compared to other statistical models for SHM and MHF geometries (Tiago A. Balbino et al., 2013; Kastner et al., 2014), the  $R^2$  values are similar. Our model did not show curvature for TFR, indicating a simple linear interaction related to this variable and liposomes size.

Considering that drug delivery systems require liposomes with a size range from 45 nm (DauXome®) to 180 nm (Myocet®) (Sedighi et al., 2019), we used the model to identify the flow conditions that could lead to this size range with an emphasis in finding the minimum realizable liposome size.

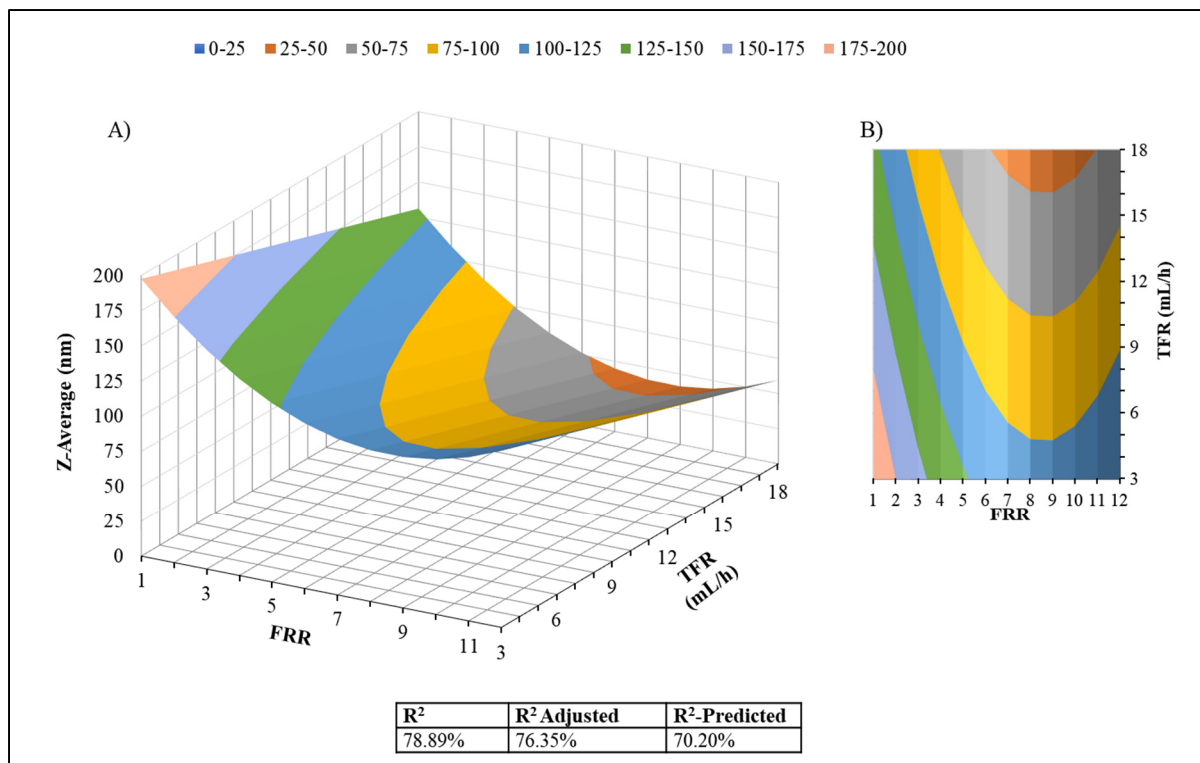


Figure 3.10 Surface Response Model derived from the Central Composite Circumscribed Rotatable Design Data. The model level of significance is  $p < 0.05$  A) 3-dimensional B) Contours representation

We used the model and optimized the factor values without restrictions within the experimental range to minimize the function, which, in this case, is liposome size (Z-average). The minimum average size predicted was 41.07 nm, with a 95% confidence range between 25.10 nm and 57.03 nm. The factors levels are FRR = 8.56 and TFR = 18 mL/h.

### 3.2.3.3 Polydispersity Index Modeling

The PDI range in the experimental results is from 0.06 to 0.27, or from highly monodisperse populations to low polydispersed populations. These values are comparable with MHF and SHM micromixers for liposome production.

We proceeded using a similar approach to analyze the influence of the two factors, FRR and TFR, over the response PDI. In this case, we also eliminated terms that are not statistically significant ( $p > 0.05$ ), as in the previous model. The quadratic term  $TFR^2$  and the interaction term  $TFR \cdot FRR$  were eliminated. Equation (3.3) shows the final model with four terms.

$$PDI = 0.0663 + 0.03181 FRR + 0.00319 TFR - 0.001905(FRR)^2 \quad (3.3)$$

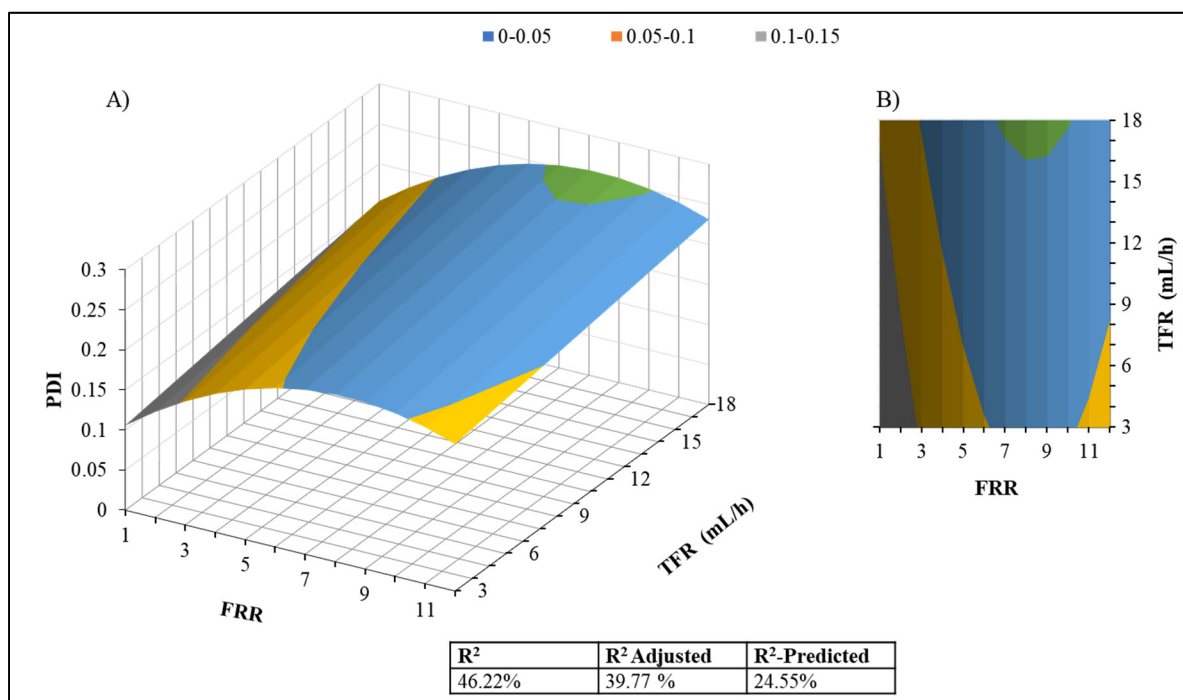


Figure 3.11 PDI Surface Response Model as well as the  $R^2$ ,  $R^2$ -adjusted, and  $R^2$ -predicted. The model has a  $p < 0.05$   
 A) 3-dimensional B) Contours representation

The surface response model for PDI is shown in Figure 3.11. Equation (3.3) shows that the value of the PDI is proportional to the  $FRR^2$  and TFR. Most of the model results for PDI are ranging between 0.1 and 0.3 for the experimental range.

To better understand the reasons behind  $R^2$  results, we performed a Tukey pairwise comparison to group the significantly different PDI means (95% confidence level), as shown in Table 3.4.

Table 3.4 Grouping information using the Tukey method at a 95% confidence level

Condition	N	Mean	Grouping		
<b>9 (FRR = 12.0 TFR = 10.5)</b>	3	0.24	A		
<b>6 (FRR = 6.5 TFR = 18.0)</b>	3	0.24	A	B	
<b>4 (FRR = 6.5 TFR = 10.5)</b>	5	0.23	A	B	
<b>3 (FRR = 2.6 TFR = 15.8)</b>	3	0.22	A	B	
<b>2 (FRR = 2.6 TFR = 5.2)</b>	3	0.22	A	B	
<b>7 (FRR = 10.4 TFR = 15.8)</b>	3	0.21	A	B	
<b>8 (FRR = 10.4 TFR = 5.2)</b>	3	0.18		B	
<b>5 (FRR = 6.5 TFR = 3.0)</b>	3	0.18		B	
<b>1 (FRR = 1.0 TFR = 10.5)</b>	3	0.07			C

The comparison detected three entirely statistically different conditions among the nine tested in this work for the PDI, with a mean of 0.07, 0.18, and 0.24. It could be inferred from the experimental conditions that a low FRR value results in highly monodisperse populations; however, above  $FRR = 2.6$ , the PDI values are mostly the same and only when  $FRR = 12.0$ , another PDI population appears. This behavior might indicate that the PDM has well-delimited operation regimes.

### 3.2.3.4 Zeta Potential Relationship with TFR and FRR

Finally, the zeta potential values range was limited from  $-38.8$  to  $-23.1$  mV on average. The means of each condition are not statistically significantly different from each other, according



to grouping information using the Tukey method and 95% confidence. Figure 3.12 shows the zeta potential for the nine different conditions. This factor showed itself to be independent of TFR and FRR; thus, the model was not significant.

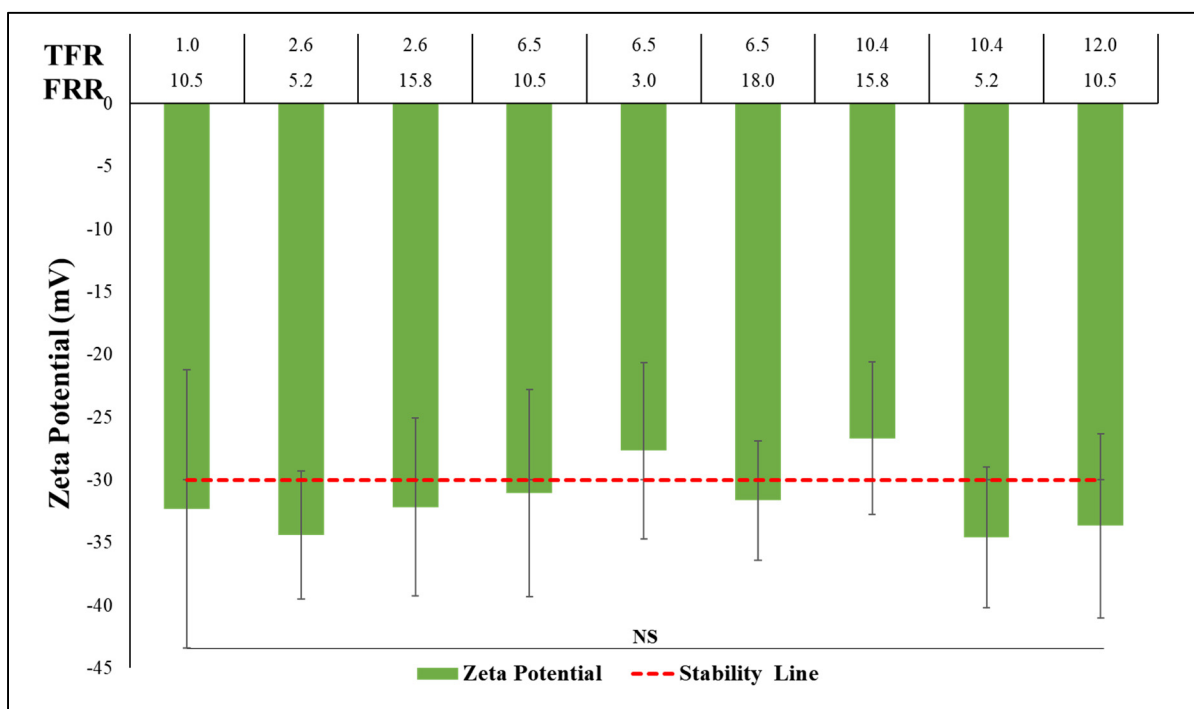


Figure 3.12 Zeta potential measurements result for the nine different conditions. The error bars show  $1.96\sigma$ , indicating the limits of 95% confidence ( $n = 3$ )

### 3.2.3.5 Statistical Model for Controlling Liposome Characteristics

The statistical information, together with the models, indicates that liposome size could be tuned by modifying TFR and FRR. On the other hand, PDI has three different groups, which might be related to the micromixer operation regime. Finally, neither the TFR nor FRR has any influence over zeta potential results using a PDM. Results from other types of micromixers indicate that only composition plays a role in liposome zeta potential (Shende, Ture, Gaud, & Trotta, 2019). Table 3.5 shows a summary of the statistical models.

Table 3.5 Statistically significant coefficients for each model  
( $p < 0.05$ ) and model statistics summary

Response	Significant Coefficients	R <sup>2</sup>	P-value	F-value
Size	FRR, FRR <sup>2</sup> , TFR	78.89%	$1 \times 10^{-8}$	31.14
PDI	FRR, FRR <sup>2</sup> , TFR	46.22%	0.001	7.16
Zeta Potential	None	NA	NA	NA

### 3.2.3.6 Model Prediction vs. Experimental Validation Run

The flow conditions which the model predicted would lead to the minimum liposome size were validated, as were the conditions in the vicinity of the prediction. The model predicted a minimum size at approximately FRR = 9 and TFR = 18 mL/h. The predicted size was 41 nm. Figure 3.13 shows the size immediately after production, after six months, and the predicted size using the model presented previously. The model predicted, with reasonable accuracy, the size for an FRR of 3, 5, and 12. The size for FRR of 1, 7, and 9 was out of the Standard Error (SE) fit value. Liposome size reduction reaches a plateau before reaching high FRR values.

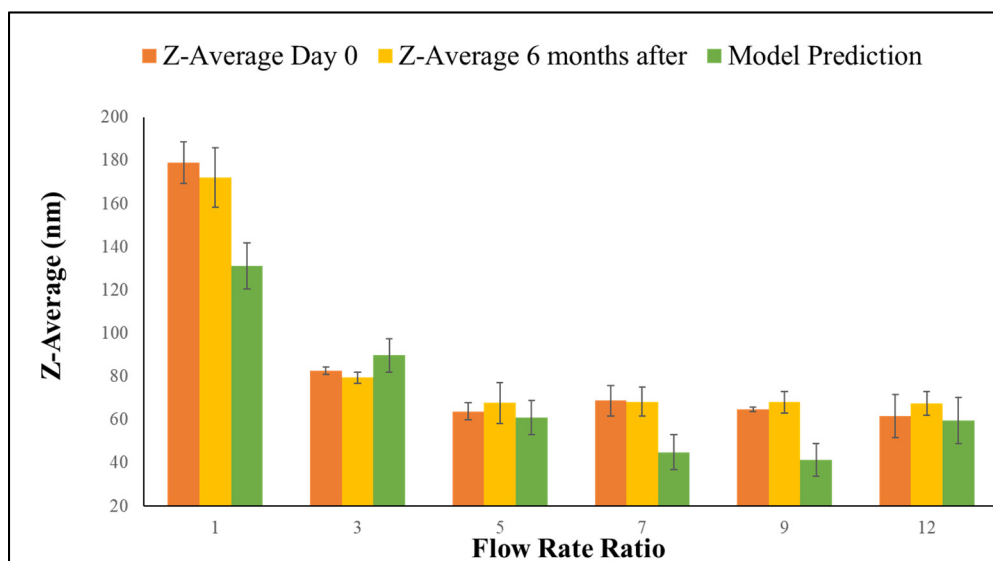


Figure 3.13 Z-average (nm) vs. FRR ( $n = 3$ ). Error bars indicate  $\pm 1$  standard deviation (SD) for samples and SE fit for the model prediction.

These results may represent the limit for the presented conditions and the PDM. This size plateauing at high FRR is found in other types of micromixers such as the VFF (R. R. Hood & DeVoe, 2015) and recently published 3D printed devices for liposome production (Chen et al., 2019). The asymptotic behavior of the liposome size is challenging to predict using a quadratic model.

Moreover, there was not a statistical difference in liposome size six months after production. This result indicates the high stability of the liposome nanoparticles produced, which suggests a suitable shelf life of such a product.

Finally, the PDI for measurements performed immediately after liposome production, six months after, and the model predictions were compared, as shown in Figure 7. In this case, even if the model is not a good fit ( $R^2$ -predicted = 24.55), it predicted values that are close to the measured values due to the low variation of PDI and because of the change induced by FRR is minimal. It could be considered that PDI is independent of the experimental range for values above  $FRR = 3$ , indicating an intrinsic process property. Number-wise, PDI values do not change significantly. However, this variation has an impact on liposome population classification between monodispersed and low polydispersed populations.

### 3.2.3.7 Relationship Between the Mixing Process and Liposome Properties

To investigate further Z-average and PDI results, the mixing efficiencies inside the microchannel were evaluated using the numerical model detailed in section above. Liposomes are formed when lipids initially diluted in ethanol agglomerate first in intermediate disk-shaped structures due to the polarity change caused by the mix of ethanol and water. As the polarity continues to increase, as a consequence of a lower ethanol concentration in the binary mixture, these disk-shaped agglomerates are forced to close into spheres to avoid lipids tails exposure to a high polarity value media (Lasic, 1988). How fast the transition occurs from agglomeration to self-assembly highly determines liposome size (Maeki et al., 2017). The mixing speed and uniformity modulate this transition from low polarity to high polarity.

In the presented validation experiments, FRR modulated the speed at which ethanol and water mixed, as illustrated in Figure 3.14. The separation between where each condition crosses 90% of mixing efficiency is reduced at each step. This feature closely relates to liposome size decrease as shown in Figure 6. Moreover, the slope of the curve for  $FRR = 1$  is very different compared to all the other conditions. The latter indicates that PDI might be modulated by the speed at which mixing efficiency increases.

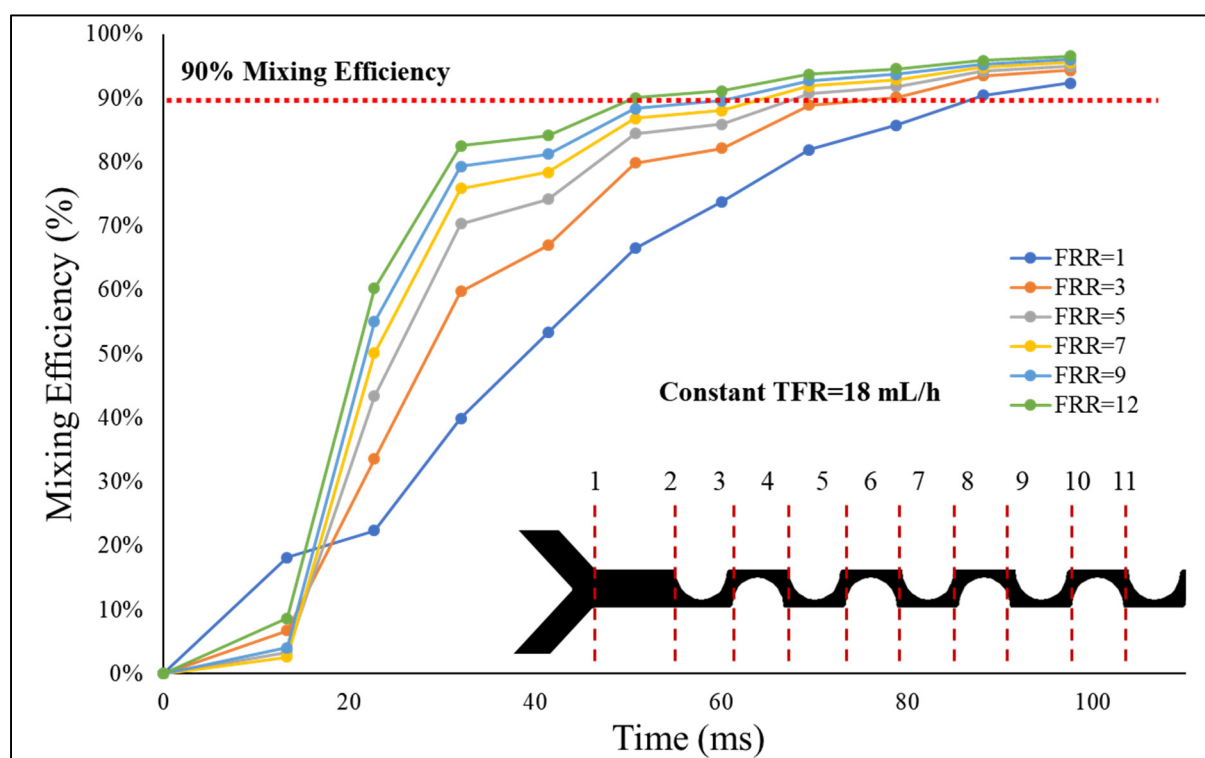


Figure 3.14 Mixing efficiency at different FRRs. Each data point corresponds to a cross-section for a total of 11 data points from 1–11

The relationship between concentration profiles uniformity and PDI has been investigated for VFF mixers (R. R. Hood & DeVoe, 2015), where the aspect ratio controls the concentration profile uniformity. By contrast, in the PDM, FRR modulates the profile uniformity. PDI results indicate that a threshold value separating monodispersed populations and low polydisperse populations exist at  $FRR \geq 3$ . These results could be related to a more uniform mixing profile at  $FRR = 1$  compared with other FRR values. FRR defines the width of the diluted species at

the beginning of the channel. Higher FRRs values mean a narrower ethanol interface, which allows a faster dispersion perpendicular to the main advection direction resulting in smaller liposomes. Although higher FRRs results in non-uniform concentration profiles that might result in more polydisperse populations. This difference in the concentration profile is illustrated in Figure 3.15 in different cross-sections for FRR = 1 and FRR = 3.

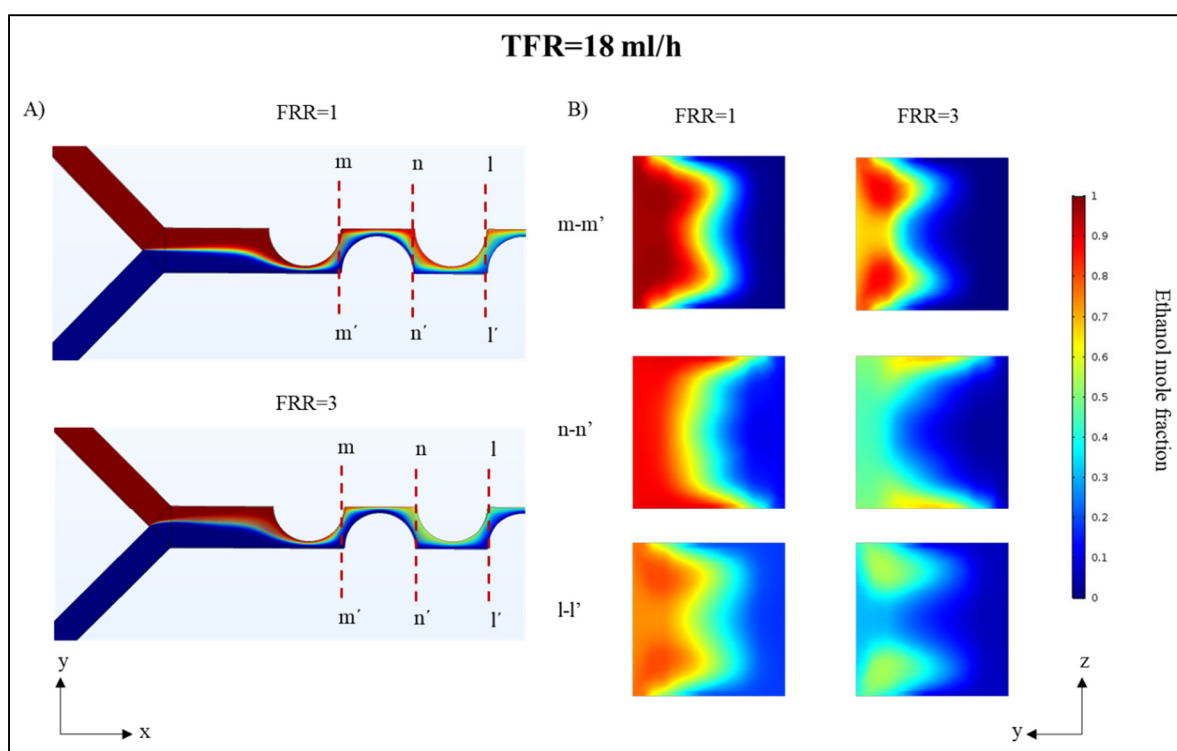


Figure 3.15 Numerical simulations comparing the concentration profiles at FRR = 1 and FRR = 3 at a constant TFR = 18 mL/h A) Top view of the mixing channels and position of the cross-sections B) Cross-sections at different FRRs

### 3.2.4 Conclusions

In this work, we used DoE and RSM to model, control, and optimize liposome properties in a Periodic Disturbance Mixer. FRR and TFR control liposome Z-average (size), as the model predicted. On the other hand, PDI showed three statistically distinct mean values, indicating likely operating regime ranges. One of these PDIs is remarkably different from the other two

at low FRR. This behavior could suggest that centripetal forces start to produce Dean vortices only after specific flow conditions are reached in our proposed micromixer. Lastly, zeta potential values under different experimental conditions are not statistically different from each other, indicating that FRR and TFR do not influence this variable. These results also suggest that the liposomes' zeta potential is controlled by another factor not studied in this work.

The size range of liposomes produced by our proposed device is comparable to currently available liposome formulations in the market.

Additionally, through numerical simulations, we investigated the relationship between the mixing conditions in the PDM and liposome properties such as size and PDI. Mixing time was related to liposome size, while the uniformity of the mixing profile was related to PDI.

Further studies are needed to understand why there are different flow regimes affecting size and PDI. Moreover, other properties influencing liposomes' self-assembly at a molecular level should be addressed.

### **3.3 Chapter 3 conclusions**

In this chapter, Section 3.1, we presented a methodological approach to identify the most critical factors controlling liposome properties in a PDM. Later, in Section 3.2, those variables were used as a starting point to create a model to predict those properties. The selected factors (FRR and TFR) showed to control liposomes size in a range from 52 to 200 nm. Finally, through numerical modeling, we explored mixing conditions inside the PDM, and calculated the mixing efficiency. We offered a glance at how mixing occurs inside PDM microchannels and how this mixing relates to liposome properties. In the next chapter, this exploration is expanded.

## **CHAPTER 4**

### **PARAMETRIC STUDY OF THE FACTORS INFLUENCING LIPOSOME PHYSICOCHEMICAL CHARACTERISTICS IN A PERIODIC DISTURBANCE MIXER**

Dean flow dynamics-based micromixers, such as the periodic disturbance mixer (PDM), have shown to produce controlled size liposomes in a scalable and reproducible way. However, contrary to micromixers based on molecular diffusion or chaotic advection, their production factors and their influence over liposome properties have not yet been addressed thoroughly. In this chapter, we present a comprehensive parametric study of the effects of flow conditions and molecular factors such as concentration, lipid type and temperature on the physicochemical characteristics of liposomes. Numerical models and confocal images are used to quantitatively and qualitatively evaluate liposome production conditions and their relationship with vesicle properties. This chapter extends the exploration of the factors suggested in Chapter 3.

#### **4.1 Introduction**

Different production factors such as flow conditions (Andreas Jahn et al., 2010), mixing index (Maeki et al., 2017), geometry (R. R. Hood & DeVoe, 2015; Michelon et al., 2017; Zizzari et al., 2017), lipid concentration (Maeki et al., 2017), temperature (Zook & Vreeland, 2010), lipids mixtures (M. Jo et al., 2020), and binary mixtures (organic-aqueous solvent mix)(Perli et al., 2019; Webb et al., 2019) have been extensively explored for molecular diffusion and chaotic advection based micromixers. However, these studies are generally not directly comparable since the device mixing principles or the reagents are different.

One mixing strategy that has yet to be fully explored is Dean flow dynamics-aided mixing (Kimura et al., 2018; Jisun Lee et al., 2013; M. G. Lee et al., 2009; Valencia et al., 2010; Y. Wu et al., 2012).

In this chapter, liposomes are synthesized using a PDM (López et al., 2020) to investigate the effect of various production factors. The influence of FRR, TFR, lipid concentration, lipid fatty acid length, and temperature are evaluated over liposome properties (average size, size distribution, and zeta potential). None of these factors influence the zeta potential of vesicle nanoparticles. Numerical models are also created to correlate the mixing index (MI) to average liposome size and size distribution, showing a clear correlation between these variables.

## **4.2 Materials and methods**

In this chapter, the same device presented in Section 3.2, was used to investigate liposome production. Besides, the lipid preparation, liposome characterization, numerical modeling, fluid, and flow imaging are previously described in Chapter 2.

The specifics of the methods used in this chapter are described below.

### **4.2.1 Lipid preparation**

A mixture containing DMPC or 1,2-Distearoyl-sn-glycero-3-phosphocholine (DSPC), Cholesterol, and DHP was prepared in a molar ratio of 5:4:1.

### **4.2.2 Liposome characterization**

Average liposome size, PDI, and zeta potential were measured for each of the samples collected. Liposome concentration was assessed using NTA for selected samples. In this chapter, the liposome average size results presented are number-based as opposed to Chapter 3 and Chapter 5, which are intensity-based. This approach was taken to assess the size by number results and compare it with other number-based works in the literature.



We used the Zetasizer software to transform intensity-based size distributions into number-based size distributions. The validity of this transformation was later tested by characterizing several samples using a native number-based method (NTA).

#### **4.2.2.1 Dynamic light scattering**

Samples were measured at a stable temperature of 25 °C. The average hydrodynamic diameter (Z-average) and PDI of at least three independent measurements were recorded and averaged. Size distribution by intensity was transformed into size distribution by number using Zetasizer Software 7.11.

#### **4.2.2.2 Zeta potential**

Zeta potential was measured by placing each sample in a disposable cuvette (1850 µl), readings were taken using the ZetaPlus (Brookhaven Instrument Corp.) at a stable temperature of 25 °C. Zeta potential average is a result of 3 stable cycles and ten measurements per sample.

#### **4.2.2.3 Transmission electron microscopy**

To confirm the production of liposomes using the PDM. TEM was used to image nanoparticles, as described in Chapter 2.10.4.

#### **4.2.2.4 Nanoparticle tracking analysis**

Liposome size and concentration were evaluated using NTA. Measurements were made using Nanosight NS500 with a 532 nm laser (Nanosight Ltd, UK). Three recordings of 30 s at 25 °C were documented and processed using the software NTA version 3.0.

#### **4.2.2.5 Intensity-based vs. Number-based size transformation validation**

In order to validate the intensity-based size distribution transformation into number-based size distributions using Zetasizer Software 7.11, representative samples were selected to be characterized both using DLS and NTA. DLS transformed to number-based size distributions were compared with NTA native number-based size distributions.

#### **4.2.3 Statistical analysis**

The average size (number-based), the PDI, and the zeta potential of at least three independent experiments were calculated for each condition described in this work as well as the standard deviation (SD). One-way analysis of variance (ANOVA) was used to assess statistical difference, with a  $p < 0.05$  considered as significant and marked with an asterisk \*. The Post hoc Tukey test with a 95% confidence interval was also applied to evaluate if means among different conditions differed significantly. For assessing liposome stability, a paired Student t-test was used. All statistical analyses were performed using Minitab 19 software.

### **4.3 Results and discussion**

In order to glean insights into the mixing process, confocal microscopy images, together with numerical models, were used to characterize mixing qualitatively and quantitatively. To better understand the factors influencing liposome physicochemical properties (average size, size distribution, and zeta potential), liposomes were produced under various fluid flow conditions. The influence of lipid concentration, lipid acid chain length, and temperature on liposome production was also investigated. Finally, liposome stability and production yield were measured.

### 4.3.1 Alternating centripetal force direction induces mixing

The semicircular structures of the PDM channel force the flow streams through a curvilinear path. Each circular path portion accelerates the flow towards the center of the semicircles. As the center point of each subsequent semicircular structure changes, these accelerations oscillate from one direction to the other, forcing the mixing process. The component of these flows perpendicular to the major advection direction creates vortices that rotate in opposite directions for a  $(De) \approx 10$ , as demonstrated before for similar mixing devices (M. G. Lee et al., 2009). This directional change is repeated all along the mixing channel, in contrast with previously described mixers (Jisun Lee et al., 2013). A wide range of flow conditions were investigated, from TFR = 5 mL/h, which corresponds to a  $De$  of 3.38 to TFR = 20 mL/h, which corresponds to a  $De$  of 13.5. The experimental range covers values above and below the Dean vortices formation threshold.

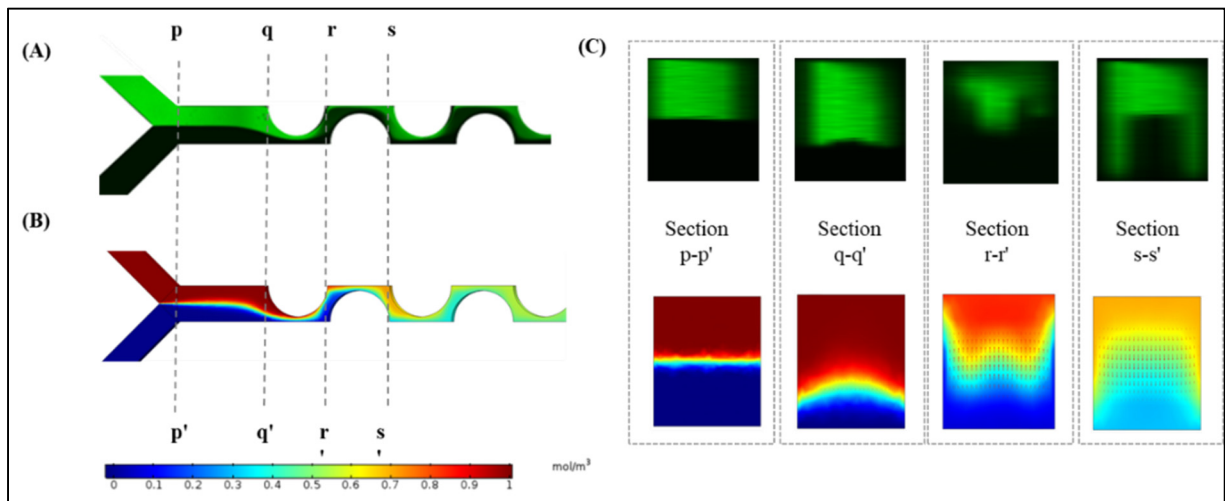


Figure 4.1 Micromixing in PDM at a FRR = 1 and TFR = 18 mL/h (A) Confocal image showing a top view of the PDM (B) Micromixer numerical model with the ethanol flow in red and the water flow in blue. Milli-Q. The bar represents the ethanol concentration (C) Cross-sections of the confocal images and their numerical model counterparts

Figure 4.1A shows the confocal image of the typical mixing process in the PDM, and Figure 4.1B shows its numerical model counterpart for  $FRR = 1$  and  $TFR = 18 \text{ mL/h}$ , these values were chosen because they represent the lowest dilution as well as a TFR at which Dean forces are present in the micromixer. As expected, the direction of the flow perpendicular to the principal advection path changes in each semicircular structure, as shown in Figure 4.1C. The cross-section  $r-r'$  shows how the centripetal forces push the diluted species (green) in a different direction than in section  $s-s'$ . The numerical model counterparts are shown below the confocal image. This periodic change enables an accelerated mixing process by moving the diluted species in a perpendicular direction to the main advection direction.

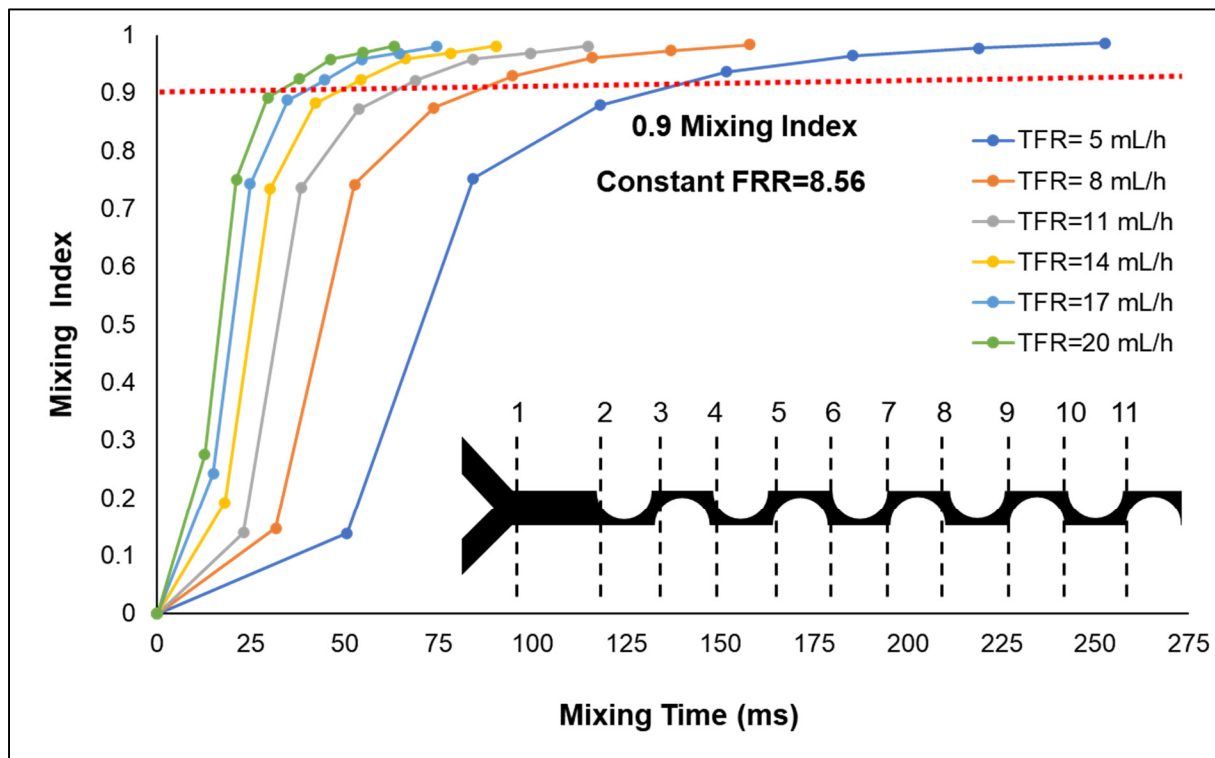


Figure 4.2 Mixing index versus time for a constant  $FRR = 8.56$  at various TFR (5-20 mL/h). Each data point corresponds to the 11 different cross sections in the diagram below

The mixing index was calculated using the numerical model and plotted against time. Figure 4.2 shows the MI for a given  $FRR = 8.56$  and variable TFR. These TFR and FRR values come

from previously presented models to predict the experimental conditions to produce liposomes in the order of nanometers. As TFR increases, the time to a mixing index of 0.9 (dotted red line) decreases. At first, this time rapidly decreases for  $5 \leq \text{TFR} \leq 11$  mL/h; however, for  $\text{TFR} > 11$  mL/h, the time only differs approximately 10 ms from each other. A TFR above 14 mL/h corresponds to the conditions under which the *De* gets close to or above 10, when Dean vortices are created, according to calculations made from the numerical model. Additionally, the maximum *Re* number for all flow conditions remained below 37, showing that the flow in the mixing channel is laminar.

For FRR, as shown in Chapter 4, at a  $\text{TFR} = 18$  mL/h value, modulates the mixing index change rate, and consequently the polarity change rate. This affects the liposome self-assembly process as well as the liposome size distribution (López et al., 2020).

#### 4.3.2 Intensity- based size vs number-based size validation

To validate the transformation done by the Zetasizer Software 7.11 from intensity to number-based size distribution, two samples were characterized by DLS and NTA. One sample was produced at  $\text{FRR} = 1$  and  $\text{TFR} = 18$  mL/h; the second one was produced at  $\text{FRR} = 9$  and  $\text{TFR} = 18$  mL/h. Table 4.1 shows detailed information for each sample. The second column shows DLS results and the third shows NTA results. The Z-average is the intensity-based size mean. The mean size by number is the number-based mean transformed by the Zetasizer software. Both Z-average (DLS) and mean (NTA) show similar results. Furthermore, the mean size by number and mode (the most repeated size) in NTA are similar.

Table 4.1 DLS vs NTA characterization

Flow Conditions		DLS				NTA		
FRR	TFR (mL/h)	Z-Average (nm)	Mean Size by Number	PDI	SD by Number (nm)	Mean (nm)	Mode (nm)	SD (nm)
1	18	199.3	149.00	0.063	43.83	189.8	146.1	67.7
9	18	65.47	37.61	0.247	11.28	62.5	40.4	49.1

NTA has a better resolution to detect individual particle populations, as it is shown in Figure 4.5. Interestingly, the peaks of both, the transformed DLS size distribution by number and the NTA peaks are similar. These results suggest that the transformation done by the software and NTA native by number size distribution results are interchangeable for this set of experiments.

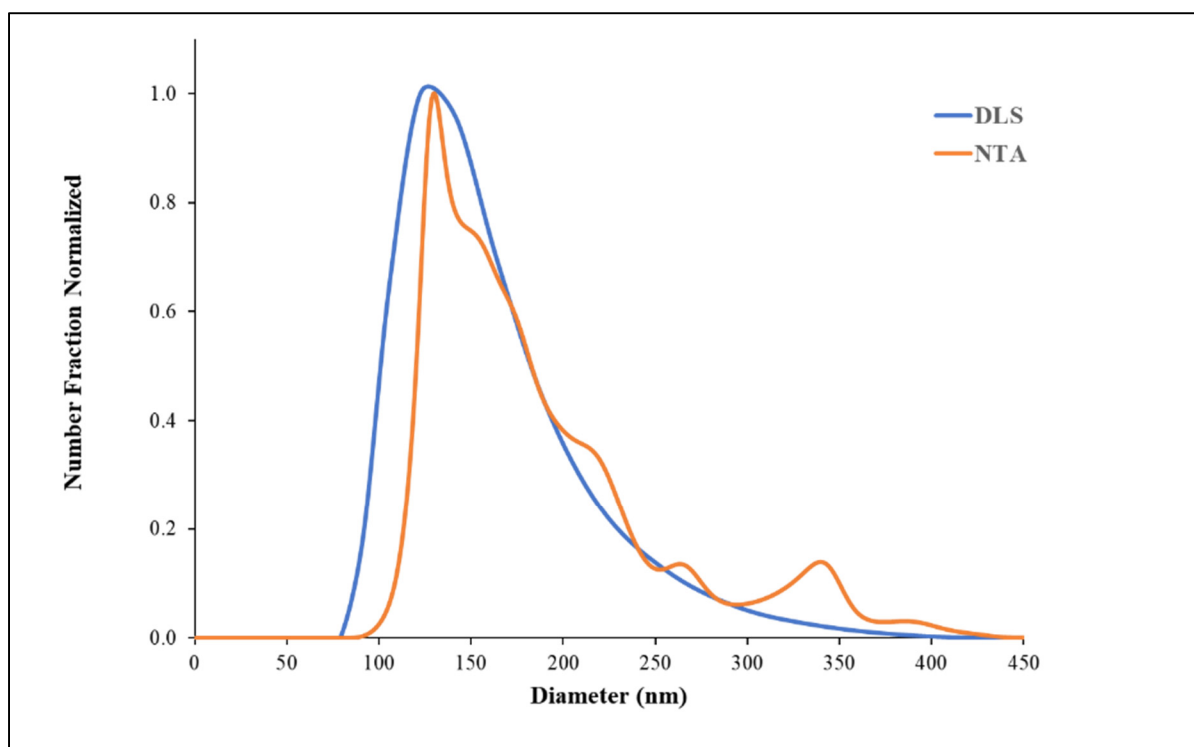


Figure 4.3 Size distribution by number normalized for the same sample produced at FRR = 1 and TFR = 18 mL/h. Characterized in the DLS (blue) and NTA (orange)

Similarly, a sample with a smaller diameter and with a higher PDI showed consistent results. In this case NTA shows 5 different peaks, however, the main peak remains similar to the one measure by the DLS as shown in Figure 4.6.

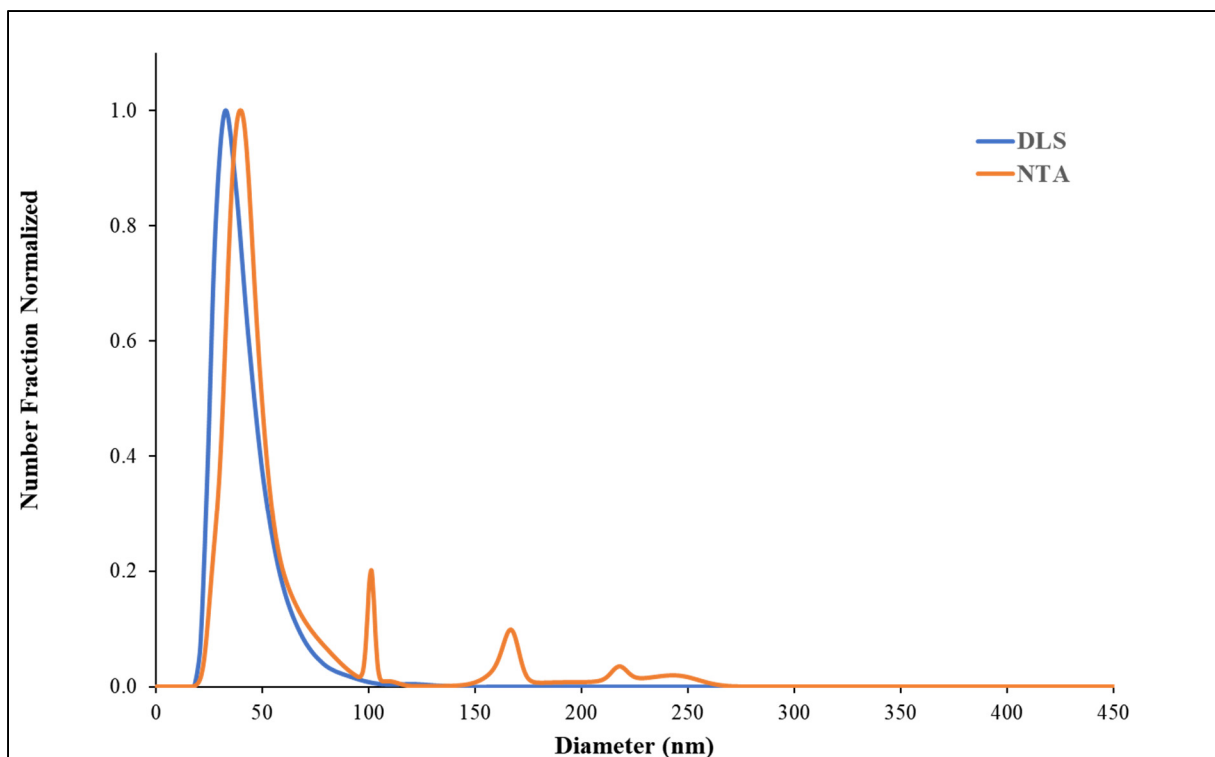


Figure 4.4 Size distribution by number normalized for the same sample produced at FRR = 1 and TFR = 18 mL/h. Characterized in the DLS (blue) and NTA (orange)

Size distributions characterized by the NTA and the DLS transformation showed similar results. This data indicates that for the specific experimental range, DLS by number size distribution can be used to estimate the real size distributions by number.

### 4.3.3 TFR controls liposome size

Under a FRR set at 8.56, the TFR exerted a clear influence over liposome size. Up to 14 mL/h, an increase in TFR led to a decrease in liposome size (Figure 4.5A). This TFR threshold corresponds to the transition of  $De$  from below 10 to above 10. The Tukey test revealed three statistically different mean groups corresponding to 5, 8, and all TFR values above or equal to 11 mL/h. These means show the effective TFR control range over average liposome size. The liposome diameter reduction observed while increasing TFR corresponds to a mixing time

decrease to reach a mixing index = 0.9. As the  $De$  gets closer to 10, Dean vortices formation improves the mixing process, thus reducing liposome size.

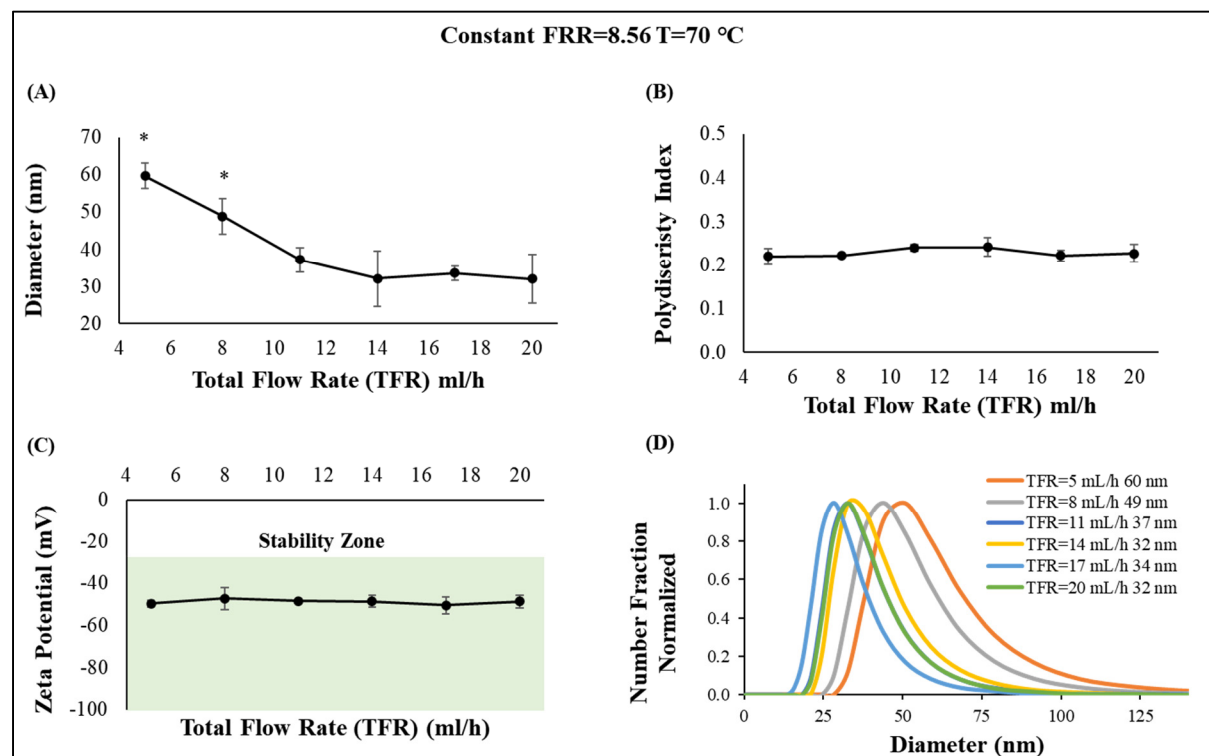


Figure 4.5 Effect of the TFR on various liposome properties

The TFR did not influence liposome PDI (Figure 4.5B) for the values studied. Liposome size distribution by number was consistent for a wide range of conditions (Figure 4.5D). This mixing device property is particularly important when developing drug delivery systems that might target different tissues and organs.

As shown in Figure 4.5C, the liposome zeta potential was relatively constant, with a mean of -47 mV, under various TFR conditions. The data suggest that zeta potential is not influenced by TFR, as previously shown for the SHM (Kastner et al., 2014). Moreover, the zeta potential is within the stability zone (green) for particles suspended in a media which is above  $|30 \text{ mV}|$  (Kumar & Dixit, 2017), so it is expected that particles will remain stable for several weeks,



contributing to a potentially long shelf life. Similar results are found in all experiments through this work.

Overall, liposome diameter can be tuned by varying the TFR, our results indicate that this parameter modulates the magnitude of centripetal forces inside mixing channels. Once TFR approaches to the value at which Dean vortices are created, ethanol dilution in water significantly increases. Consequently, the polarity change rate timescale decreases, forcing a faster assembly of lipid intermediate structures into liposomes resulting in smaller nanoparticles .

#### **4.3.4 FRR controls liposome size in a defined range**

FRR showed an impact on liposome diameter. Increasing FRR value from 1 to 3 at a constant TFR = 18 mL/h decreased liposomes diameter from 142 nm to 40 nm, as shown in Figure 4.6A. This abrupt variation in size indicates a change in the micromixing regime inside the microdevice. As FRR increases above 3, liposome diameters slightly change, reaching a value of 29 nm at FRR = 7, followed by a small increase of 7 nm until finally reaching a minimum size of 27 nm at FRR = 12. It is noteworthy that the PDM produces liposomes with a diameter of around 40 nm at a FRR of only 3, resulting in a much lower dilution for producing nanoparticles compared with other micromixers. Statistically, the average liposome size has only two different value means: one at  $FRR < 3$  and the other at  $FRR \geq 3$ . This FRR range is comparable with chaotic advection-based micromixers, and much narrower than for molecular diffusion-based micromixers.

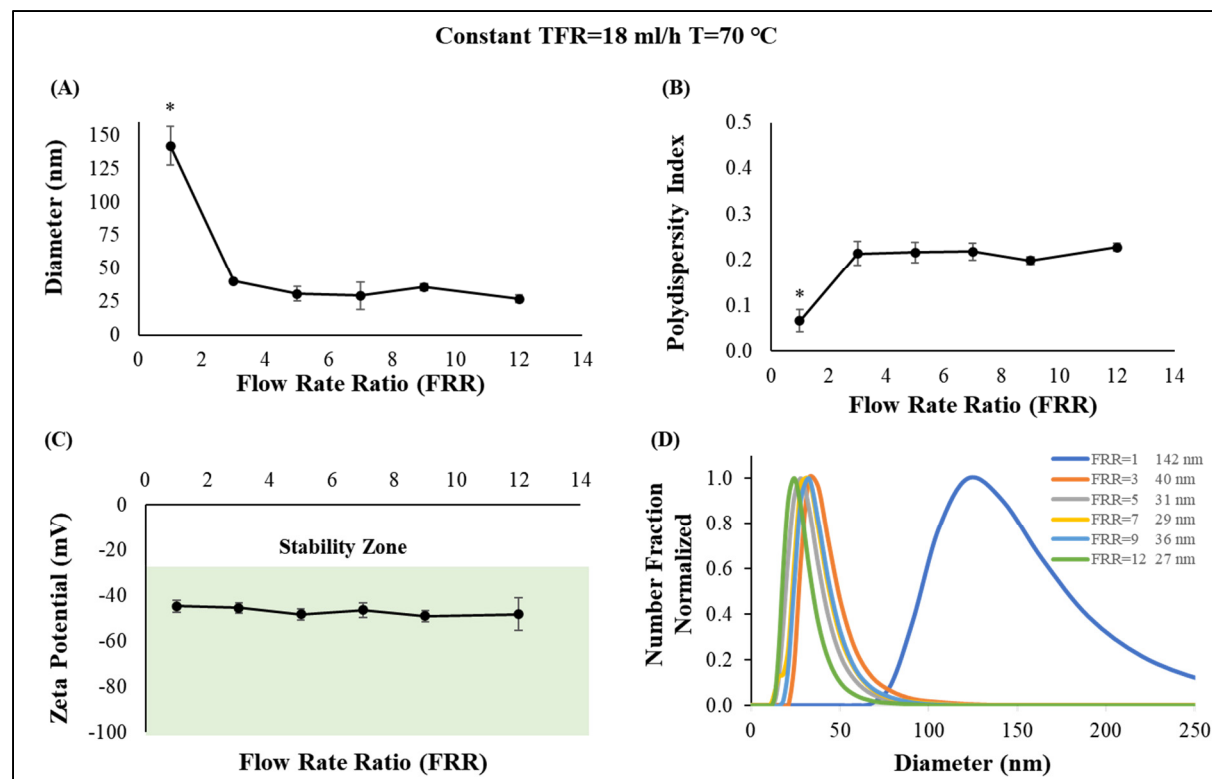


Figure 4.6 The effect of FRR over liposomes properties

In the previous chapter we have shown that a FRR value of approximately three is a threshold that divides highly monodispersed and low polydispersed liposome populations (see Figure 4.6B). This behavior might be caused by the decrease in the uniformity of the concentration profile (López et al., 2020).

Previously discussed results contrast with the SHM in the commercially available microfluidic system in which FRR greater than 3 produces liposomes with PDI above 0.4, leading to much more polydispersed populations (Kastner et al., 2014). This shows another advantage of the PDM over other micromixers which PDI is not affected noticeably after FRR = 3, producing low polydispersed populations in contrast with the highly polydispersed populations of the SHM.

Like TFR, evidence suggests that for the studied range, FRR does not influence liposome zeta potential, as shown in Figure 4.6C. Finally, Figure 4.6D shows normalized size distributions by number for different FRRs. Average liposome size and size distribution are similar for  $FRR \geq 3$ .

The data suggest that FRR modulates liposome size in a small range, affecting mainly PDI when it changes from 1 to 3. Previously presented numerical models suggest that this could be related to the concentration profile uniformity (López et al., 2020). The PDM can produce liposomes below 40 nm at low FRR, comparable to the SHM, but without increasing liposome population PDI. The latter could be useful when trying to keep a low polydispersity in liposomes that need to be small to passively target organs and tissues with high specificity.

#### **4.3.5 Lipid concentration influences liposome size**

In this section, the lipid concentration effects on liposome physicochemical characteristics are investigated. The tested concentrations ranged from 5 to up to 40 mM. Each concentration level studied was the double of the previous one. In this section, the lipid concentration effects on liposome physicochemical characteristics are investigated. The tested concentrations ranged from 5 up to 40 mM. The flow conditions were set to a constant  $FRR = 8.56$  and a  $TFR = 18$  mL/h, according to the previously presented statistical model, these flow conditions produced the smallest liposomes in PDM. The hot plate temperature was set to 40 °C. Average liposome size increased rapidly from 44 nm to 74 nm when lipid concentration was doubled; from that point on, liposome size increased almost linearly even though concentration was doubling, as shown in Figure 4.7A. According to Tukey test grouping, there are three liposome size mean groups: one at 5 mM, another grouping from 10 mM to 20 mM, and a final one at 40 mM. Similar results are reported for SHM mixers (Maeki et al., 2017) and contrast with previously presented for other types of mixers such as VFF (R. R. Hood & DeVoe, 2015) where liposome size does not change dramatically by changing lipid concentration from 5 mM to 40 mM.

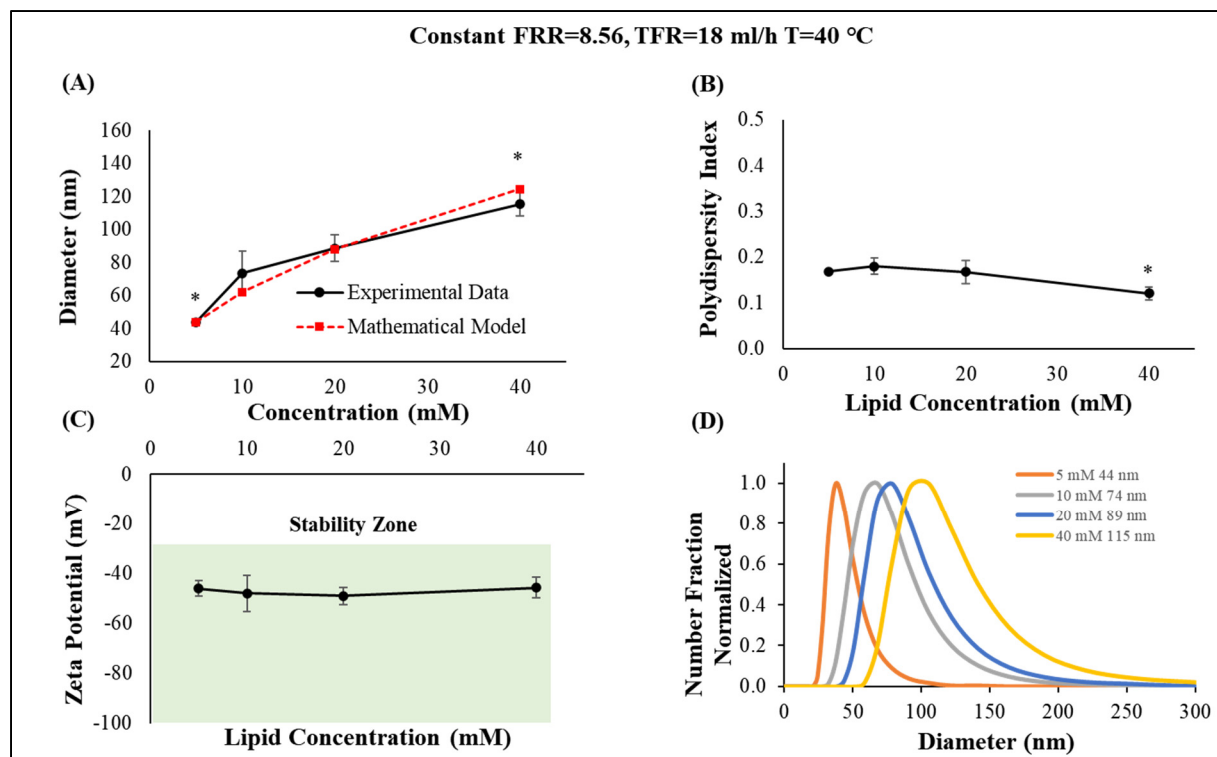


Figure 4.7 Initial lipid concentration effects over liposome size

By contrast, PDI and zeta potential were not remarkably affected by the variation of the initial lipid concentration, as shown in Figure 4.7B and Figure 4.7C. The zeta potential is in the stability zone (shaded green). Increases in lipid concentration lead to increasingly higher average liposome size (Figure 4.7D). This behavior could be explained by the increased nucleation of the intermediated disk-shaped structures at the beginning of the mixing channel. This result indicates that a higher initial concentration results in larger liposomes, as opposed to more liposomes with similar size.

To better understand the average liposome size grow due to the increase in the concentration, the process was modeled using the next assumptions. Liposomes in micromixers start as intermediate disk-shaped lipid bilayers with a surface area  $A_{d0}$  directly proportional to the lipid concentration (assumption 1). The surface area of this intermediate disk-shaped structure is equal to the surface area of a spherical liposome made from this intermediate structure, as shown in Equation (4.1). As the initial concentration doubles, the surface area of this lipid

bilayer increases proportionally as shown in Equation (4.2), implying that this area is not broken into small pieces (assumption 2). Thus, the diameter of the liposome when the initial concentration is doubled is given by Equation (4.3).

$$A_{d0} = A_{s0} = \pi D_{s0}^2 \quad (4.1)$$

$$A_{d1} = 2A_{d0} = \pi D_{s1}^2 = 2\pi D_{s0}^2 \quad (4.2)$$

$$D_{s1} = \sqrt{2} D_{s0} \quad (4.3)$$

Where  $A_{d0}$  is the surface area of the intermediate disk-shaped lipid bilayer at a given initial concentration,  $A_{s0}$  is the surface area of the spherical liposome and  $D_{s0}$  is the diameter of the liposomes given the initial concentration. Starting from a given concentration and knowing liposome diameter, one can calculate subsequent liposome diameters for each liposome concentration doubling using Equation (4.4) or more generally for any given constant proportional increase X, as shown in Equation (4.5).

$$D_{sn} = 2^{\frac{n}{2}} D_{s0} \quad (4.4)$$

$$D_{sn} = X^{\frac{n}{2}} D_{s0} \quad (4.5)$$

Where n is the value of the index in the series. This model was compared with the experimental values. Other authors have had similar results using energetic considerations.(Phapal et al., 2017). The model predicted values are within the range of one standard deviation of experimental results as shown in Figure 4.7A. In the next section, we explore if this model is applicable for a lipid with a longer fatty acid chain and a different transition temperature.

### 4.3.6 Lipid fatty acid chain length influence over liposome size

The influence of the nature of the lipid constituent over liposome properties was also investigated. The original lipid mixture was modified by replacing DMPC by DSPC. The latter possesses an almost identical structure compared to DMPC, except for the fact that it has more carbons in its fatty acid chain (18 DSPC vs 14 DMPC). This difference has a direct impact on lipid transition temperature, which is 24 °C for DMPC and 55°C for DSPC, as well as on the elastic bending energy of the intermediate disk-shaped structures (Zook & Vreeland, 2010). Liposomes produced at 40 °C using DSPC as the primary lipid resulted in larger liposomes compared with DMPC, as shown in Figure 4.8A. Average liposome size was far below the value predicted for the previously presented model. In this case, lipid concentration increase did not result in liposome diameter increase, as stated by Equation (4.4), indicating that disk-shaped intermediate structures are disrupted before they assemble into liposomes.

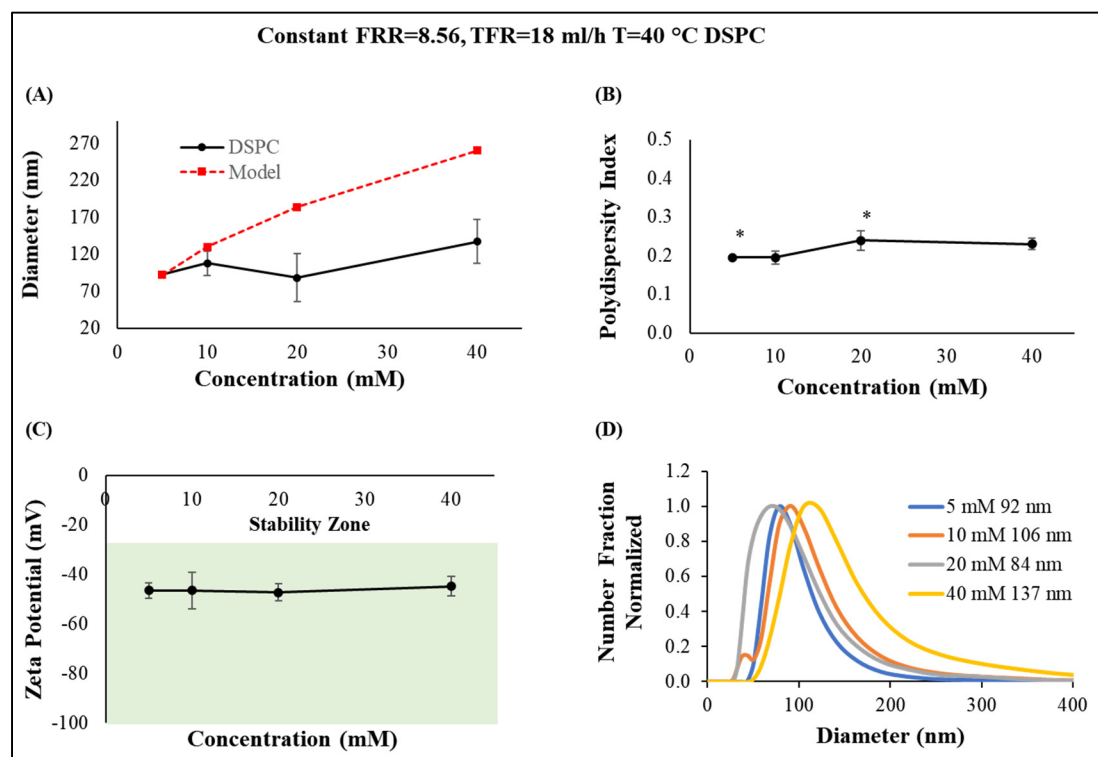


Figure 4.8 Liposome properties produced using DSPC, cholesterol, and DHP in a molar ratio 5:4:1

PDI, on the other hand, oscillated around 0.2, without substantial variations compared with different concentrations or lipid mixture type (as shown in Figure 4.8B)

On the other hand, liposome zeta potential did not show any statistically significant difference compared with DMPC liposomes prepared under the same conditions (see Figure 4.8C). Both lipids have the same terminal head group. These results suggest that zeta potential is controlled by terminal group properties and not by lipid concentration or fatty acid chain length.

Finally, size distributions are mostly monomodal populations except for the one prepared with 10 mM concentration, which exhibits two peaks as it is shown in Figure 4.8D.

#### **4.3.7 Temperature and liposome size are negatively correlated**

Liposomes containing DMPC as the primary lipid were produced at four different temperatures, 25 °C (close to DMPC transition temperature), 40 °C, 55 °C and 70 °C.

A higher temperature implies a lower elastic bending energy of the lipid-made membranes; thus, smaller liposomes, as shown in Figure 4.9A. Intermediate disk-shaped structures bend faster as temperature increases. The Tukey test revealed that there were only two statistically significant means groups for size: one for 25 °C, and the other for temperatures above 40 °C.

By contrast, PDI shows a similar pattern compared to previously presented experiments (see Figure 4.9B). Finally, zeta potential values are not statistically significant at different temperatures, confirming that this characteristic is independent of temperature (see Figure 4.9C). Finally, all populations are monomodal see Figure 4.9D.

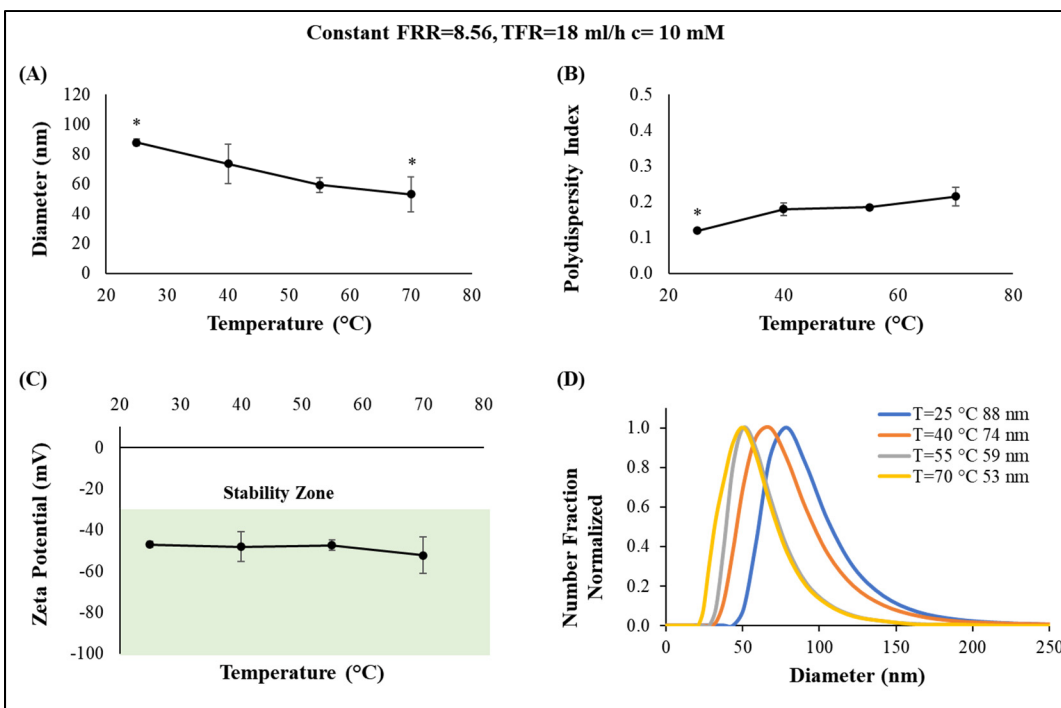


Figure 4.9 Temperature effects on liposome properties

#### 4.3.8 Liposomes are stable in the long term

Average liposome size and size distribution stability were of interest because the centripetal forces at which liposomes were exposed during the mixing process in the semicircular structures or ethanol residues that might have a detrimental effect on lipid bilayer stability. Stability was assessed 50 days after synthesis. Average liposome size and PDI variations were 3 and 0.016 nm, respectively. The samples with the smallest size or PDI were the most susceptible to variation. However, most of these variations are within one standard deviation (SD). Figure 4.10A shows the sample with the most significant relative variation among liposomes produced at different TFR and FRR. Figure 4.10B shows a typical sample.

Neither centripetal forces nor ethanol residues showed an effect on liposome long-term size and size distribution stability. One could conclude that ethanol residues in the membrane are not significant enough to degrade the lipid bilayers



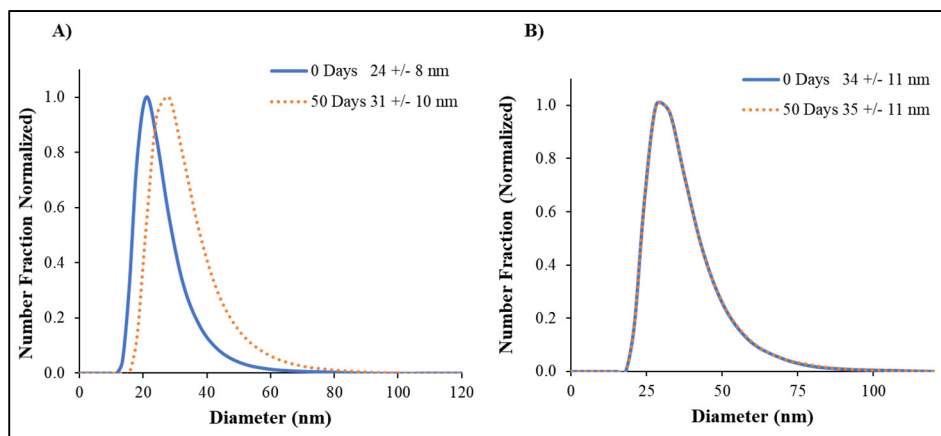


Figure 4.10 Liposomes stability after 50 days diameter mean  $\pm$  1 SD

A) Liposome sample synthesized at FRR = 12 and TFR = 18 mL/h,

B) FRR = 8.56 TFR = 20 mL/h T = 70 °C

In order to evaluate liposome integrity, liposomes were imaged using TEM. Images indicated that liposomes preserve their structure three months after production, as shown in Figure 4.11.

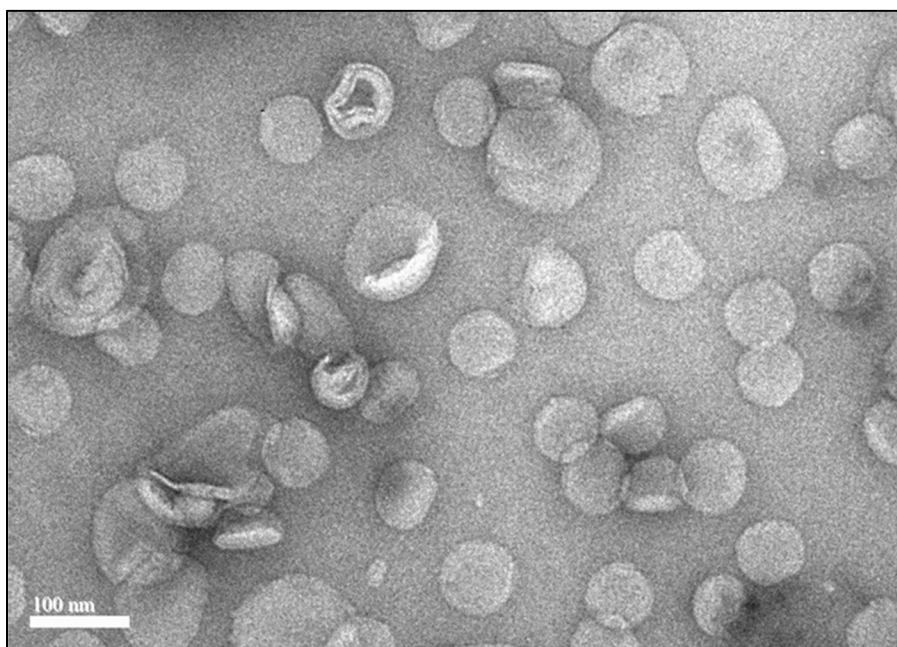


Figure 4.11 Liposomes produced at FRR = 8.56 TFR = 18 mL/h, initial lipid concentration of 10 mM, T = 40 °C made of DMPC:CHOL:DHP at a molar ratio 5:4:1 three months after production

#### 4.3.9 Liposome production rate

Regarding industrial scalability, liposome production rate is an important parameter as size and size distribution. The PDM production rate was 24.63 mg/h or approximately  $10^{14}$  liposomes/h with a liposome diameter of 142 nm using an initial lipid concentration of 5 mM. FRR = 1 and TFR = 18 mL/h. The production rate order of magnitude was confirmed using the concentration results from NTA as shown in Table 4.2 for a sample diluted to 1 µg/mL.

Table 4.2 Theoretical vs. Measured particle concentration  
produce at FRR = 1 TFR = 18 mL/h

Theoretical concentration solving Equation (2.15)	Measured Concentration using NTA
$4.23 \times 10^9$ particles/mL	$7.15 \times 10^9$ particles/mL

At a FRR = 8.56 and TFR = 18 mL/h using a 40 mM initial concentration, the final production rate is calculated to be 41.22 mg/h with a liposome size of 115 nm as shown in Figure 4.8. Even considering the low initial concentration (5 mM) in this work experiments, together with the relatively low total flow rates (max 20 mL/h), the PDM production rate is comparable with the VFF (R. R. Hood & DeVoe, 2015) order of magnitude, and far above previous described Tesla Structures (Valencia et al., 2010) or 3D mixers (Y. Wu et al., 2012).

#### 4.4 Chapter 4 conclusions

In this chapter, we performed a comprehensive parametric evaluation of crucial variables controlling liposome physicochemical characteristics inherent to a Dean Flow dynamics-based micromixer. Mixing index, average liposome size, and PDI variations were shown to be closely related in this device. Liposome size was mainly controlled by TFR and, in a limited range, by FRR. TFR also modulated liposome production rate, so it contributed to producing small liposomes at high yield in contrast with other mixers, which require higher dilutions to produce liposome nanoparticles. FRR was shown to control PDI by setting a threshold between highly

monodisperse and low polydispersed liposome populations. It was also demonstrated that this platform can produce liposome nanoparticles at low dilution factors ( $FRR = 3$ ).

Additionally, we investigated molecular-related factors such as lipid concentration, fatty acid chain length, and temperature. These variables affect liposome size and size distribution. A model explaining how lipid concentration affects average liposome size was presented. We contrasted the validity of the model against liposomes produced using two different lipid mixtures. It was demonstrated that, for liposomes composed primarily of DMPC, the model predicts the average liposome size. On the other hand, increasing the production temperature was shown to decrease liposome size. Finally, liposome zeta potential was not affected by any of the studied variables in this work. Through this work, it was shown that the PDM has the potential to be used in the production of delivery systems.



## CHAPTER 5

### **THE EFFECT OF DIFFERENT ORGANIC SOLVENTS IN LIPOSOME PROPERTIES PRODUCED IN A PERIODIC DISTURBANCE MIXER: TRANSCUTOL®, A POTENTIAL ORGANIC SOLVENT REPLACEMENT**

In this chapter, to assess the organic solvent influence over liposome characteristics, we investigated three conventional organic solvents: ethanol, methanol, and isopropanol, as well as Transcutol®. Also, it was proposed for the first time, the use of Transcutol® instead of conventional solvents has the potential to avoid the need for removing this substance from the final liposome formulation.

#### **5.1 Introduction**

Diethylene glycol monoethyl ether (DEGEE), or more commonly known for years under the trade name Transcutol® (Gattefossé, Lyon, France), is a liquid solvent used as an excipient in numerous commercial formulations. It plays an important role as a penetration enhancer since it can penetrate the epidermis (first layer of the skin), and decrease its resistance barrier by temporarily weakening its impermeability, enabling transdermal delivery; therefore, it is principally applied in topical and dermal products (Javadzadeh, Adibkia, & Hamishekar, 2015). This hydroalcoholic solvent, which is gaining interest in different fields of application, can also be found in dietary supplements and nutraceutical products used as a strong solubilizer (Ha et al., 2019). Unfortunately, Transcutol® is contaminated with ethylene glycol and diethylene glycol, two impurities identified as toxic substances for humans. Before the 90s, the solvent had a low purity and showed some adverse effects. Nevertheless, it is suggested that these problems were due to its contaminants and not the solvent itself (Srivastava et al., 2019). The long history of Transcutol® use in personal care products and food proved safe in human usage. Nowadays, the Transcutol® used in pharmaceutical products is a high purity (HP), with over 99.9% of DEGEE (Osborne & Musakhanian, 2018). At this grade, it is safe and well-tolerated, which makes it more appealing to new oral or parenteral administrations such as liposomal DDS (Ha et al., 2019). This fact is one of the main motivations for this chapter to

investigate the use of Transcutol® on liposome synthesis since these solvent residues could even help drug delivery as opposed to other organic solvents such as methanol or IPA, substances well known to be toxic.

Ways to control and modulate liposome characteristics in micromixers have been explored, such as flow rate (Kastner et al., 2014), micromixer geometry (Michelon et al., 2017), aqueous solvent ionic strength (Perli et al., 2019) and nanoparticle composition (M. Jo et al., 2020). However, the study of the effects of different organic solvents or aqueous solvents has not been thoroughly explored in micromixers, except for the study of four different binary mixtures (Joshi et al., 2016), another in aqueous solvents (Guner & Oztop, 2017) and a very recent work using conventional organic solvents (Webb et al., 2019). However, the use of various methods, devices, or lipid compositions in these research works does not enable a proper comparison.

Therefore, the purpose of this chapter work is to generate comparable data, utilizing different organic solvents with a well-defined micromixer, lipid concentration, and temperature production conditions, allowing the study of the effects on particle size, size distribution, and zeta potential. Additionally, the effects of lipid concentration and temperature are studied for only two of these solvents (ethanol and Transcutol®, and the stability of lipid nanoparticles is assessed.

The organic solvents investigated in this work are ethanol, IPA, methanol and Transcutol®. Ethanol has been chosen as a control solvent or benchmark due to its wide application in this field, and well-known toxicity profile. On the other hand, IPA is known to be a suitable solvent for cholesterol and has a stabilizing effect on the edges of the bilayer discs, and consequently, a proven effect on liposome size (Zook & Vreeland, 2010). Methanol has shown in previous investigations to produce smaller size range vesicles than ethanol when mixed with PBS (Joshi et al., 2016). Finally, a solvent which is commercially known as Transcutol®, which despite its long history of use in topical formulations and cosmetics, has never been studied in liposome synthesis using micromixers.

## 5.2 Materials and methods

The same microfluidic device employed in previous chapters with an  $AR = 1$  was used in the next set of experiments. The general description of methods is given in Chapter 2. The details of this chapter experiments are described below.

### 5.2.1 Lipids preparation and nanoparticle production

Ethanol (100%), IPA, methanol and chloroform (all last three HPLC grade) were purchased from Sigma Aldrich Canada, while Transcutol® was provided by Gattefossé (Gattefossé, Canada Inc, Montreal, Canada). The Transcutol® used was HP grade, containing at least 99.9 % of diethylene glycol monoethyl ether. The same lipid mixture used in the previous chapter was prepared (DMPC: CHOL: DHP 5:4:1 molar ratio). Lipids mixtures were again diluted individually in the four cited organic solvents. The final concentration of lipids in the solvents was set according to the experimental design shown in section 6.2.4.

TFR in the device for all the experiments was 18 mL/h. FRR between Milli-Q Water and the organic solvent flow was 8.56. These values were predicted to produce the smallest nanoparticles using ethanol, as shown before in section 3.2 (López et al., 2020). Both inlet stream flows were controlled using Harvard Apparatus syringe pumps (Harvard Apparatus Canada, Montreal, Canada) connected to a computer interface. The control application was programmed in Python programming language. It controls both flow conditions and the hot plate temperature. The micromixer device was placed on the top of a hot plate. The hot plate was used to set a constant and specific production temperature for each experiment.

As part of the nanoparticle production process, a fluid stabilization time of 330 seconds was established before starting the sample collection. This duration is selected to allow the flow inside the channel to develop and reach a steady state.

### 5.2.2 Nanoparticle characterization

Nanoparticle size and size distribution were measured using the DLS technique. The averaged results per condition based on intensity are presented. Zeta potential average is a result of 3 stable cycles and ten repetitions for each sample. The measurements of vesicle size, polydispersity, particle size distribution, and zeta potential were all carried out at 25 °C.

### 5.2.3 Experimental design and statistical analysis

Three sets of experiments were designed to investigate the influence of different organic solvents over liposome properties. First, the four organic solvents were tested one by one under the same fluid flow conditions (FRR = 8.56 and TFR = 18 mL/h), at a production temperature of 40 °C and with a lipid concentration of 10 mM. Next, a set of 8 different experiments was performed using just ethanol and Transcutol®. This set tested the remaining lipid concentrations at 40 °C. Finally, a set of 6 more experiments using ethanol and Transcutol® were executed for all three remaining temperatures at a 10 mM lipid concentration. The temperature range was set to be above DMPC transition temperature (24 °C). A summary of the experiments performed is shown in Table 5.1, the organic solvent, temperature, and lipid concentration for each of the tested conditions are shown. E = Ethanol, T = Transcutol®, M = Methanol, and I = Isopropanol. Three repeats were produced for each condition. Additionally, a stability assessment 50 days after production was performed on all samples.

Table 5.1 Experimental design. All the experiments were performed at FRR = 8.56 and TFR = 18 mL/h

Concentration\Temperature	25 °C	40 °C	55 °C	70 °C
<b>5 mM</b>	x	E/T	x	x
<b>10 mM</b>	E/T	M/I/E/T	E/T	E/T
<b>20 mM</b>	x	E/T	x	x
<b>40 mM</b>	x	E/T	x	x



The average, as well as the standard deviation of the Z- average, PDI, and zeta potential, were calculated. ANOVA ( $p < 0.05$ ) with the Pairwise Tukey Grouping Method was used to group means with a confidence level of 95%. This analysis was performed using Minitab® 19.1 software.

### **5.3 Results and discussion**

For a fixed aqueous solvent as in this case water, the organic solvent determines the gradient and thus the polarity change rate. In order to assess the influence of this factor, liposomes were produced using different organic solvents and characterized, and their properties were analyzed using statistical tools. Later, ethanol and Transcutol® as organic solvents and their effects on liposomes properties were investigated at different temperatures and concentrations.

#### **5.3.1 Liposome production using different organic solvents**

For the first set of experiments, nanoparticles were produced using four different organic solvents, comprising ethanol, IPA, methanol and Transcutol®, and the same aqueous solvent (Milli-Q Water). Fig. 2A Y-axis represents the Z-Average (diameter) and the X-axis represents the organic solvent used to produce the particles.

According to the Tukey grouping method, ethanol and methanol Z-average size correspond to the same mean, while IPA and Transcutol® are part of another group with smaller lipid nanoparticles.

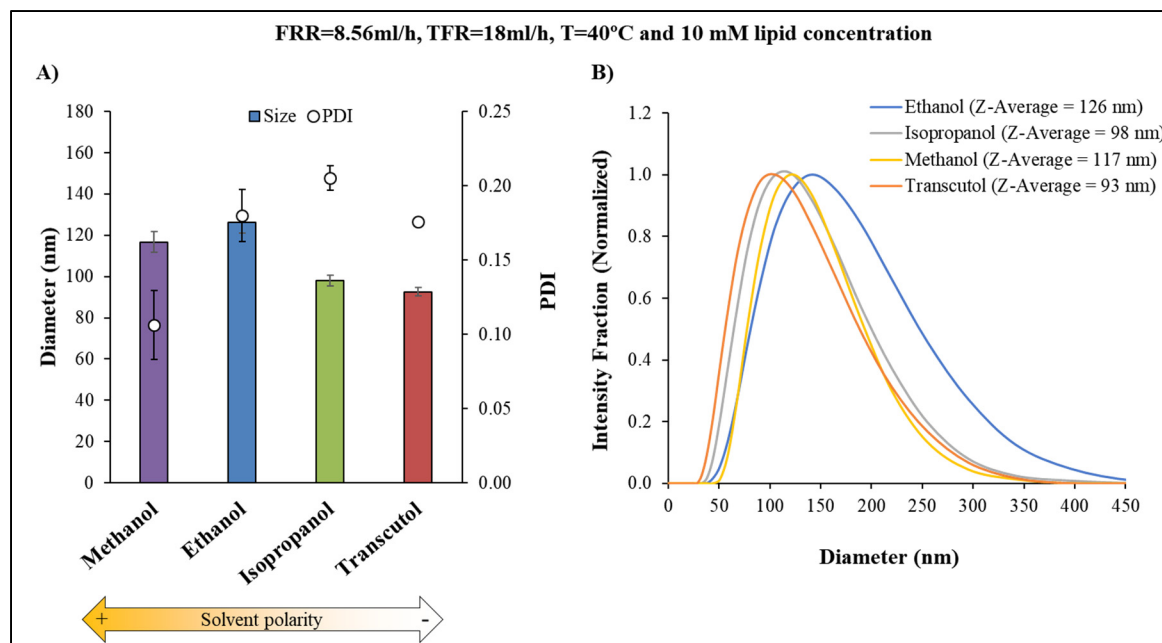


Figure 5.1 Liposomes synthesized using an FRR = 8.56 and TFR = 18 mL/h at 40 °C using different organic solvents with a 10 mM lipid concentration A) Z-Average and PDI. The bars indicate  $\pm 1$  SD  $n = 3$  B) Size Distribution by Intensity Normalized

The particle polydispersity index is also shown in Fig. 2A, on the secondary Y-axis (right side). PDI can vary from 0 to 1, where lower values indicate a more homogeneous size distribution. Values under 0.2 are considered as low polydispersed populations. In this case, all PDI values except isopropanol were below 0.2. Additionally, the PDI value of methanol (0.106) is considered a monodisperse population.

There are only two different mean groups for the PDI value. The first one contains ethanol, IPA, and Transcutol®, and the other contains methanol. Hence, only methanol is statistically different from the other solvents.

Size Distribution by Intensity, as well as the Z-Average mean value (displayed in parentheses), are presented in Fig. 2B. The intensity was normalized between 0 and 1. The graph shows that the smallest nanoparticles were produced using Transcutol® as a solvent. On the other hand, Size Distribution by Number also shows that Transcutol® produced the smallest nanoparticles

considering the peak of this distribution, as is shown in Figure 5.2 (the value in parentheses is the peak average of the size distribution by number).

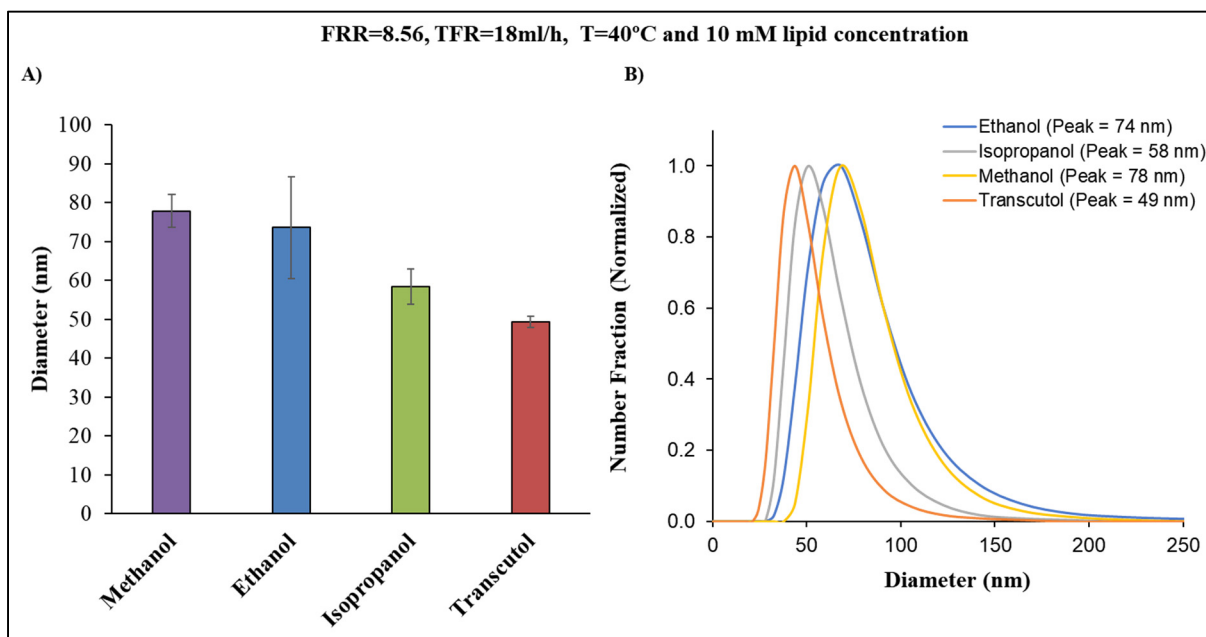


Figure 5.2 Liposomes synthesized using an FRR = 8.56 and TFR = 18 mL/h at 40 °C using different organic solvents with a 10 mM lipid concentration A) Diameter by number. The bars indicate  $\pm 1$  SD n = 3 B) Size Distribution by Number Normalized

This size variance between solvents could stem from their different polarities. It is known that the mixing of an aqueous solvent with the organic solvent produces an increase in polarity, which in turn causes the lipids to become less soluble triggering liposome self-assembly. Other authors have shown that control of the mixing speed enables the control of liposome size. Furthermore, a lower mixing time results in smaller nanoparticles (Maeki et al., 2017). In this case, a greater gradient in polarity between the organic and the aqueous solvent leads to a more drastic, and hence faster polarity change, which produces smaller particles (as seen in Figure 5.3). Transcutol® has a lower dielectric constant, and hence lower polarity than IPA, which in turn, has a lower polarity than ethanol and methanol (Osborne & Musakhanian, 2018). This translates into a higher polarity gradient, considering the fixed aqueous solvent (water) as well as an increased polarity change rate.

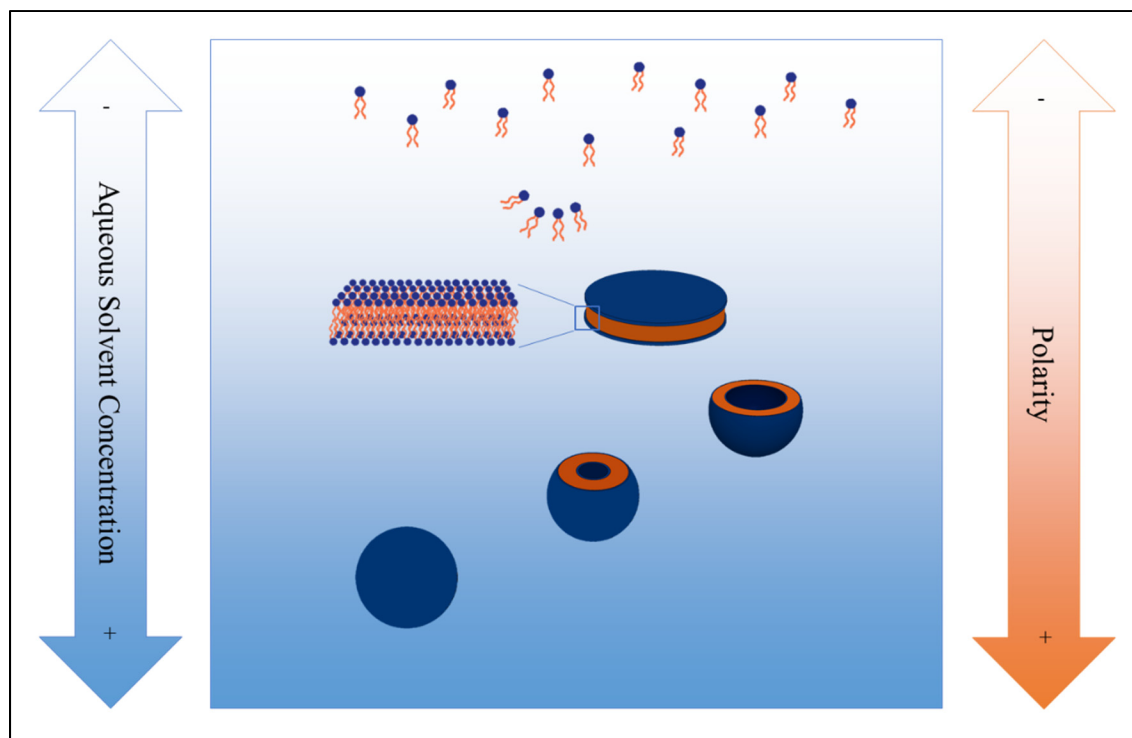


Figure 5.3 Nanoparticle formation process. The increase of the aqueous solvent concentration, and hence the polarity of the mixture, causes the lipids to self-assemble in disk-shaped structures, which finally bend and close into liposomes

Additionally, studies on binary mixtures polarities indicate that some mixtures of organic solvents (like methanol and IPA) with water undergo a steep increase in polarity when the solvent is low in concentration (less than 40% solvent) (Bosch & Rosés, 1992), which appears to be the concentration region in which liposomes are formed according to previous works (40%) (Andreas Jahn et al., 2004), (25%-50%) (Phapal et al., 2017). However, there is no consensus about the exact figure (Maeki et al., 2017).

Alternatively, the variation in the solvent viscosity does not appear to have an essential effect on liposome size in this type of micromixer. Prior studies showed a possible relation between viscosity and mixing speed in micro hydrodynamic focusing devices, where higher viscosity would slow down the fluid flow and posterior mixing (Z. Wu & Nguyen, 2005a). More viscous fluids would then be expected to produce bigger nanoparticles. However, IPA and Transcutol® have a viscosity value of 2.35 and 4.8 cP (Osborne & Musakhanian, 2018) at 20 °C, whereas

ethanol and methanol have values of 1.2 and 0.594 cP, respectively, and yet IPA and Transcutol® produce smaller nanoparticles in the PDM.

Finally, the particle zeta potential means were statistically the same for all four organic solvents, meaning that regardless of the organic solvent used, zeta potential values were similar as shown in Figure 5.4. The zeta potential values obtained are considered over the stability threshold ( $\pm 30$  mV). A very recently published work in which liposomes were produced using different organic solvents (ethanol, methanol and IPA) with two commercially available microfluidic systems, presented similar results, where, as in this work, liposome zeta potential was unaffected by the solvent selection. However, in terms of liposome size, they presented contradictory results, finding that IPA yielded the largest liposomes, while methanol yielded the smallest ones (Webb et al., 2019). This finding may be an indicator that the mixing method plays a role in the size of liposomes.

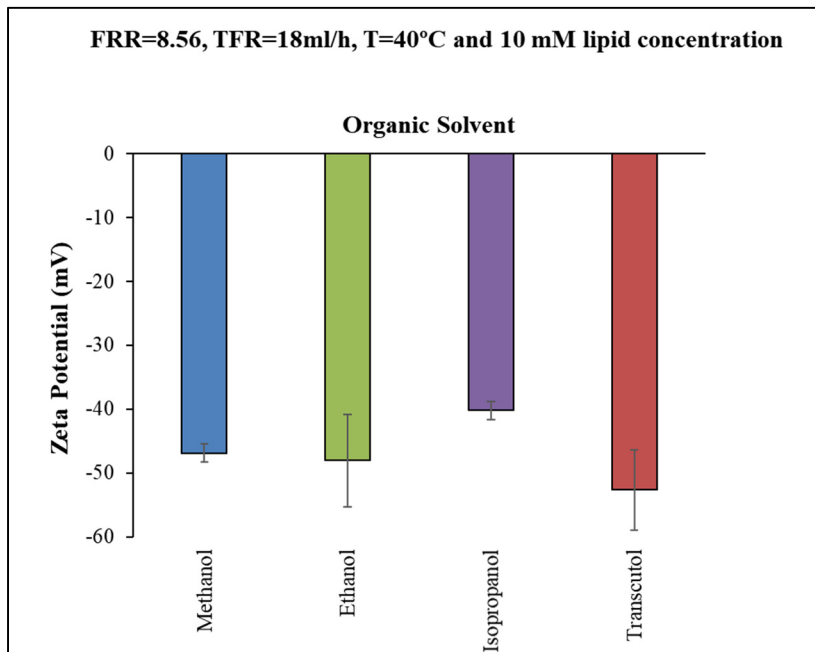


Figure 5.4 Zeta Potential of liposomes synthesized using an FRR = 8.56 and TFR = 18 mL/h at 40 °C

Our results using different organics solvents prove that Transcutol® not only enables the production of lipid nanoparticles but also presents better results in terms of size versus ethanol or methanol (the particles produced are smaller). For this reason, the two new sets of experiments were also designed using Transcutol®, testing in these cases the lipid concentration and temperature effects on size, PDI and zeta potential. The same experiments were also run with ethanol, as a benchmark solvent, to compare the obtained results, while methanol and IPA were dismissed due to their toxicity.

### **5.3.2 Concentration effects on liposomes produced with ethanol and Transcutol®**

Lipid nanoparticles were produced at different concentrations of 5, 10, 20 and 40 mM. The production temperature was set to 40 °C. The two organic solvents investigated were ethanol and Transcutol®, and the same aqueous solvent (Milli-Q water).

Nanoparticles produced with ethanol and Transcutol® increased in size as lipid concentration increased, as observed in Figure 5.5A; Y-axis shows the diameter (Z-Average) while X-axis displays the lipid concentration. This phenomenon supports the results from previous studies where lipid nanoparticles produced with ethanol increased in size with lipid concentration. The reason behind this behavior is the availability of more lipids to grow and fuse into the intermediate disk-shaped structures, to finally self-assemble into larger liposomes (Maeki et al., 2017).

Transcutol® produces smaller nanoparticles than ethanol, except for the extreme cases at 5 and 40 mM lipid concentrations, where both means belong to the same group according to the Tukey method. The analysis also indicates that there is no statistically significant difference between ethanol at 20 and 40 mM, and between Transcutol® at 5 and 10 mM.

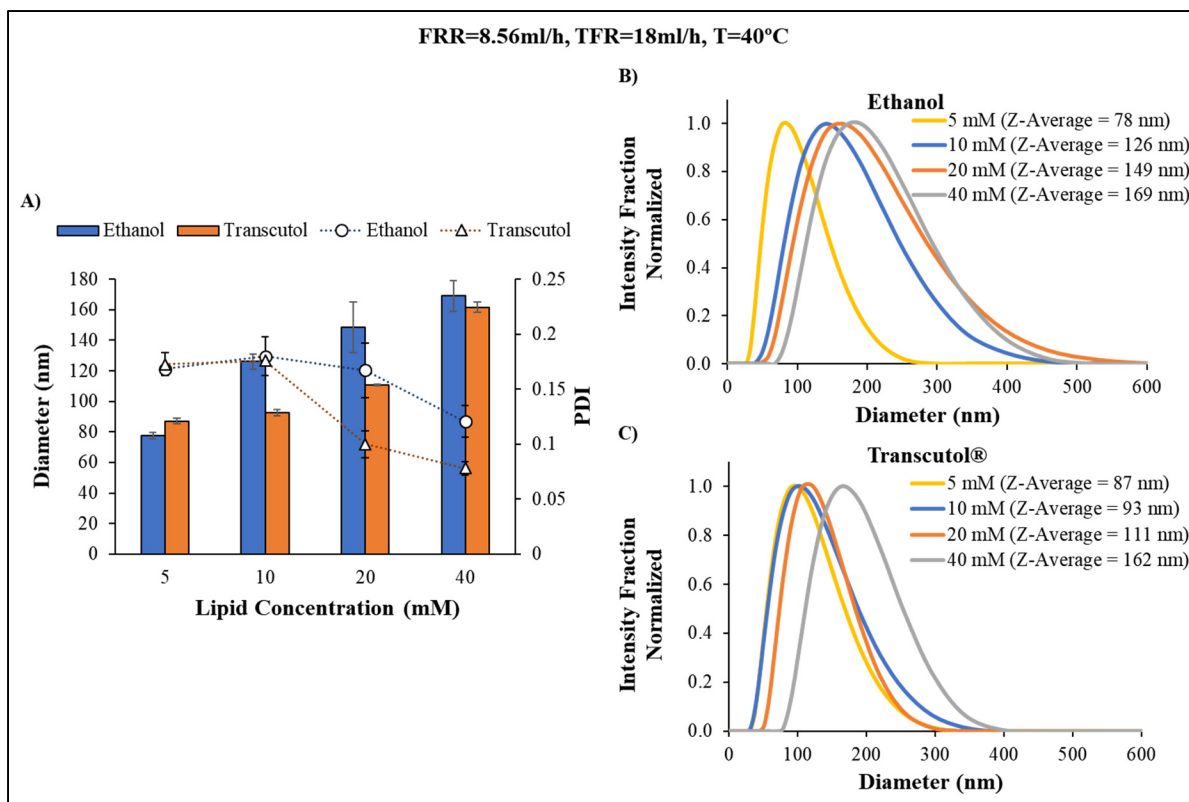


Figure 5.5 Liposomes synthesized using two different organic solvents and different lipid concentrations at 40 °C, with an FRR = 8.56 and TFR = 18mL/h A) Average size and PDI. The bars indicate +/- 1 SD n = 3 B) Size Distribution by Intensity Normalized for ethanol C) Size Distribution by Intensity Normalized for Transcutol®

The two organic solvents presented low PDI values. However, at higher lipid concentrations, Transcutol® offers a significantly smaller PDI, which is comparable to monodispersed populations.

Size Distribution by Intensity and Z-Average mean value (displayed in parentheses) for both ethanol and Transcutol® are found in Figure 5.5B and Figure 5.5C, respectively. Ethanol size distribution is shifted to the right compared with the one of Transcutol®, meaning bigger size. Additionally, high lipid concentration curves are wider, which implies that populations are less homogeneous.

The statistical analysis for zeta potential confirms once again that the electrokinetic potential is stable, meaning that regardless of the organic solvent used and the lipid concentration, all liposome zeta potential value means were statistically the same (see Figure 5.6).

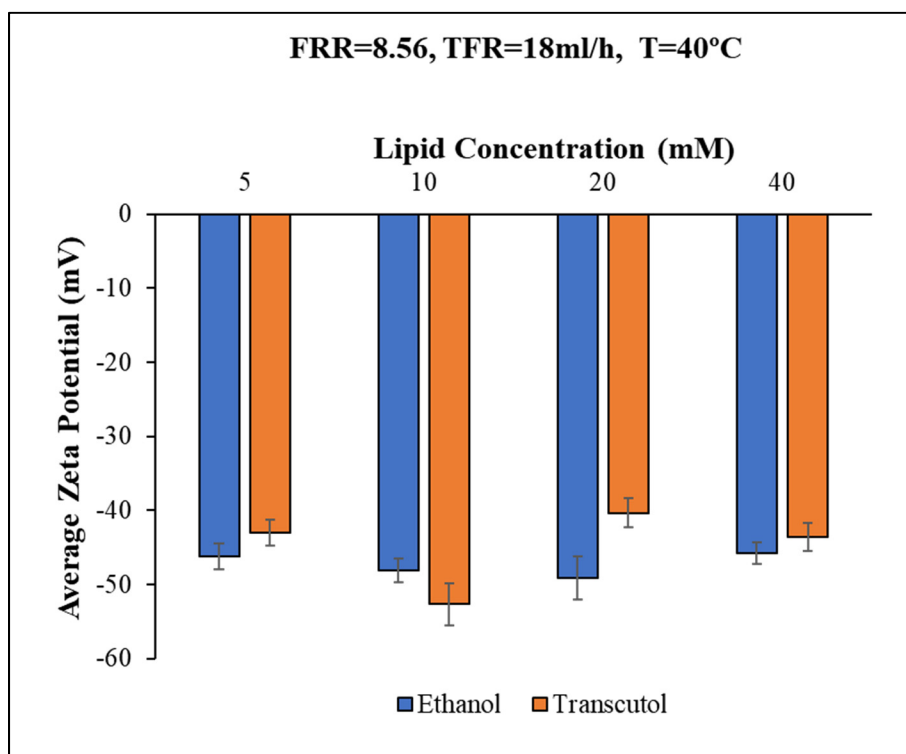


Figure 5.6 Zeta Potential of liposomes synthesized using two different organic solvents and different lipid concentrations at 40 °C, with an FRR = 8.56 and TFR = 18mL/h. The bars indicate +/- 1 SD  
n = 3

### 5.3.3 Temperature effects on liposomes produced with ethanol and Transcutol®

The third and last set of experiments shows the results of the effect of production temperature on nanoparticles with a 10 mM lipid concentration. Again, both ethanol and Transcutol® were used as organic solvents and Milli-Q water as an aqueous solvent.



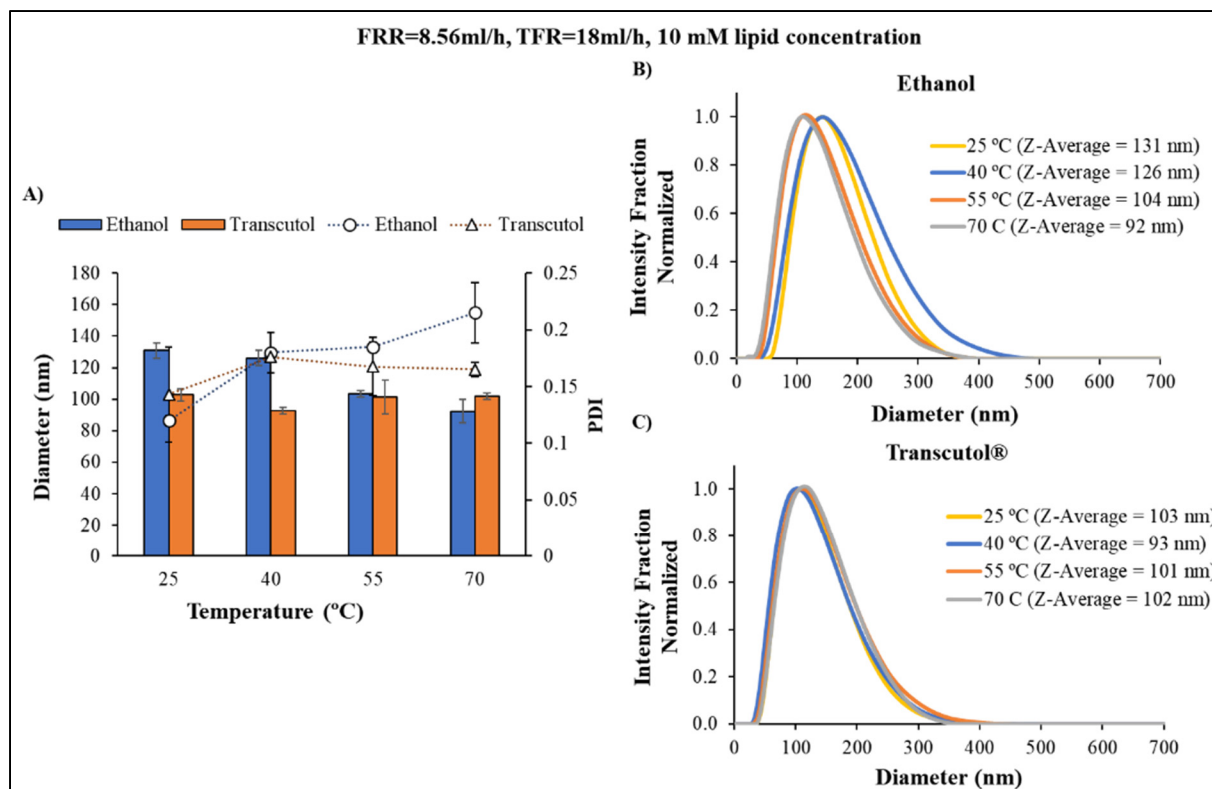


Figure 5.7 Liposomes synthesized using two different organic solvents and different production temperatures at 10 mM lipid concentration, with an FRR = 8.56 and TFR = 18mL/h A) Average size and PDI. The bars indicate  $\pm 1$  SD  $n = 3$  B) Size Distribution by Intensity Normalized for ethanol C) Size Distribution by Intensity Normalized for Transcutol®

When using ethanol, a relationship can be observed between temperature and diameter (see Figure 5.7), which is consistent with previous work on temperature effects (Zook & Vreeland, 2010). According to the Tukey method, there are only two different mean groups, one containing 25° and 40 °C, and another one with 55° and 70 °C. This behavior could be explained by the proximity to the gel-to-liquid crystalline phase transition temperature of the lipids and its relation to the elasticity modulus. Other authors have shown that liposome size increased when formed far below the transition temperature, as the membrane elasticity modulus is larger, and hence the membrane is much stiffer (Zook & Vreeland, 2010). As production temperature approaches the transition temperature, liposomes decrease in size, since the membrane becomes more elastic and bends faster in a closed vesicle. By contrast, above the

transition temperature, membrane elasticity modulus is much less dependent on temperature and liposome size suffers less variation. DMPC transition temperature is 24 °C, but when mixed with cholesterol it can widen the phase transition up to 10° to 15 °C, reaching 40 °C. This behavior explains why there is no significant difference between the two low temperatures. Above the transition temperature, size comes to be less dependent on temperature. Thus, 55° and 70 °C show no significant difference either (Zook & Vreeland, 2010).

Transcutol®, on the other hand, does not present this kind of behavior but shows a more stable average size. In fact, size averages at all four temperatures are statistically equal. There is neither a significant difference between the two solvents at 55° nor 70 °C. Thus, Transcutol® only offers statistically significant smaller particles at production temperatures below 55 °C.

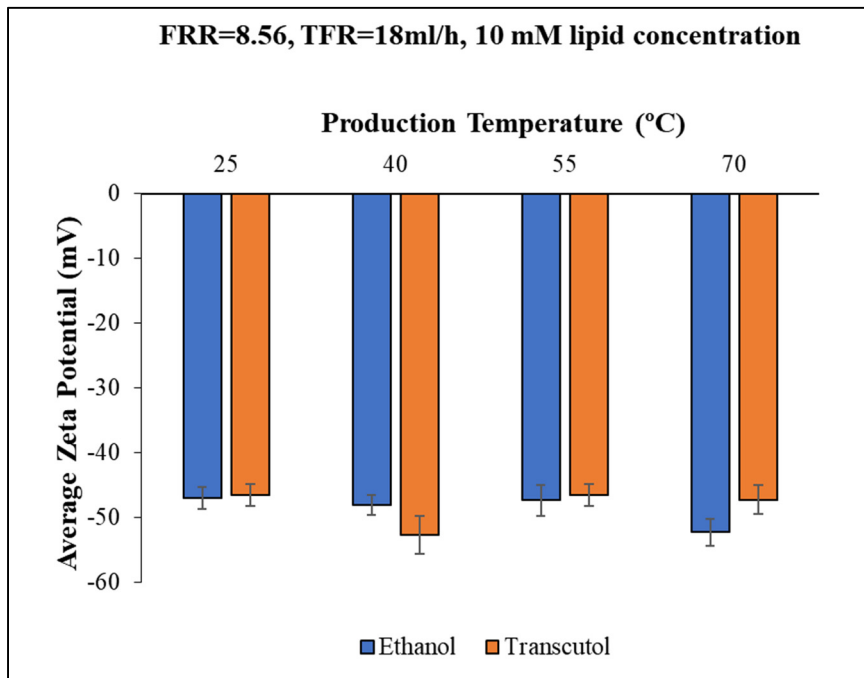


Figure 5.8 Zeta Potential of liposomes synthesized using two different organic solvents and different production temperatures at 10 mM lipid concentration, with an FRR = 8.56 and TFR = 18mL/h. The bars indicate +/- 1 SD  
n = 3

PDI, displayed in Figure 5.7A, is below 0.2 for all temperatures and solvents once again.

Finally, the statistical analysis for zeta potential confirms once more that the electrokinetic potential is stable, showing that regardless of the organic solvent used and the production temperature, all means were not statistically different (see Figure 5.8).

### 5.3.4 Liposome size stability

The characterization of the nanoparticles was performed one day after their synthesis. Fifty days later, after storing the solutions at 4 °C, a new characterization was carried out to study the size stability of these particles. In Fig. 6, a comparison between the two characterizations when using ethanol is presented. Fig. 6A shows Size Distributions by Intensity of the three sample groups that suffered less change, while Fig. 6B shows the ones which suffered the most significant change. In the first case, the means are statistically the same, whereas case B represents two significantly different means.

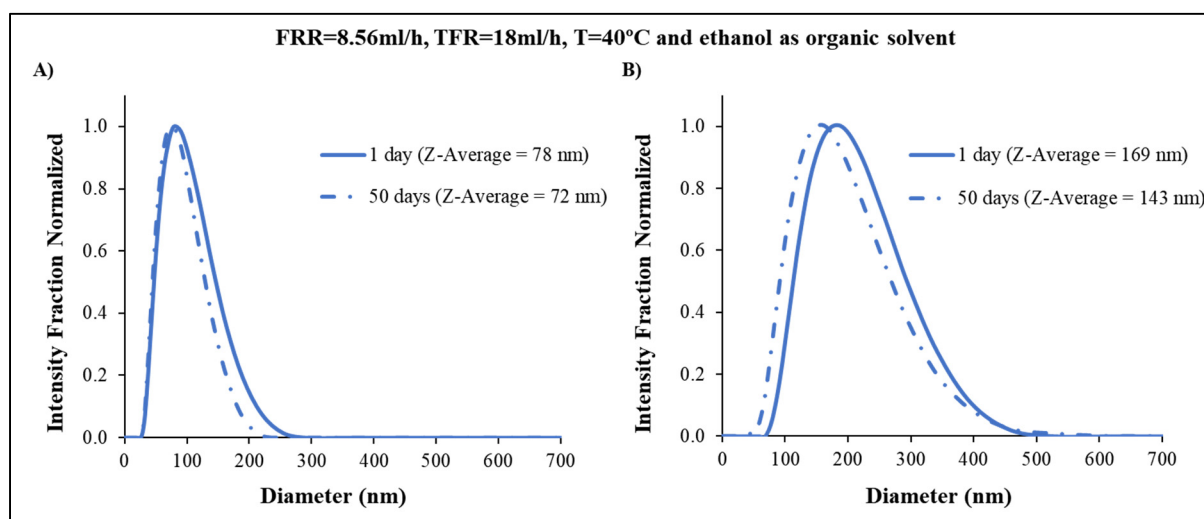


Figure 5.9 Liposome size evolution synthesized with ethanol at 40 °C using an FRR = 8.56 and TFR = 18 mL/h. 1-day vs. 50 days after synthesis characterization  
 A) Size Distribution by Intensity of the least changing sample synthesized with a 5 mM lipid concentration  
 B) Size Distribution by Intensity of the most changing sample synthesized with a 40 mM lipid concentration

Size distributions presented in Figure 7A and Figure 7B correspond respectively to the least and most changing particle size means, for the nanoparticles produced with Transcutol®. The characterizations were performed one day and 50 days after synthesis. Statistical analysis shows that in both cases, means are statistically equal. Transcutol® liposomes are consequently more size stable over time than ethanol liposomes.

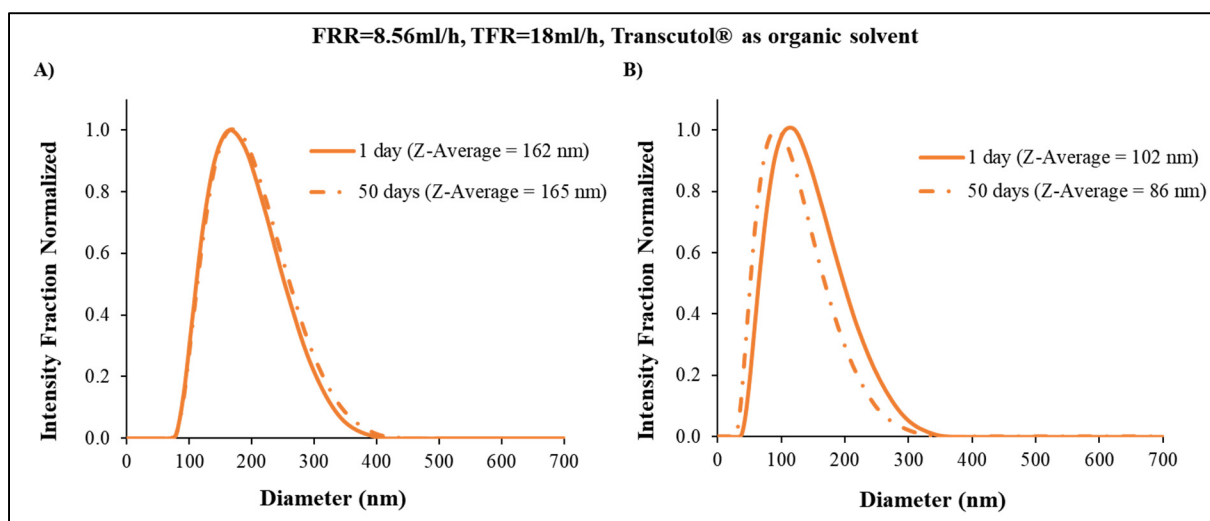


Figure 5.10 Liposome size evolution synthesized with Transcutol® using an FRR = 8.56 and TFR = 18mL/h. 1-day vs. 50 days after synthesis characterization A) Size Distribution by Intensity of the least changing sample produced at 40 °C and with a 40 mM lipid concentration B) Size Distribution by Intensity of the most changing sample produced at 70 °C and with a 10 mM lipid concentration

Size distributions presented in Figure 5.11A and Figure 5.11B correspond respectively to the least and most changing particle size means, for the nanoparticles produced with Transcutol®. The characterizations were performed one day and 50 days after synthesis. Statistical analysis shows that in both cases, means are statistically equal. Transcutol® liposomes are consequently more size stable over time than ethanol liposomes.

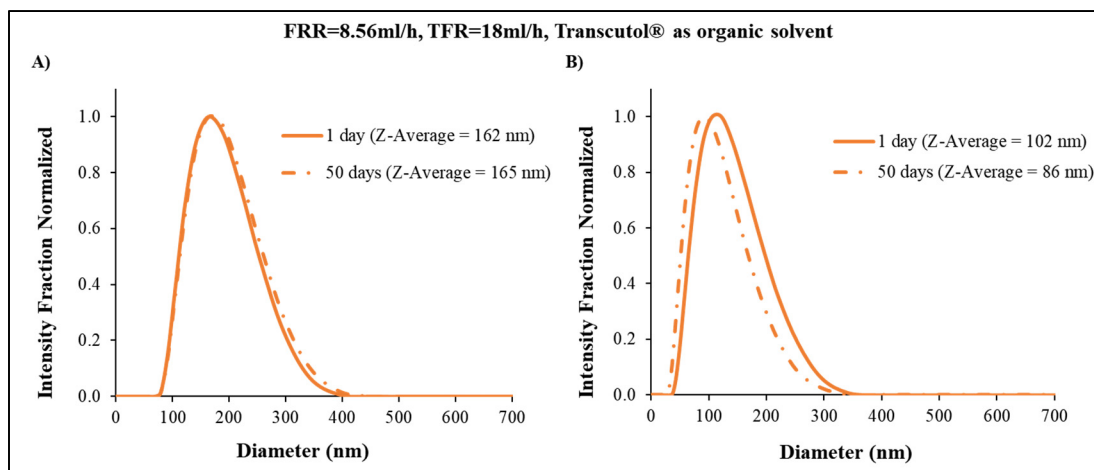


Figure 5.11 Liposome size evolution synthesized with Transcutol® using an FRR = 8.56 and TFR = 18mL/h. 1-day vs. 50 days after synthesis characterization  
 A) Size Distribution by Intensity of the least changing sample produced at 40 °C and with a 40 mM lipid concentration  
 B) Size Distribution by Intensity of the most changing sample produced at 70 °C and with a 10 mM lipid concentration

## 5.4 Chapter 5 conclusions

In this chapter, we investigated the liposome properties produced in a micromixer (PDM) using conventional organic solvents such as ethanol, IPA, and methanol, but also, and for the first time Transcutol®.

The substitution of the organic solvent by Transcutol® could help avoid additional filtration steps by virtue of its improved safety profile compared with other organic solvents. Moreover, it could be used as a skin permeation/penetration enhancer for liposomal DDS and provides a clear difference compared to methanol or IPA regarding safety issues.

The obtained results demonstrate that IPA and Transcutol® produce smaller nanoparticles than ethanol and methanol under the studied condition, while Transcutol® produces smaller particles under several different temperatures and lipid concentration conditions compared with ethanol. The studies also showed that the organic solvent used, production temperature, and lipid concentration have no effect on the nanoparticle zeta potential.



## CHAPTER 6

### FUTURE WORK: TOWARDS BIOMEDICAL APPLICATIONS

In this chapter, we describe research findings derived from this work as well as potential research lines for future work. Most of them are focused on accelerating the technology transfer from the laboratory to biomedical applications for the benefit of patients. This objective could be fulfilled by facilitating micromixers fabrication, reduce its cost as well as increase liposome production yield. Finally, liposome characterization methods can be used to investigate cell to cell communication.

#### 6.1 Alternative microfabrication process: 3D printing

3D-printing has recently attracted the interest of researchers in microfluidics. This technology has proved its potential as a way of fabricating microchannels, offering an automated, low-cost, and straight-forward approach compared with the laborious soft-lithography method (N. Bhattacharjee, Urrios, Kang, & Folch, 2016). 3D-printing enables rapid prototyping. Microfluidic devices can be produced using an additive 3D-printing method such as fused deposition modeling (FDM), with channels width in the order of hundreds of micrometers. These devices can be used for testing new topologies, geometries, and concepts before investing in other costlier methods. However, the study of the fluid flows inside microfluidic devices requires optical access to microchannels. Unfortunately, even transparent materials such as Poly lactic acid (PLA) produce translucent 3D prints, that are not optically transparent, because of the layering process in 3D-printing. We proposed a way of creating an optical window by using an open channel approach delimited by cyclic olefin copolymer (COC). This approach enabled us to monitor liquid flow inside the device using biocompatible materials.

We fabricated a MHF micromixer using 3D-printing. This device was first proposed more than 20 years ago (Knight, Vishwanath, Brody, & Austin, 1998), it has proved useful for multiple applications from liposomes synthesis (Andreas Jahn et al., 2004) to microdroplet generation (Anna, Bontoux, & Stone, 2003).

We proposed a 3D-printed-PLA micromixer with COC as a ceiling, enabling optical access and biocompatibility. Moreover, this method can be completed in a few steps, making it ideal for low-cost rapid prototyping and proof of concept. Figure 6.1 shows the fabrication process of the proposed device.

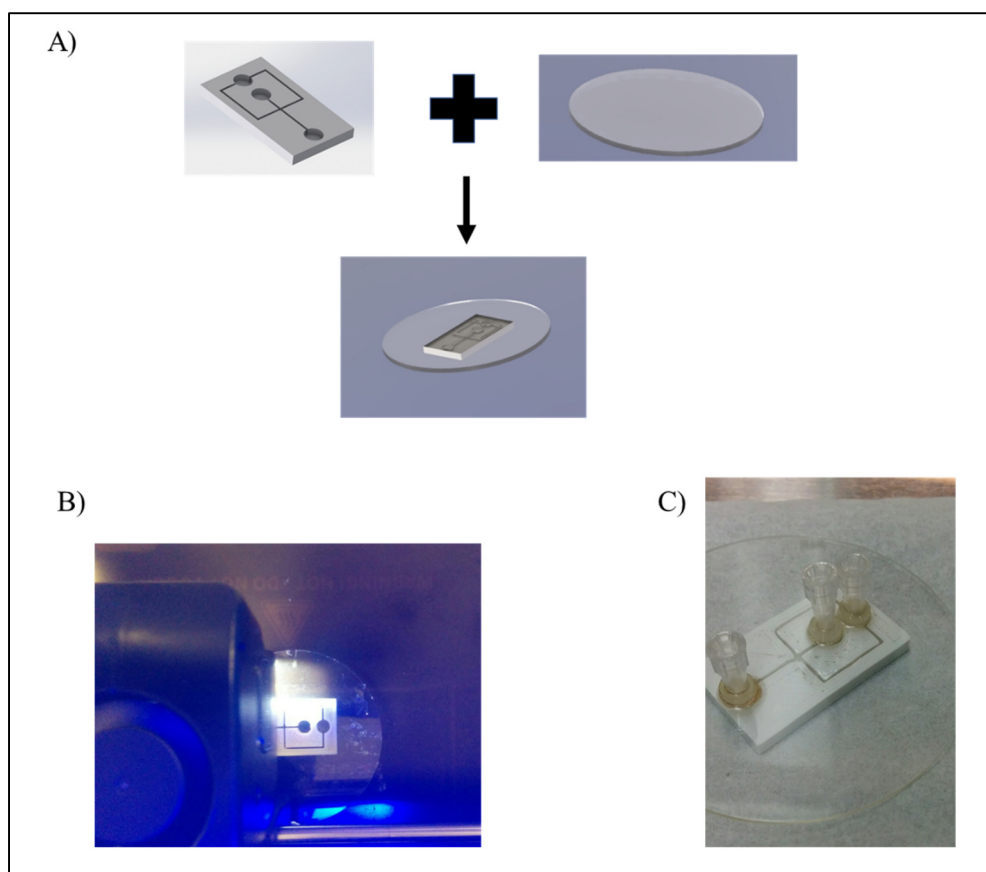


Figure 6.1 Microfabrication process of 3D printed-PLA-COC device A) PLA device and COC “ceiling” B) 3D printing the microfluidic device C) A completed device with connectors

This work was presented in NEWCAS 2019, Montreal, Canada (Lopez, Nerguizian, & Stiharu, 2018). Future work on this subject includes the creation of microfluidic devices molds using 3D printing, as well as the complete fabrication of the device, and connectors in one single step for different types of micromixers.



Other methods, such as SLA, might offer better dimensional resolution in the order of tens of micrometers.

## **6.2 Geometry optimization for an improved liposome production yield**

The PDM dimensional aspects play a crucial role in mixing, and thus on liposome production. Numerical model results have shown that the mixing process is completed in the first ten semicircular structures (see Section 3.2.3.7). Thus, the microfluidic device could be shortened. Theoretically, liposomes will be produced under the same conditions. This approach will enable to reduce the device footprint as well as limit alignment manipulations. This planar optimization can save space to create a dense array of micromixers to parallelize production and increase the liposome yield. An array of at least 6 PDMs could be easily fitted in a 100-mm wafer with an estimated production of 247 mg/h of liposomes.

Also, the effects of the microchannel height must be further studied. It is predicted that a lower aspect ratio device will cause an increase in the flow speed in the PDM narrowest sections, increasing centripetal forces, therefore speeding the mixing process, and consequently producing smaller liposomes than higher aspect ratio devices. This last point must be experimentally corroborated.

## **6.3 Approaches to facilitate liposome production implementation**

In this work, liposome production was demonstrated using a novel passive micromixer. This approach utilizes syringe pumps, a computer interface to control these pumps, the microfluidic device, and a hot plate to control the production temperature. This setup is required to produce liposomes at a scale of milliliters to liters. However, this method could not be ideal for researchers whose primary interest is testing different formulations rapidly using quantities in the range of  $\mu\text{L}$  with high repeatability. The need for an external driving force, as in this case pumps, hinders the use of this method in a standard biology laboratory setting, where this

process is just one among many others. Other more bench-friendly approaches are required with a low-entry-cost to produce liposomes and prepare liposomes medications at the bedside.

One possible solution is to remove the active elements (pumps) of the experimental setup and leave only the microfluidic device itself. Nevertheless, this approach requires other forces to move the liquids into the channels to mix the reagents and thus produce liposomes. These mechanisms could be capillarity forces, vacuum, gravity, or centrifuge compatible devices. Capillarity is a motor force that has been explored before (Zimmermann, Schmid, Hunziker, & Delamarche, 2007), in a micromixer with baffle structures (C.-T. Lee & Lee, 2012). However, as far as the author knows, this approach has never been assessed for liposome production. A pumpless liposome production approach can be useful to make liposome research more accessible to laboratories working on drug delivery, transfection, and imaging.

#### **6.4 EVs characterization for cancer research**

Recently, EVs have attracted attention mainly because of their role as messengers between cells. EVs transport proteins, genetic material, and other biologically relevant molecules inside their lipid bilayers. EVs are released from cells; their size is in the range of 40 nm to 1  $\mu\text{m}$ . The size of these vesicles is highly heterogenous (Raposo & Stoorvogel, 2013).

Moreover, EVs play a crucial role in modulating tumorigenic behavior (Xu, Liao, & Zhou, 2018). EVs properties play a role in how effective biomolecules cargo can be transferred between cells (Horibe, Tanahashi, Kawauchi, Murakami, & Rikitake, 2018). However, until now, it is not clear which variables are more important for this transfer. Size, size distribution, zeta potential, surface moieties, and lipid composition might play a crucial role.

By using the same methods to characterize liposomes, EVs can be further studied to understand how their physicochemical characteristics influence *invitro* and *invivo* interactions and their relationship with cancer malignancy. Following this approach, we studied EVs derived from 3 primary uveal melanoma (UM) cell lines (MP41, MP46, OCM), a metastatic (OMM2.5) UM

cell line and fibroblasts (HTB 102) as control were extracted by ultracentrifugation. EV size and size distribution were characterized using DLS. The zeta potential of EVs was calculated from their electrophoretic mobility.

This characterization is the first complete analysis of the physicochemical characterization of EVs derived from UM cells. Our data showed a difference in the physicochemical features of EVs derived from primary and metastatic UM cell lines as well as non-cancerous cells.

The work summarized in the previous paragraphs was accepted to be presented as a poster in the Association for Research in Vision and Ophthalmology (ARVO) 2020 Conference in Baltimore, USA. (Cancelled due to COVID-19). Future work includes an extensive characterization of EVs extracted from other cell lines.

## **6.5 Gene delivery applications**

Liposomes can deliver genetic material inside cells (transfection). Positively charged vesicles, also known as cationic liposomes form through electrostatic interactions complexes with the negatively charged DNA or RNA, this complex can be delivered inside the cells (P. L. Felgner et al., 1987). The platform presented in this work could be used to produce gene delivery systems. An optimization of this delivery could be achieved using a similar approach to the one shown in Chapter 3.2. This statistically modeling approach has been tried for MHF devices for liposomes with transfection applications (Tiago A. Balbino et al., 2013), but it has not attempted before for micromixers based on Dean flow dynamics. An example of the factors and responses in gene delivery systems production is shown in Figure 6.2, on the left the production factors and on the right the responses.

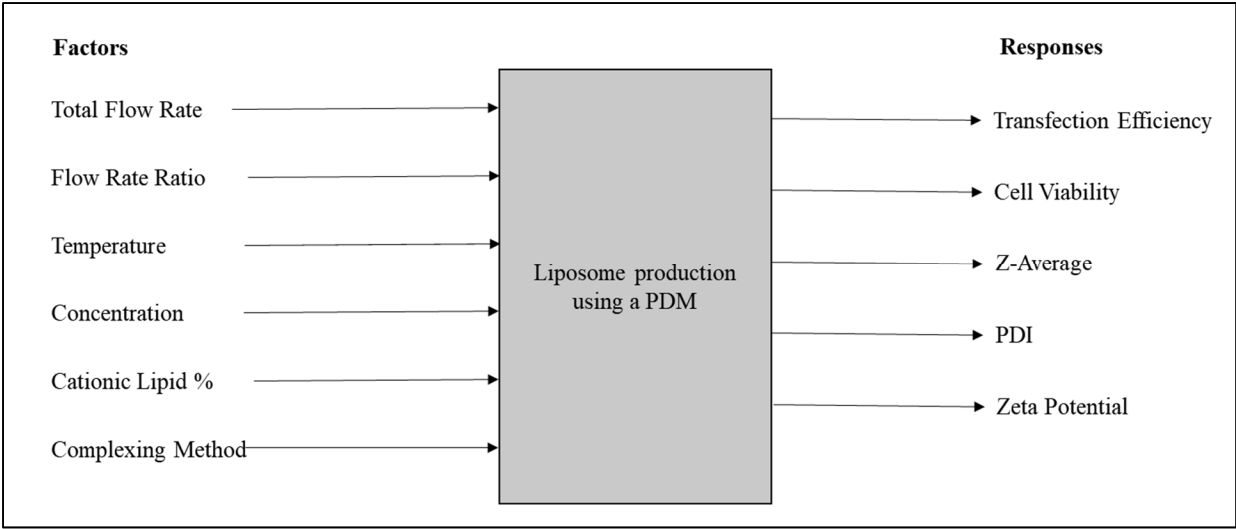


Figure 6.2 Factors influencing gene delivery systems production

## CONCLUSIONS

Liposomes production on an industrial scale with high reproducibility is required to deploy liposomes for biomedical applications effectively. This doctoral dissertation investigates the production of LNPs using a novel Dean dynamic flow-based micromixer, the PDM. We showed the relationship between mixing efficiency and liposome properties. Liposomes produced using the PDM have a size range from 27 nm to more than 200 nm. This range is relevant for applications in drug, gene, and imaging delivery systems.

Additionally, liposome populations were mostly monomodal, from highly monodispersed to low polydispersed populations. This result is particularly important for ensuring that all particles will end in the same place, similar to a quality factor. Additionally, we demonstrated how liposome size and size distribution are controlled by TFR, FRR, concentration, temperature, lipid mixture, and organic solvent. Furthermore, we showed that the zeta potential of liposomes was controlled only by the liposome lipid composition.

In this work, we showed that the PDM could produce liposomes at a rate of 41 mg/h. This production yield is comparable only with high-aspect-ratio and chaotic advection-based devices. This production yield can be further increased by increasing TFR and by microfluidic device parallelization means. The PDM can produce nanosized lipid nanoparticles at low FRR, improving the final liposome concentration.

Liposome properties are consistent under the same production conditions; thus, the presented method is reproducible. Furthermore, liposome size and size distribution are stable for up to 6 months, showing that the centripetal forces do not have a negative impact on the membrane's integrity. This stability is crucial for the shelf-life of drug delivery systems.

To investigate liposome production in the PDM, a methodology to first identify and then model the key factors controlling liposome production was used to find the experimental conditions under which liposomes of suitable size would be produced. The model was validated with

further experimentation. Finally, a numerical model, including concentration-dependent variables, was used to assess the mixing index and its relationship with the physicochemical characteristics of liposomes. This methodology is relevant for investigating micromixers designs tailored to liposome production.

To extend our understanding of liposome production, further parametric experiments, including fluid flow and related molecular variables, were performed as well as additional confocal imaging to observe and analyze the mixing phenomenon qualitatively. We found out that TFR played a crucial role in controlling liposome size in a wide range of conditions. By contrast, FRR showed to separate highly monodispersed and low polydispersed liposome populations with a threshold of around three. Similarly, we found out a negatively correlated relationship between temperature and liposome size. We also presented a model that relates concentration with the nonlinear liposome size increase, which works for liposomes produced above the transition temperature.

Finally, the influence of the organic solvent used for liposome production over liposome physicochemical characteristics was investigated. We demonstrated that the polarity change rate could also be modulated by selecting different organic solvents. The substitution of conventional organic solvents by Transcutol® could potentially prevent the need for additional filtration steps for toxicity reduction.

In summary, we investigated several factors influencing liposome physicochemical properties, which provided a glance in the fundamental aspects of liposome formation using micromixers. The proposed method proved to be suitable for producing liposomes in continuous flow at high production rates. This approach could also be used in other amphiphilic-based nanoparticles, such as copolymers. Innovative approaches in microfabrication such as 3D printing and pumpless production of liposomes might accelerate the translation of this technology to laboratories working on developing new liposomal formulations. Furthermore, this platform has the potential to be a powerful tool to produce drug and gene delivery systems as well as to investigate EVs' role in cancer dissemination and cell to cell communication.

## RECOMMENDATIONS

This brief section's objective is to compare the presented approach with currently available solutions, discuss opportunity areas, and recommend new avenues of research. There are three critical aspects groups in regard to liposome research and production that will significantly accelerate liposome adoption as a widely used delivery system. The first one is the ease of the production and modulation of liposome properties from early research stages to mass production. The second is the scalability and the production rate. Finally, the third is about overcoming the nanoprecipitation method limitations, mainly the use of organic solvents that could be detrimental for drug delivery applications.

First, the production of liposomes must be easy and as few steps as possible. The reason is twofold. At a research level, this will help the adoption of liposomes by reducing the risk of testing innovative formulations. Nowadays, researchers in the field have to face a difficult decision; doing liposomes using outdated methods with inconsistent results, buying liposomes that are not tailored to their research objectives, or acquiring equipment that is extremely expensive to buy and operate. The solution at an abstract level is a device, without technical difficulties that adapt well to the existing research environment, with a low financial risk to try. One probable solution could be achieved by simplifying the platform presented in this work by eliminating the pumps, the hot plate, and using innovative approaches to move and mix liquids inside the microfluidic device. Currently, there is not a commercially available device capable of producing liposomes using only a microfluidic device without active components. At an industrial level, the simplification will result in fewer steps and the reduction of costs.

In this work, average liposome size and size distribution were controlled mainly by varying the FRR, TFR, temperature, lipid type, initial lipid concentration, and binary mixture. Remarkably, the PDI of the particles does not change dramatically for different flow conditions ( $PDI \approx 0.2$ ). In PDI terms, the liposomes produced in PDM are in between the pure molecular

diffusion devices and the micromixers based on chaotic advection such as the SHM. A more extensive experimental range would provide a better understanding of how the liposome population homogeneity could be further improved. In terms of zeta potential, the data presented suggest that this property is influenced by the liposome lipid composition, a complete study focusing on this topic will be useful for developing new liposomal formulations. Finally, new micromixer designs, geometric parameters, and principles should be explored. This approach could be aided by numerical models and rapid prototyping techniques such as high precision 3D printing using stereolithography. Very recently, pure molecular diffusion micromixers have been optimized using this approach.

The second key aspect are scalability and production rate. Liposome production using micromixers can be scaled by parallelization means. One limitation of this research is that the actual length and number of structures required to produce liposomes were not studied. Such data will give future researchers the tools to optimize the microfluidic footprint crucial to get as many as possible of these devices in a reduced area. A second limitation is related to the production rate. The demonstrated liposome yield in this work was in the same order of magnitude than high aspect ratio devices based only on flow focusing. However, it was below the devices based on chaotic advection. Higher initial lipid concentrations and total flow rates will further improve liposome production yield. In this work, the use of soft lithography constraints the aspect ratios, the pressure inside the microchannels (or the total flow rate) and the binary mixtures that can be safely used. Other biocompatible materials such as cyclic olefin copolymer and production methods such as hot embossing will significantly increase liposome production capacities overcoming fabrication constraints.

Finally, the nanoprecipitation method has a pitfall; the presence of the organic solvent is detrimental for the function of the liposomes. In this work, it was demonstrated for the first time that an alternative hydroalcoholic solvent (Transcutol) could be used to produce liposomes with expected reduced toxicity eliminating a step (solvent removal). Ideally, this solvent removal step should be incorporated in one chip, though some efforts to remove this



out of the chip have been presented elsewhere. The use of membranes inside the microchannels might help to incorporate a filtration step, producing liposomes ready to be used.

In summary, there are several avenues of research that include improving the mixing process, the ease of production and modulation of liposome properties as well as the incorporation of filtration steps into one single chip and step. Liposomes are a system that has the potential to foster the pharmaceutical industry for the benefit of patients.



## APPENDIX I

### PUBLICATIONS DURING PH.D. STUDIES

López, R. R., Ocampo, I., G. Font de Rubinat, P., Sánchez, L.-M., Alazzam, A., Tsering, T., Bergeron, K.-F., Camacho-León, S., Burnier, J. V., Mounier, C., Stiharu, I., & Nerguizian, V. (2020). *Parametric Study of the Factors Influencing Liposome Physicochemical Characteristics in a Periodic Disturbance Mixer*. Manuscript submitted.

López, R. R., G. Font de Rubinat, P., Sánchez, L.-M., Ocampo, I., Alazzam, A., Bergeron, K.-F., Mounier, C., Stiharu, I., & Nerguizian, V. (2020). *Transcutol®: A promising drug solubilizer suitable for in continuous flow liposome production in a Periodic Disturbance  $\mu$ mixer*. Paper presented at the 7th FIP Pharmaceutical Sciences World Congress (PSWC2020), Montreal, Canada. (Accepted and to be presented as poster).

López, R. R., G. Font de Rubinat, P., Sánchez, L.-M., Alazzam, A., Stiharu, I., & Nerguizian, V. (2020). *Lipid Fatty Acid Chain Influence over Liposome Physicochemical Characteristics Produced in a Periodically Disturbed Micromixer*. Paper presented at the IEEE Nano 2020, Montreal. (Accepted and to be presented as oral presentation).

López, R. R., Tsering, T., Bustamante, P., G. Font de Rubinat, P., Stiharu, I., Burnier, J. V., & Nerguizian, V. (2020). *Unraveling uveal melanoma-derived extracellular vesicles: a physicochemical characterization*. Paper presented at the Association for Research in Vision and Ophthalmology (ARVO 2020), Baltimore, USA. (Accepted and to be presented as poster).

López, R. R., & Olivares-Quiroz, L. (2020). *Liposomas, de la Física Biológica a la Medicina Molecular*. Revista Ciencia, (Trimestral, 2020). Academia Mexicana de Ciencias, Ciudad de México. Manuscript submitted

López, R. R., G. Font de Rubinat, P., Sánchez, L.-M., Alazzam, A., Bergeron, K.-F., Mounier, C., Stiharu, I., & Nerguizian, V. (2020). *The Effect of Different Organic Solvents in Liposome Properties Produced in a Periodic Disturbance Mixer: Transcutol®, a potential organic solvent replacement*. Manuscript submitted

- López, R. R., Ocampo, I., Sánchez, L.-M., Alazzam, A., Bergeron, K.-F., Camacho-León, S., Mounier, C., Stiharu, I., & Nerguizian, V. (2020). Surface Response Based Modeling of Liposome Characteristics in a Periodic Disturbance Mixer. *Micromachines*, 11(3), 235. (Published)
- López Salazar, R. R., Ocampo, I., Bergeron, K.-F., Alazzam, A., Mounier, C., Stiharu, I., & Nerguizian, V. (2019). *Assessment of the Factors Influencing Liposome Size in Dean Forces Based  $\mu$ mixers*. Paper presented at the  $\mu$ TAS 2019 The 23rd International Conference on Miniaturized Systems for Chemistry and Life Sciences Basel, Switzerland. (Presented as poster).
- Lopez, R., Nerguizian, V., & Stiharu, I. (2018, 24-27 June 2018). *Low-Cost 3D-Printed PLA-COC Micro Hydrodynamic Focused Device*. Paper presented at the 2018 16th IEEE International New Circuits and Systems Conference (NEWCAS). (Presented and published).
- Lopez, R. R., Nerguizian, V., & Stiharu, I. (2018). Mass Production of Liposomes—Pushing Forward Next-Generation Therapies. *Substance ÉTS*. (In press).

## BIBLIOGRAPHY

- Allen, T. M., & Cullis, P. R. (2013). Liposomal drug delivery systems: from concept to clinical applications. *Adv Drug Deliv Rev*, 65(1), 36-48. doi:10.1016/j.addr.2012.09.037
- Amrani, S., & Tabrizian, M. (2018). Characterization of Nanoscale Loaded Liposomes Produced by 2D Hydrodynamic Flow Focusing. *ACS Biomaterials Science & Engineering*, 4(2), 502-513. doi:10.1021/acsbmaterials.7b00572
- Angelova, M., & Dimitrov, D. S. (1988). A mechanism of liposome electroformation. In V. Degiorgio (Ed.), *Trends in Colloid and Interface Science II* (pp. 59-67). Darmstadt: Steinkopff.
- Anna, S. L., Bontoux, N., & Stone, H. A. (2003). Formation of dispersions using “flow focusing” in microchannels. *Applied Physics Letters*, 82(3), 364-366. doi:doi:<http://dx.doi.org/10.1063/1.1537519>
- Arrieta, O., Medina, L.-A., Estrada-Lobato, E., Ramírez-Tirado, L.-A., Mendoza-García, V.-O., & de la Garza-Salazar, J. (2014). High liposomal doxorubicin tumour tissue distribution, as determined by radiopharmaceutical labelling with <sup>99m</sup>Tc-LD, is associated with the response and survival of patients with unresectable pleural mesothelioma treated with a combination of liposomal doxorubicin and cisplatin. *Cancer Chemotherapy and Pharmacology*, 74(1), 211-215. doi:10.1007/s00280-014-2477-x
- B. Knight, J., Vishwanath, A., Brody, J., & Austin, R. (1998). *Hydrodynamic Focusing on a Silicon Chip: Mixing Nanoliters in Microseconds* (Vol. 80).
- Baker, M. T., & Heriot, W. A. (2005). US006855296B1.
- Balbino, T. A., Aoki, N. T., Gasperini, A. A. M., Oliveira, C. L. P., Azzoni, A. R., Cavalcanti, L. P., & de la Torre, L. G. (2013). Continuous flow production of cationic liposomes at high lipid concentration in microfluidic devices for gene delivery applications. *Chemical Engineering Journal*, 226, 423-433. doi:<http://dx.doi.org/10.1016/j.cej.2013.04.053>
- Balbino, T. A., Azzoni, A. R., & de la Torre, L. G. (2013). Microfluidic devices for continuous production of pDNA/cationic liposome complexes for gene delivery and vaccine therapy. *Colloids and Surfaces B: Biointerfaces*, 111, 203-210. doi:<http://dx.doi.org/10.1016/j.colsurfb.2013.04.003>
- Balbino, T. A., Serafin, J. M., Radaic, A., de Jesus, M. B., & de la Torre, L. G. (2017). Integrated microfluidic devices for the synthesis of nanoscale liposomes and

- lipoplexes. *Colloids and Surfaces B: Biointerfaces*, 152, 406-413. doi:<https://doi.org/10.1016/j.colsurfb.2017.01.030>
- Bangham, A. D., De Gier, J., & Greville, G. D. (1967). Osmotic properties and water permeability of phospholipid liquid crystals. *Chemistry and Physics of Lipids*, 1(3), 225-246. doi:[http://dx.doi.org/10.1016/0009-3084\(67\)90030-8](http://dx.doi.org/10.1016/0009-3084(67)90030-8)
- Barenholz, Y. (2012). Doxil® — The first FDA-approved nano-drug: Lessons learned. *Journal of Controlled Release*, 160(2), 117-134. doi:<http://dx.doi.org/10.1016/j.jconrel.2012.03.020>
- Batzri, S., & Korn, E. D. (1973). Single bilayer liposomes prepared without sonication. *Biochimica et Biophysica Acta (BBA) - Biomembranes*, 298(4), 1015-1019. doi:[http://dx.doi.org/10.1016/0005-2736\(73\)90408-2](http://dx.doi.org/10.1016/0005-2736(73)90408-2)
- Beckett, C., Laugharn, J. A., & Kakumanu, S. K. (2017). US9776149.
- Belliveau, N. M., Huft, J., Lin, P. J. C., Chen, S., Leung, A. K. K., Leaver, T. J., . . . Cullis, P. R. (2012). Microfluidic Synthesis of Highly Potent Limit-size Lipid Nanoparticles for In Vivo Delivery of siRNA. *Molecular Therapy. Nucleic Acids*, 1(8), e37. doi:10.1038/mtna.2012.28
- Bernardes, A. T. (1996). Computer Simulations of Spontaneous Vesicle Formation. *Langmuir*, 12(24), 5763-5767. doi:10.1021/la960209j
- Bhattacharjee, N., Urrios, A., Kang, S., & Folch, A. (2016). The upcoming 3D-printing revolution in microfluidics. *Lab on a Chip*, 16(10), 1720-1742. doi:10.1039/C6LC00163G
- Bhattacharjee, S. (2016). DLS and zeta potential – What they are and what they are not? *Journal of Controlled Release*, 235, 337-351. doi:<https://doi.org/10.1016/j.jconrel.2016.06.017>
- Blanco, E., Shen, H., & Ferrari, M. (2015). Principles of nanoparticle design for overcoming biological barriers to drug delivery. *Nature Biotechnology*, 33(9), 941-951.
- Bleul, R., Thiermann, R., & Maskos, M. (2015). Techniques To Control Polymersome Size. *Macromolecules*, 48(20), 7396-7409. doi:10.1021/acs.macromol.5b01500
- Bosch, E., & Rosés, M. (1992). Relationship between ET polarity and composition in binary solvent mixtures. *Journal of the Chemical Society, Faraday Transactions*, 88(24), 3541-3546. doi:10.1039/FT9928803541
- Bottaro, E., Mosayyebi, A., Carugo, D., & Nastruzzi, C. (2017). Analysis of the Diffusion Process by pH Indicator in Microfluidic Chips for Liposome Production. *Micromachines*, 8(7), 209. doi:10.3390/mi8070209

- Buck, J., Grossen, P., Cullis, P. R., Huwyler, J., & Witzigmann, D. (2019). Lipid-Based DNA Therapeutics: Hallmarks of Non-Viral Gene Delivery. *ACS Nano*, 13(4), 3754-3782. doi:10.1021/acsnano.8b07858
- Business-Wire. (2019). Global Nanopharmaceuticals Market to Surpass US\$ 168.91 Billion by 2026. Retrieved from <https://www.bloomberg.com/press-releases/2019-02-15/global-nanopharmaceuticals-market-to-surpass-us-168-91-billion-by-2026>
- Campardelli, R., Trucillo, P., & Reverchon, E. (2018). Supercritical assisted process for the efficient production of liposomes containing antibiotics for ocular delivery. *Journal of CO2 Utilization*, 25, 235-241. doi:<https://doi.org/10.1016/j.jcou.2018.04.006>
- Capreto, L., Cheng, W., Hill, M., & Zhang, X. (2011). *Microfluidics : technologies and applications* (L. Bingcheng Ed. 1 ed. Vol. 304). Berlin; New York: Springer-Verlag Berlin Heidelberg.
- Carugo, D., Bottaro, E., Owen, J., Stride, E., & Nastruzzi, C. (2016). Liposome production by microfluidics: potential and limiting factors. *Scientific reports*, 6, 25876. doi:10.1038/srep25876
- Castor, T. P. (1996). US5554382A.
- Castor, T. P., & Chu, L. (1998). US5776486.
- Chen, Z., Han, J. Y., Shumate, L., Fedak, R., & DeVoe, D. L. (2019). High Throughput Nanoliposome Formation Using 3D Printed Microfluidic Flow Focusing Chips. *Advanced Materials Technologies*, 0(0), 1800511. doi:doi:10.1002/admt.201800511
- Cheung, C. C. L., & Al-Jamal, W. T. (2019). Sterically stabilized liposomes production using staggered herringbone micromixer: Effect of lipid composition and PEG-lipid content. *International Journal of Pharmaceutics*, 566, 687-696. doi:<https://doi.org/10.1016/j.ijpharm.2019.06.033>
- Cho, K., Wang, X., Nie, S., Chen, Z. G., & Shin, D. M. (2008). Therapeutic nanoparticles for drug delivery in cancer. *Clinical Cancer Research*, 14(5), 1310-1316. doi:10.1158/1078-0432.CCR-07-1441
- Cinquerrui, S., Mancuso, F., Vladislavljević, G. T., Bakker, S. E., & Malik, D. J. (2018). Nanoencapsulation of Bacteriophages in Liposomes Prepared Using Microfluidic Hydrodynamic Flow Focusing. *Frontiers in Microbiology*, 9(2172). doi:10.3389/fmicb.2018.02172
- Costa, A. P., Xu, X., & Burgess, D. J. (2014). Freeze-Anneal-Thaw Cycling of Unilamellar Liposomes: Effect on Encapsulation Efficiency. *Pharmaceutical Research*, 31(1), 97-103. doi:10.1007/s11095-013-1135-z

- Costa, A. P., Xu, X., Khan, M. A., & Burgess, D. J. (2016). Liposome Formation Using a Coaxial Turbulent Jet in Co-Flow. *Pharmaceutical Research*, 33(2), 404-416. doi:10.1007/s11095-015-1798-8
- Croci, R., Bottaro, E., Chan, K. W. K., Watanabe, S., Pezzullo, M., Mastrangelo, E., & Nastruzzi, C. (2016). Liposomal Systems as Nanocarriers for the Antiviral Agent Ivermectin. *International Journal of Biomaterials*, 2016, 15. doi:10.1155/2016/8043983
- Danckwerts, P. V. (1952). The definition and measurement of some characteristics of mixtures. *Applied Scientific Research, Section A*, 3(4), 279-296. doi:10.1007/bf03184936
- Dimov, N., Kastner, E., Hussain, M., Perrie, Y., & Szita, N. (2017). Formation and purification of tailored liposomes for drug delivery using a module-based micro continuous-flow system. *Sci Rep*, 7(1), 12045. doi:10.1038/s41598-017-11533-1
- Dolomite. (2020). <https://www.dolomite-microfluidics.com/microfluidic-systems/liposome-synthesis/>. Retrieved from <https://www.dolomite-microfluidics.com/microfluidic-systems/liposome-synthesis/>
- Du, Y., Zhang, Z., Yim, C., Lin, M., & Cao, X. (2010). A simplified design of the staggered herringbone micromixer for practical applications. *Biomicrofluidics*, 4(2), 024105. doi:10.1063/1.3427240
- Durst, F., Ray, S., Ünsal, B., & Bayoumi, O. A. (2005). The Development Lengths of Laminar Pipe and Channel Flows. *Journal of Fluids Engineering*, 127(6), 1154-1160. doi:10.1115/1.2063088
- Ehrlich, P. (1913). Address in Pathology, ON CHEMIOOTHERAPY: Delivered before the Seventeenth International Congress of Medicine. *British Medical Journal*, 2(2746), 353-359. doi:10.1136/bmj.2.2746.353
- Erdogan, S., Medarova, Z. O., Roby, A., Moore, A., & Torchilin, V. P. (2008). Enhanced tumor MR imaging with gadolinium-loaded polychelating polymer-containing tumor-targeted liposomes. *Journal of Magnetic Resonance Imaging*, 27(3), 574-580. doi:10.1002/jmri.21202
- Eş, I., Montebugnoli, L. J., Filippi, M. F. P., Malfatti-Gasperini, A. A., Radaic, A., de Jesus, M. B., & de la Torre, L. G. (2020). High-throughput conventional and stealth cationic liposome synthesis using a chaotic advection-based microfluidic device combined with a centrifugal vacuum concentrator. *Chemical Engineering Journal*, 382, 122821. doi:<https://doi.org/10.1016/j.cej.2019.122821>
- Fang, S., Chang, S., WildSukhjinder, A., Sidhu, S., Ma, K., Versteeg, B. A., & Leaver, T. (2017). USD800336.



- Felgner, J. H., Kumar, R., Sridhar, C. N., Wheeler, C. J., Tsai, Y. J., Border, R., . . . Felgner, P. L. (1994). Enhanced gene delivery and mechanism studies with a novel series of cationic lipid formulations. *Journal of Biological Chemistry*, 269(4), 2550-2561. Retrieved from <https://www.scopus.com/inward/record.uri?eid=2-s2.0-0028024919&partnerID=40&md5=87c04a9b8db40bc83f1ba0b7546d4d54>
- Felgner, P. L., Gadek, T. R., Holm, M., Roman, R., Chan, H. W., Wenz, M., . . . Danielsen, M. (1987). Lipofection: a highly efficient, lipid-mediated DNA-transfection procedure. *Proceedings of the National Academy of Sciences of the United States of America*, 84(21), 7413-7417. Retrieved from <http://www.ncbi.nlm.nih.gov/pmc/articles/PMC299306/>
- Fessi, H., Puisieux, F., Devissaguet, J. P., Ammoury, N., & Benita, S. (1989). Nanocapsule formation by interfacial polymer deposition following solvent displacement. *International Journal of Pharmaceutics*, 55(1), R1-R4. doi:[https://doi.org/10.1016/0378-5173\(89\)90281-0](https://doi.org/10.1016/0378-5173(89)90281-0)
- Food, U., & Administration, D. (2018). *Liposome Drug Products Chemistry, Manufacturing, and Controls; Human Pharmacokinetics and Bioavailability; and Labeling Documentation*. 10001 New Hampshire Ave., Hillandale Bldg., 4th Floor U.S. Department of Health and Human Services Retrieved from <https://www.fda.gov/media/70837/download>
- Forbes, N., Hussain, M. T., Briuglia, M. L., Edwards, D. P., Ter Horst, J. H., Szita, N., & Perrie, Y. (2019). Rapid and scale-independent microfluidic manufacture of liposomes entrapping protein incorporating in-line purification and at-line size monitoring. *International Journal of Pharmaceutics*, 556, 68-81.
- Fraley, R. R. (1980). Introduction of liposome-encapsulated SV40 DNA into cells. *Journal of Biological Chemistry*, 255(21), 10431-10435.
- Funakoshi, K., Suzuki, H., & Takeuchi, S. (2007). Formation of Giant Lipid Vesiclelike Compartments from a Planar Lipid Membrane by a Pulsed Jet Flow. *Journal of the American Chemical Society*, 129(42), 12608-12609. doi:10.1021/ja074029f
- Gabizon, A., Catane, R., Uziely, B., Kaufman, B., Safra, T., Cohen, R., . . . Barenholz, Y. (1994). Prolonged circulation time and enhanced accumulation in malignant exudates of doxorubicin encapsulated in polyethylene-glycol coated liposomes. *Cancer Research*, 54(4), 987-992. Retrieved from <https://www.ncbi.nlm.nih.gov/pubmed/8313389>
- González, B., Calvar, N., Gómez, E., & Domínguez, Á. (2007). Density, dynamic viscosity, and derived properties of binary mixtures of methanol or ethanol with water, ethyl acetate, and methyl acetate at T=(293.15, 298.15, and 303.15)K. *The Journal of Chemical Thermodynamics*, 39(12), 1578-1588. doi:10.1016/j.jct.2007.05.004

- Gregoriadis, G., & Ryman, B. E. (1971). Liposomes as carriers of enzymes or drugs: a new approach to the treatment of storage diseases. *The Biochemical journal*, 124(5), 58P-58P. doi:10.1042/bj1240058p
- Guimarães Sá Correia, M., Briuglia, M. L., Niosi, F., & Lamprou, D. A. (2017). Microfluidic manufacturing of phospholipid nanoparticles: Stability, encapsulation efficacy, and drug release. *International Journal of Pharmaceutics*, 516(1–2), 91-99. doi:<http://dx.doi.org/10.1016/j.ijpharm.2016.11.025>
- Guner, S., & Oztop, M. H. (2017). Food grade liposome systems: Effect of solvent, homogenization types and storage conditions on oxidative and physical stability. *Colloids and Surfaces A: Physicochemical and Engineering Aspects*, 513, 468-478. doi:<http://doi.org/10.1016/j.colsurfa.2016.11.022>
- Ha, E.-S., Lee, S.-K., Choi, D. H., Jeong, S. H., Hwang, S.-J., & Kim, M.-S. (2019). Application of diethylene glycol monoethyl ether in solubilization of poorly water-soluble drugs. *Journal of Pharmaceutical Investigation*. doi:10.1007/s40005-019-00454-y
- Hafner, A., Lovrić, J., Lakoš, G. P., & Pepić, I. (2014). Nanotherapeutics in the EU: an overview on current state and future directions. *International journal of nanomedicine*, 9, 1005-1023. doi:10.2147/IJN.S55359
- Hak Soo, C., Wenhao, L., Misra, P., Tanaka, E., Zimmer, J. P., Itty Ipe, B., . . . Frangioni, J. V. (2007). Renal clearance of quantum dots. *Nature Biotechnology*, 25(10), 1165-1170. doi:10.1038/nbt1340
- Hamano, N., Böttger, R., Lee, S. E., Yang, Y., Kulkarni, J. A., Ip, S., . . . Li, S.-D. (2019). A robust microfluidic technology and a new lipid composition for fabrication of curcumin-loaded liposomes: Effect on the anticancer activity and safety of cisplatin. *Molecular Pharmaceutics*.
- Havel, H. A. (2016). Where Are the Nanodrugs? An Industry Perspective on Development of Drug Products Containing Nanomaterials. *The AAPS Journal*, 1-3. doi:10.1208/s12248-016-9970-6
- Hood, R., & Devoe, D. L. (2019). US010434065B2.
- Hood, R. R., & DeVoe, D. L. (2015). High-Throughput Continuous Flow Production of Nanoscale Liposomes by Microfluidic Vertical Flow Focusing. *Small*, 11(43), 5790-5799. doi:10.1002/smll.201501345
- Hood, R. R., DeVoe, D. L., Atencia, J., Vreeland, W. N., & Omiatek, D. M. (2014). A facile route to the synthesis of monodisperse nanoscale liposomes using 3D microfluidic hydrodynamic focusing in a concentric capillary array. *Lab on a Chip*, 14(14), 2403-2409. doi:10.1039/C4LC00334A

- Hood, R. R., Vreeland, W. N., & DeVoe, D. L. (2014). Microfluidic remote loading for rapid single-step liposomal drug preparation. *Lab on a Chip*, 14(17), 3359-3367. doi:10.1039/C4LC00390J
- Horibe, S., Tanahashi, T., Kawauchi, S., Murakami, Y., & Rikitake, Y. (2018). Mechanism of recipient cell-dependent differences in exosome uptake. *BMC Cancer*, 18(1), 47. doi:10.1186/s12885-017-3958-1
- Hoy, S. M. (2018). Patisiran: First Global Approval. *Drugs*, 78(15), 1625-1631. doi:10.1007/s40265-018-0983-6
- Hua, S., de Matos, M. B. C., Metselaar, J. M., & Storm, G. (2018). Current Trends and Challenges in the Clinical Translation of Nanoparticulate Nanomedicines: Pathways for Translational Development and Commercialization. *Frontiers in Pharmacology*, 9(790). doi:10.3389/fphar.2018.00790
- Huang, X., Caddell, R., Yu, B., Xu, S., Theobald, B., Lee, L. J., & Lee, R. J. (2010). Ultrasound-enhanced microfluidic synthesis of liposomes. *Anticancer Research*, 30(2), 463-466. Retrieved from <https://www.ncbi.nlm.nih.gov/pubmed/20332455>
- ISO. (1996). ISO 13321:1996 Particle size analysis — Photon correlation spectroscopy. In: International Organization for Standardization.
- ISO. (2017). ISO 22412: 2017 particle size analysis—dynamic light scattering (DLS). In: International Organization for Standardization.
- Jaafar-Maalej, C., Charcosset, C., & Fessi, H. (2011). A new method for liposome preparation using a membrane contactor. *Journal of Liposome Research*, 21(3), 213-220. doi:10.3109/08982104.2010.517537
- Jahn, A., Lucas, F., Wepf, R. A., & Dittrich, P. S. (2013). Freezing Continuous-Flow Self-Assembly in a Microfluidic Device: Toward Imaging of Liposome Formation. *Langmuir*, 29(5), 1717-1723. doi:10.1021/la303675g
- Jahn, A., Stavis, S. M., Hong, J. S., Vreeland, W. N., DeVoe, D. L., & Gaitan, M. (2010). Microfluidic Mixing and the Formation of Nanoscale Lipid Vesicles. *ACS Nano*, 4(4), 2077-2087. doi:10.1021/nn901676x
- Jahn, A., Vreeland, W., Locascio, L., & Gaitan, M. (2015). US Patent No. 20050112184A1.
- Jahn, A., Vreeland, W. N., DeVoe, D. L., Locascio, L. E., & Gaitan, M. (2007). Microfluidic Directed Formation of Liposomes of Controlled Size. *Langmuir*, 23(11), 6289-6293. doi:10.1021/la070051a
- Jahn, A., Vreeland, W. N., Gaitan, M., & Locascio, L. E. (2004). Controlled Vesicle Self-Assembly in Microfluidic Channels with Hydrodynamic Focusing. *Journal of the American Chemical Society*, 126(9), 2674-2675. doi:10.1021/ja0318030

- Javadzadeh, Y., Adibkia, K., & Hamishekar, H. (2015). Transcutol® (Diethylene Glycol Monoethyl Ether): A Potential Penetration Enhancer. In N. Dragicevic & H. I. Maibach (Eds.), *Percutaneous Penetration Enhancers Chemical Methods in Penetration Enhancement: Modification of the Stratum Corneum* (pp. 195-205). Berlin, Heidelberg: Springer Berlin Heidelberg.
- Jia, X., Wang, W., Han, Q., Wang, Z., Jia, Y., & Hu, Z. (2016). Micromixer Based Preparation of Functionalized Liposomes and Targeting Drug Delivery. *ACS Medicinal Chemistry Letters*, 7(4), 429-434. doi:10.1021/acsmedchemlett.6b00028
- Jo, M., Park, K.-M., Park, J.-Y., Yu, H., Choi, S. J., & Chang, P.-S. (2020). Microfluidic assembly of mono-dispersed liposome and its surface modification for enhancing the colloidal stability. *Colloids and Surfaces A: Physicochemical and Engineering Aspects*, 586, 124202. doi:<https://doi.org/10.1016/j.colsurfa.2019.124202>
- Jo, M. C., & Guldiken, R. (2013). Dual surface acoustic wave-based active mixing in a microfluidic channel. *Sensors and Actuators A: Physical*, 196, 1-7. doi:<http://dx.doi.org/10.1016/j.sna.2013.03.028>
- Joshi, S., Hussain, M. T., Roces, C. B., Anderluzzi, G., Kastner, E., Salmaso, S., . . . Perrie, Y. (2016). Microfluidics based manufacture of liposomes simultaneously entrapping hydrophilic and lipophilic drugs. *International Journal of Pharmaceutics*, 514(1), 160-168. doi:<http://dx.doi.org/10.1016/j.ijpharm.2016.09.027>
- Kanra, G., Marchisio, P., Feiterna-Sperling, C., Gaedicke, G., Lazar, H., Durrer, P., . . . Principi, N. (2004). Comparison of immunogenicity and tolerability of a virosome-adjuvanted and a split influenza vaccine in children. *The Pediatric infectious disease journal*, 23(4), 300-306.
- Kastner, E., Kaur, R., Lowry, D., Moghaddam, B., Wilkinson, A., & Perrie, Y. (2014). High-throughput manufacturing of size-tuned liposomes by a new microfluidics method using enhanced statistical tools for characterization. *International Journal of Pharmaceutics*, 477(1-2), 361-368. doi:<http://dx.doi.org/10.1016/j.ijpharm.2014.10.030>
- Kastner, E., Verma, V., Lowry, D., & Perrie, Y. (2015). Microfluidic-controlled manufacture of liposomes for the solubilisation of a poorly water soluble drug. *International Journal of Pharmaceutics*, 485(1-2), 122-130. doi:<http://dx.doi.org/10.1016/j.ijpharm.2015.02.063>
- Khadke, S., Roces, C. B., Cameron, A., Devitt, A., & Perrie, Y. (2019). Formulation and manufacturing of lymphatic targeting liposomes using microfluidics. *J Control Release*, 307, 211-220. doi:10.1016/j.jconrel.2019.06.002

- Khorasani, S., Danaei, M., & Mozafari, M. R. (2018). Nanoliposome technology for the food and nutraceutical industries. *Trends in Food Science & Technology*, 79, 106-115. doi:<https://doi.org/10.1016/j.tifs.2018.07.009>
- Kimura, N., Maeki, M., Sato, Y., Note, Y., Ishida, A., Tani, H., . . . Tokeshi, M. (2018). Development of the iLiNP Device: Fine Tuning the Lipid Nanoparticle Size within 10 nm for Drug Delivery. *ACS Omega*, 3(5), 5044-5051. doi:10.1021/acsomega.8b00341
- Knight, J. B., Vishwanath, A., Brody, J. P., & Austin, R. H. (1998). Hydrodynamic Focusing on a Silicon Chip: Mixing Nanoliters in Microseconds. *Physical Review Letters*, 80(17), 3863-3866. Retrieved from <http://link.aps.org/doi/10.1103/PhysRevLett.80.3863>
- Kumar, A., & Dixit, C. K. (2017). 3 - Methods for characterization of nanoparticles. In S. Nimesh, R. Chandra, & N. Gupta (Eds.), *Advances in Nanomedicine for the Delivery of Therapeutic Nucleic Acids* (pp. 43-58): Woodhead Publishing.
- Langhals, H. (1982). Polarity of Binary Liquid Mixtures. *Angewandte Chemie International Edition in English*, 21(10), 724-733. doi:10.1002/anie.198207241
- Lasic, D. D. (1988). The mechanism of vesicle formation. *Biochemical Journal*, 256(1), 1-11. Retrieved from <http://www.ncbi.nlm.nih.gov/pmc/articles/PMC1135360/>
- Lasič, D. D. (1987). A general model of vesicle formation. *Journal of Theoretical Biology*, 124(1), 35-41. doi:[http://dx.doi.org/10.1016/S0022-5193\(87\)80250-3](http://dx.doi.org/10.1016/S0022-5193(87)80250-3)
- Lee, C.-T., & Lee, C.-C. (2012). A capillary-driven micromixer: idea and fabrication. *Journal of Micromechanics and Microengineering*, 22(10), 105034. doi:10.1088/0960-1317/22/10/105034
- Lee, J., Goh, U., Lee, H.-J., Kim, J., Jeong, M., & Park, J.-H. (2017). Effective Retinal Penetration of Lipophilic and Lipid-Conjugated Hydrophilic Agents Delivered by Engineered Liposomes. *Molecular Pharmaceutics*, 14(2), 423-430. doi:10.1021/acs.molpharmaceut.6b00864
- Lee, J., Lee, M. G., Jung, C., Park, Y.-H., Song, C., Choi, M. C., . . . Park, J.-K. (2013). High-throughput nanoscale lipid vesicle synthesis in a semicircular contraction-expansion array microchannel. *BioChip Journal*, 7(3), 210-217. doi:10.1007/s13206-013-7303-8
- Lee, M. G., Choi, S., & Park, J.-K. (2009). Rapid laminating mixer using a contraction-expansion array microchannel. *Applied Physics Letters*, 95(5), 051902. doi:10.1063/1.3194137
- Leung, A. W. Y., Amador, C., Wang, L. C., Mody, U. V., & Bally, M. B. (2019). What Drives Innovation: The Canadian Touch on Liposomal Therapeutics. *Pharmaceutics*, 11(3), 26. doi:10.3390/pharmaceutics11030124

- Lin, B., & Basuray, S. (2011). *Microfluidics : technologies and applications* (B. Lin Ed. 1 ed.). Berlin; New York: Springer.
- Liu, Q., & Boyd, B. J. (2013). Liposomes in biosensors. *Analyst*, 138(2), 391-409. doi:10.1039/C2AN36140J
- Löb, P., Drese, K. S., Hessel, V., Hardt, S., Hofmann, C., Löwe, H., . . . Werner, B. (2004). Steering of Liquid Mixing Speed in Interdigital Micro Mixers – From Very Fast to Deliberately Slow Mixing. *Chemical Engineering & Technology*, 27(3), 340-345. doi:10.1002/ceat.200401995
- Lopez, R., Nerguizian, V., & Stiharu, I. (2018, 24-27 June 2018). *Low-Cost 3D-Printed PLA-COC Micro Hydrodynamic Focused Device*. Paper presented at the 2018 16th IEEE International New Circuits and Systems Conference (NEWCAS).
- López, R. R., Ocampo, I., Sánchez, L.-M., Alazzam, A., Bergeron, K.-F., Camacho-León, S., . . . Nerguizian, V. (2020). Surface Response Based Modeling of Liposome Characteristics in a Periodic Disturbance Mixer. *Micromachines*, 11(3), 235. Retrieved from <https://www.mdpi.com/2072-666X/11/3/235>
- López Salazar, R. R., Ocampo, I., Bergeron, K.-F., Alazzam, A., Mounier, C., Stiharu, I., & Nerguizian, V. (2019). *Assessment of the Factors Influencing Liposome Size in Dean Forces Based  $\mu$ mixers*. Paper presented at the  $\mu$ TAS 2019 The 23rd International Conference on Miniaturized Systems for Chemistry and Life Sciences Basel, Switzerland.
- Ma, L., Kohli, M., & Smith, A. (2013). Nanoparticles for Combination Drug Therapy. *ACS Nano*, 7(11), 9518-9525. doi:10.1021/nn405674m
- Maeki, M., Fujishima, Y., Sato, Y., Yasui, T., Kaji, N., Ishida, A., . . . Tokeshi, M. (2017). Understanding the formation mechanism of lipid nanoparticles in microfluidic devices with chaotic micromixers. *PLoS One*, 12(11), e0187962. doi:10.1371/journal.pone.0187962
- Magnan, C., Badens, E., Commenges, N., & Charbit, G. (2000). Soy lecithin micronization by precipitation with a compressed fluid antisolvent — influence of process parameters. *The Journal of Supercritical Fluids*, 19(1), 69-77. doi:[http://dx.doi.org/10.1016/S0896-8446\(00\)00076-0](http://dx.doi.org/10.1016/S0896-8446(00)00076-0)
- Manual, Z. N. S. U. (2013). Size Theory. In: Chapter.
- Martinez Paino, I. M., Santos, F., & Zucolotto, V. (2017). Biocompatibility and toxicology effects of graphene oxide in cancer, normal, and primary immune cells. *Journal of Biomedical Materials Research Part A*, 105(3), 728-736. doi:10.1002/jbm.a.35946



- Massing, U., Cicko, S., & Ziroli, V. (2008). Dual asymmetric centrifugation (DAC)—A new technique for liposome preparation. *Journal of Controlled Release*, 125(1), 16-24. doi:<http://dx.doi.org/10.1016/j.jconrel.2007.09.010>
- Matsumura, Y., & Maeda, H. (1986). A New Concept for Macromolecular Therapeutics in Cancer Chemotherapy: Mechanism of Tumoritropic Accumulation of Proteins and the Antitumor Agent Smancs. *Cancer Research*, 46(12 Part 1), 6387-6392.
- Michelon, M., Oliveira, D. R. B., de Figueiredo Furtado, G., Gaziola de la Torre, L., & Cunha, R. L. (2017). High-throughput continuous production of liposomes using hydrodynamic flow-focusing microfluidic devices. *Colloids and Surfaces B: Biointerfaces*, 156(Supplement C), 349-357. doi:<http://dx.doi.org/10.1016/j.colsurfb.2017.05.033>
- Mie, G. (1908). Beiträge zur Optik trüber Medien, speziell kolloidaler Metallösungen. *Annalen der Physik*, 330(3), 377-445. doi:10.1002/andp.19083300302
- New, R. R. C., Chance, M. L., Thomas, S. C., & Peters, W. (1978). Antileishmanial activity of antimonials entrapped in liposomes. *Nature*, 272(5648), 55-56. Retrieved from <http://dx.doi.org/10.1038/272055a0>
- Nguyen, N.-T. (2012a). Chapter 1 - Introduction. In *Micromixers (Second Edition)* (pp. 1-8). Oxford: William Andrew Publishing.
- Nguyen, N.-T. (2012b). Chapter 2 - Fundamentals of mass transport in the microscale. In *Micromixers (Second Edition)* (pp. 9-72). Oxford: William Andrew Publishing.
- Nguyen, N.-T., & Wu, Z. (2005). Micromixers a review. *J. Micromech. Microeng. Journal of Micromechanics and Microengineering*, 15(2), R1-R16.
- Osborne, D. W., & Musakhanian, J. (2018). Skin Penetration and Permeation Properties of Transcutol®—Neat or Diluted Mixtures. *AAPS PharmSciTech*, 19(8), 3512-3533. doi:10.1208/s12249-018-1196-8
- Otake, K., Imura, T., Sakai, H., & Abe, M. (2001). Development of a New Preparation Method of Liposomes Using Supercritical Carbon Dioxide. *Langmuir*, 17(13), 3898-3901. doi:10.1021/la010122k
- Patil, Y. P., & Jadhav, S. (2014). Novel methods for liposome preparation. *Chemistry and Physics of Lipids*, 177, 8-18. doi:<http://dx.doi.org/10.1016/j.chemphyslip.2013.10.011>
- Pattni, B. S., Chupin, V. V., & Torchilin, V. P. (2015). New Developments in Liposomal Drug Delivery. *Chemical Reviews*, 115(19), 10938-10966. doi:10.1021/acs.chemrev.5b00046
- Perli, G., Pessoa, A. C. S. N., Balbino, T. A., & de la Torre, L. G. (2019). Ionic strength for tailoring the synthesis of monomodal stealth cationic liposomes in microfluidic

- devices. *Colloids and Surfaces B: Biointerfaces*, 179, 233-241. doi:<https://doi.org/10.1016/j.colsurfb.2019.03.056>
- Phapal, S. M., Has, C., & Sunthar, P. (2017). Spontaneous formation of single component liposomes from a solution. *Chemistry and Physics of Lipids*, 205, 25-33. doi:<https://doi.org/10.1016/j.chemphyslip.2017.04.003>
- Plackett, R. L., & Burman, J. P. (1946). The Design of Optimum Multifactorial Experiments. *Biometrika*, 33(4), 305-325. doi:10.2307/2332195
- Pratt, K. C., & Wakeham, W. A. (1974). The Mutual Diffusion Coefficient of Ethanol-Water Mixtures: Determination by a Rapid, New Method. *Proceedings of the Royal Society A: Mathematical, Physical and Engineering Sciences*, 336(1606), 393-406. doi:10.1098/rspa.1974.0026
- Rahimpour, Y., & Hamishehkar, H. (2012). Liposomes in cosmeceutics. *Expert Opin Drug Deliv*, 9(4), 443-455. doi:10.1517/17425247.2012.666968
- Ramsay, E., Taylor, R. J., Walsh, C., Belliveau, N. M., Cullis, P. R., Leaver, T., & Wild, A. (2019). US010342760B2.
- Raposo, G., & Stoorvogel, W. (2013). Extracellular vesicles: exosomes, microvesicles, and friends. *Journal of Cell Biology*, 200(4), 373-383. doi:10.1083/jcb.201211138
- Rasouli, M. R., & Tabrizian, M. (2019). An ultra-rapid acoustic micromixer for synthesis of organic nanoparticles. *Lab on a Chip*. doi:10.1039/C9LC00637K
- Rayleigh, L. (1899). XXXIV. On the transmission of light through an atmosphere containing small particles in suspension, and on the origin of the blue of the sky. *The London, Edinburgh, and Dublin Philosophical Magazine and Journal of Science*, 47(287), 375-384.
- Rhoades, T., Kothapalli, C. R., & Fodor, P. S. (2020). Mixing Optimization in Grooved Serpentine Microchannels. *Micromachines*, 11(1), 61. Retrieved from <https://www.mdpi.com/2072-666X/11/1/61>
- Richter, Y., Zelig, Y., Elmalak, O., & Eyal, D. (2018). US9993427 B2.
- Sadeghi, A. (2019). Analytical solutions for mass transport in hydrodynamic focusing by considering different diffusivities for sample and sheath flows. *Journal of Fluid Mechanics*, 862, 517-551. doi:10.1017/jfm.2018.979
- Safra, T., Muggia, F., Jeffers, S., Tsao-Wei, D. D., Groshen, S., Lyass, O., . . . Gabizon, A. (2000). Pegylated liposomal doxorubicin (doxil): Reduced clinical cardiotoxicity in patients reaching or exceeding cumulative doses of 500 mg/m<sup>2</sup>. *Annals of Oncology*, 11(8), 1029-1033. Retrieved from <http://annonc.oxfordjournals.org/content/11/8/1029.abstract>



- Sedighi, M., Sieber, S., Rahimi, F., Shahbazi, M.-A., Rezayan, A. H., Huwyler, J., & Witzigmann, D. (2019). Rapid optimization of liposome characteristics using a combined microfluidics and design-of-experiment approach. *Drug Delivery and Translational Research*, 9(1), 404-413. doi:10.1007/s13346-018-0587-4
- Senturia, S. D. (2001). *Microsystem design*: Kluwer Academic Publishers.
- Shallan, A. I., & Priest, C. (2019). Microfluidic process intensification for synthesis and formulation in the pharmaceutical industry. *Chemical Engineering and Processing - Process Intensification*, 142, 107559. doi:<https://doi.org/10.1016/j.cep.2019.107559>
- Shen, K. C., Kakumanu, S., Beckett, C. D., & Laugharn Jr, J. A. (2015). Use of Adaptive Focused Acoustics™ ultrasound in controlling liposome formation. *Ultrasonics Sonochemistry*, 27, 638-645. doi:<http://dx.doi.org/10.1016/j.ultsonch.2015.04.027>
- Shende, P., Ture, N., Gaud, R. S., & Trotta, F. (2019). Lipid- and polymer-based plexes as therapeutic carriers for bioactive molecules. *International Journal of Pharmaceutics*, 558, 250-260. doi:<https://doi.org/10.1016/j.ijpharm.2018.12.085>
- Silva, V. (2018). *Statistical Approaches With Emphasis on Design of Experiments Applied to Chemical Processes*: BoD–Books on Demand.
- Srivastava, S., Mishra, S., Dewangan, J., Divakar, A., Gupta, N., Kalleti, N., . . . Rath, S. K. (2019). Safety assessment of the pharmacological excipient, diethylene glycol monoethyl ether (DEGEE), using in vitro and in vivo systems. *DARU*, 27, 219-231. doi:10.1007/s40199-019-00264-5
- Stano, P. (2018). Is Research on “Synthetic Cells” Moving to the Next Level? *Life*, 9(1), 3. Retrieved from <http://www.mdpi.com/2075-1729/9/1/3>
- Stavis, S. M., Fagan, J. A., Stopa, M., & Liddle, J. A. (2018). Nanoparticle Manufacturing – Heterogeneity through Processes to Products. *ACS Applied Nano Materials*, 1(9), 4358-4385. doi:10.1021/acsanm.8b01239
- Stroock, A. D., Dertinger, S. K. W., Ajdari, A., Mezić, I., Stone, H. A., & Whitesides, G. M. (2002). Chaotic Mixer for Microchannels. *Science*, 295(5555), 647-651. doi:10.1126/science.1066238
- Szoka, F., & Papahadjopoulos, D. (1978). Procedure for preparation of liposomes with large internal aqueous space and high capture by reverse-phase evaporation. *Proceedings of the National Academy of Sciences of the United States of America*, 75(9), 4194-4198. Retrieved from <http://www.ncbi.nlm.nih.gov/pmc/articles/PMC336078/>
- Tamai, H., Okutsu, N., Tokuyama, Y., Shimizu, E., Miyagi, S., Shulga, S., . . . Kurita, N. (2016). A coarse grained molecular dynamics study on the structure and stability of small-sized liposomes. *Molecular Simulation*, 42(2), 122-130. doi:10.1080/08927022.2015.1020487

- Tardi, P., Harasym, T., Webb, M., & Shew, C. (2010). US007850990B2.
- Thakur, R. K., Vial, C., Nigam, K. D. P., Nauman, E. B., & Djelveh, G. (2003). Static Mixers in the Process Industries—A Review. *Chemical Engineering Research and Design*, 81(7), 787-826. doi:<http://dx.doi.org/10.1205/026387603322302968>
- Thiermann, R., Mueller, W., Montesinos-Castellanos, A., Metzke, D., Löb, P., Hessel, V., & Maskos, M. (2012). Size controlled polymersomes by continuous self-assembly in micromixers. *Polymer*, 53(11), 2205-2210. doi:<https://doi.org/10.1016/j.polymer.2012.03.058>
- Ulrich, A. S. (2002). Biophysical Aspects of Using Liposomes as Delivery Vehicles. *Bioscience Reports*, 22(2), 129-150. doi:10.1023/a:1020178304031
- Valencia, P. M., Basto, P. A., Zhang, L., Rhee, M., Langer, R., Farokhzad, O. C., & Karnik, R. (2010). Single-Step Assembly of Homogenous Lipid-Polymeric and Lipid-Quantum Dot Nanoparticles Enabled by Microfluidic Rapid Mixing. *ACS Nano*, 4(3), 1671-1679. doi:10.1021/nn901433u
- van Swaay, D., & deMello, A. (2013). Microfluidic methods for forming liposomes. *Lab on a Chip*, 13(5), 752-767. doi:10.1039/C2LC41121K
- Van Tran, V., Moon, J.-Y., & Lee, Y.-C. (2019). Liposomes for delivery of antioxidants in cosmeceuticals: Challenges and development strategies. *Journal of Controlled Release*, 300, 114-140. doi:<https://doi.org/10.1016/j.jconrel.2019.03.003>
- Wagner, A., Vorauer-Uhl, K., Kreismayr, G., & Katinger, H. (2002). The crossflow injection technique: an improvement of the ethanol injection method. *Journal of Liposome Research*, 12(3), 259-270. doi:10.1081/LPR-120014761
- Wang, L., Yang, J.-T., & Lyu, P.-C. (2007). An overlapping crisscross micromixer. *Chemical Engineering Science*, 62(3), 711-720. doi:<https://doi.org/10.1016/j.ces.2006.09.048>
- Webb, C., Khadke, S., Schmidt, S. T., Roces, C. B., Forbes, N., Berrie, G., & Perrie, Y. (2019). The Impact of Solvent Selection: Strategies to Guide the Manufacturing of Liposomes Using Microfluidics. *Pharmaceutics*, 11(12), 653. doi:10.3390/pharmaceutics11120653
- Westerhausen, C., Schnitzler, L. G., Wendel, D., Krzysztoń, R., Lächelt, U., Wagner, E., . . . Wixforth, A. (2016). Controllable Acoustic Mixing of Fluids in Microchannels for the Fabrication of Therapeutic Nanoparticles. *Micromachines*, 7(9), 150.
- Wi, R., Oh, Y., Chae, C., & Kim, D. H. (2012). Formation of liposome by microfluidic flow focusing and its application in gene delivery. *Korea-Australia Rheology Journal*, 24(2), 129-135. doi:10.1007/s13367-012-0015-0

- Wu, Y., Li, L., Mao, Y., & Lee, L. J. (2012). Static Micromixer–Coaxial Electrospray Synthesis of Theranostic Lipoplexes. *ACS Nano*, 6(3), 2245-2252. doi:10.1021/nn204300s
- Wu, Z., & Nguyen, N.-T. (2005a). Hydrodynamic focusing in microchannels under consideration of diffusive dispersion: theories and experiments. *Sensors and Actuators B: Chemical*, 107(2), 965-974. doi:<http://dx.doi.org/10.1016/j.snb.2004.11.014>
- Wu, Z., & Nguyen, N.-T. (2005b). Rapid Mixing Using Two-Phase Hydraulic Focusing in Microchannels. *Biomedical Microdevices*, 7(1), 13-20. doi:10.1007/s10544-005-6167-7
- Xu, J., Liao, K., & Zhou, W. (2018). Exosomes Regulate the Transformation of Cancer Cells in Cancer Stem Cell Homeostasis. *Stem Cells Int*, 2018, 4837370. doi:10.1155/2018/4837370
- Zhigaltsev, I. V., Belliveau, N., Hafez, I., Leung, A. K. K., Huft, J., Hansen, C., & Cullis, P. R. (2012). Bottom-Up Design and Synthesis of Limit Size Lipid Nanoparticle Systems with Aqueous and Triglyceride Cores Using Millisecond Microfluidic Mixing. *Langmuir*, 28(7), 3633-3640. doi:10.1021/la204833h
- Zimmermann, M., Schmid, H., Hunziker, P., & Delamarche, E. (2007). Capillary pumps for autonomous capillary systems. *Lab Chip*, 7(1), 119-125. doi:10.1039/b609813d
- Zizzari, A., Bianco, M., Carbone, L., Perrone, E., Amato, F., Maruccio, G., . . . Arima, V. (2017). Continuous-Flow Production of Injectable Liposomes via a Microfluidic Approach. *Materials (Basel)*, 10(12). doi:10.3390/ma10121411
- Zook, J. M., & Vreeland, W. N. (2010). Effects of temperature, acyl chain length, and flow-rate ratio on liposome formation and size in a microfluidic hydrodynamic focusing device. *Soft Matter*, 6(6), 1352-1360. doi:10.1039/B923299K



